Properties and applications of additively manufactured metallic cellular materials: A review

Anton du Plessis [a,b,*], Seyed Mohammad Javad Razavi [c], Matteo Benedetti [d], Simone Murchio [d], Martin Leary [e], Marcus Watson [e], Dhruv Bhate [f], Filippo Berto [c,*]

[a] Research Group 3DInnovation, Stellenbosch University, Stellenbosch 7602, South Africa
[b] Object Research Systems, Montreal, Canada
[c] Department of Mechanical and Industrial Engineering, Norwegian University of Science and Technology (NTNU), Richard Birkelands vei 2b, Trondheim, Norway
[d] Department of Industrial Engineering, University of Trento, 38123 Trento, Italy
[e] RMIT Centre for Additive Manufacturing, School of Engineering, RMIT University, Melbourne, VIC, Australia
[f] 3DX Research Group, Arizona State University, Mesa, AZ 85212, USA

ARTICLE INFO

ABSTRACT

Additive manufacturing (AM) refers to a collection of manufacturing methods involving the incremental addition of material to build a part directly in its final or near-final geometry, usually in a layer-by-layer process. Metal AM in particular has seen great industrial adoption and maturation. This technology enables increased freedom of design in engineered materials with complex geometries, of which architected cellular or lattice structures are particularly promising in a wide range of applications. These materials are similar to stochastic foams which have found many industrial applications over the last few decades, but regular cellular structures possess a higher degree of control over the manufactured architectures made possible by additive manufacturing. These architected porous materials have properties that can be fine-tuned for a particular application (for mechanical performance, permeability, thermal properties, etc.). The control over the design and manufacturing of such architected structures in comparison to stochastic structures opens new application possibilities and enables a range of new products and features. This potential is only starting to be realized as metal AM techniques are maturing and are increasingly being adopted in various industries, and as design-for-AM capabilities improve. This review paper summarizes the unique properties of AM lattice structures and how these have been successfully employed for specific applications so far, and highlights various application areas of potential interest for the near future. The focus in this review paper is therefore on unique achievable properties and the associated applications for metal additively manufactured lattice structures.

1. Introduction

Additive manufacturing (AM) is the term for all manufacturing processes that use incremental material addition to build parts, using a digital design model. AM is classified into seven process categories according to the ASTM ISO 52900 terminology standard [1],

---

* Corresponding authors.
  E-mail addresses: aduplessis@theobjects.com (A. du Plessis), filippo.berto@ntnu.no (F. Berto).

with a wide variety of materials that can be used including high-end engineering polymers, metals, ceramics and more [2]. The laser powder bed fusion (L-PBF) process is now widely adopted in industry and has reached a high level of maturity, with excellent part quality that can be reliably produced in a wide variety of popular metal alloys [3,4]. The L-PBF process uses a high-power focused laser beam to melt tracks of powder, with overlapping tracks and layer by layer processing until the component is complete [3]. Due to typical track widths of 0.1–0.2 mm, highly intricate and complex structures can be manufactured. The layer by layer processing allows complexity that is in many cases impossible to be achieved by any other manufacturing method. Typical maximum part sizes reach 300 mm or even larger in latest commercial systems. This size and resolution range opens many industry-relevant opportunities for key components to be produced, in optimized complex geometries, in short lead times, making the technology relevant to the aerospace, medical, automotive and general manufacturing industries [5].

Major advantages of AM include the consolidation of multiple parts (less joins between parts), shorter lead times for low-volume parts, ease of design iterations and customized designs for specific short-run or unique applications, and complex designs that were too difficult or expensive (or even impossible) to manufacture previously with traditional manufacturing methods. Complexity is a key driver in terms of light-weighting design for automotive and aerospace, as optimized geometries may be manufactured that minimize mass while performing equally well for the expected loads. These optimized geometries may include curved structures following expected load paths, with no material in low-stressed regions. This approach has been successfully demonstrated in many examples of part-scale topology optimization and biomimetic engineering design, including organic-shaped brackets and curved geometries, replacing traditional "block-shaped" designs, examples of this are discussed in the review [6]. When the expected loads are well known, such topology optimized bulk structures are a good choice and hold promise for many applications, especially those involving light-weighting applications. These structures can often be manufactured (in somewhat lower complexity) using traditional manufacturing methods, but this is often simply more expensive or more challenging for such traditional tools due to the increased complexity. In AM, the complexity "comes for free", and there is no additional cost for utilizing this complexity compared to less complex parts. Optimal use of the available complexity is therefore often key to the financial and performance benefits of AM over traditional manufacturing, hence the interest in making full use of complexity in AM. The majority of the available literature on the design and assessment of structural integrity of AM parts are focused on the bulk materials and components with simplified geometrical discontinuities. More information about these research studies can be found in [7-10]. Although the mentioned research studies are of great importance when dealing with bulk mechanical components and structures, their extension to other fields such as metamaterials can be challenging.

Some of the most complex structures that are made possible by AM are not topology optimized bulk structures as discussed above, but smaller-scale cellular or lattice structures, also known as architected cellular materials or meta-materials. These structures are similar to open-cell stochastic foams, which have found great industrial use over the last two decades [11-14]. The main difference is that porous cellular structures manufactured by AM can be highly regular and controlled, with unique properties achievable through precise control of the manufacturing process and the porous design. Typically in lattice structures, struts and nodes are connected in a regular arrangement according to some basic building block design, the unit cell design, and tessellated or repeated in 3D space. These regular strut-based lattices resemble scaffold structures with often more complex architectures. The struts and nodes may be arranged in different ways that influence the effective material stiffness, deformation behaviour and failure modes. Due to the sharp corners at the nodes where struts connect, these locations are often locations of high stress concentration under loading conditions, prompting the use of curved designs in these corners, such as fillets [15]. Besides struts and nodes, another popular cellular design approach is the use of triply periodic minimal surfaces (TPMS) that are available in different variations, with either skeletal or sheet-based varieties [16]. In both varieties, the porous structure is made of continuous curved geometries, eliminating stress concentrations. Further designs and classifications of cellular and lattice architectures are discussed in [17].

The wide array of cellular designs available and the ability to precisely tailor their design, density and other properties in 3D using additive manufacturing provides new opportunities for applications of these structures in industrially-relevant products and parts. Their application in medical implants is widely acknowledged and has driven much of the literature so far, with extensive reviews of lattices in medical implants over the last decade [18-26]. Besides medical applications, their application for light-weighting is also widely acknowledged and drives significant interest from the aerospace and automotive industries. In these efforts, much progress has been made in understanding the properties of AM lattice structures and their constraints or limits for specific applications, while literature reviews often include mentions of the varied potential applications of lattice structures [27,28]. So far, however, this literature does not yet consider extensively the wide array of potential applications of lattice structures, with most discussion concerning their use in implants and their optimization for this particular application. More generally, porous stochastic foams have found many other applications in industry over the last two decades [11-14], and AM lattice structures have the potential to outperform these in various similar applications. In order to reach this level of performance, an in-depth understanding of AM must be combined with an equally deep understanding of lattice structure design, manufacturability and testing. The mechanical properties and fatigue performance, in particular, of lattice structures is still a valid concern, due to widely disparate results reported in various studies to date. As recently reviewed in [29], the causes of this variability are currently being better understood and appropriate performance can be achieved using some guidelines and quality control approaches. In general for metal AM industrial applications, a holistic approach combining knowledge of materials, structures, design and processes is required to achieve specific desired properties [30]. Besides material choices and manufacturing quality, the design choices for lattice structures are key to their successful implementation in industry. This includes an understanding of the application requirements and how to select or optimize a cellular structure for each particular application, which is the focus of the current paper. This paper therefore takes a unique application-centric approach, focusing on the achievable properties of lattice structures and how to optimize these properties for specific applications, reviewing successes reported in the literature in each application area to date. A summary and overview is provided in Table 1, which directs the

reader to the appropriate section in the paper for each property or application type.

This contribution will be especially useful for design engineers to make appropriate choices and thereby inspires and informs future designs and design choices in each of these areas. The aim of this paper is therefore to provide a comprehensive resource for AM design engineers and researchers, to assist in selecting an appropriate cellular architecture, material and process for manufacturing of lattices for specific applications. The scope is limited to metal AM and to cellular structures manufactured primarily by L-PBF, due to the industrial importance and reliability of this technology. Much of the discussion may also be relevant to other materials and processes, such as micro- or even nanoscale cellular materials, polymers and resins (e.g. by stereolithography) or larger scale structures (e.g. by directed energy deposition). Potential exists in other AM processes and materials, but the scope in this paper is limited to metal lattice structures by L-PBF. In this paper, the terms "lattice structure" and "cellular structure" are used interchangeably with the more generic term "architected cellular materials" referring to all intentionally designed and additively manufactured porous structures. The term *meta*-material is also sometimes used, in order to emphasize the unique and sometimes superior properties of these unique materials.

2. Background

2.1. Basics and terminology of cellular structures

Materials occurring in nature are often characterized by a porous structure, in contrast to most artificially engineered materials employing solid structures, such as metals and polymers. Natural materials like bone, wood, and cork have a complex multiscale hierarchical porous architecture [11]. For illustrative purposes, Fig. 1A shows the microstructure of bone consisting of a thin solid layer of cortical bony tissue attached to a highly porous, cellular core of cancellous bony tissue. The cellular architecture of the core is complex, with intricately shaped ligaments and gradients in density – comparative architected cellular designs are shown (minimal surface geometries) in Fig. 1B. Fig. 1C shows a natural hexagonal honeycomb and 1D an example of bioinspired metallic honeycomb structure. Honeycomb structures are specifically reviewed in [31].

The architecture of natural biomaterials such as bone is in general the result of responses to external stimuli that leads to a continuous remodelling of the internal structure in order to adapt it to changing boundary conditions [35]. Multifunctional properties displayed by natural biomaterials, ranging from structural strength and stiffness to fluid permeability and thermal insulation, are not easily attainable by traditional artificial materials. Taking inspiration from nature [6,36], a new class of engineered materials is

Table 1
Selected applications of cellular materials along with the relevant desired properties and section where this is discussed in more detail.

| Application	Desired Properties	Section
Lightweight Structures	High Specific Stiffness	3.1; 3.2
	High Specific Strength	
Biomedical Implants	Tuned mechanical properties to match bone elastic modulus	3.1
	Good bone integration, enhanced by appropriate pore size, large surface area, permeability	3.4; 3.5
Crashworthiness applications	High energy absorption	3.3
	Low transmitted stress	
Vibration Control	High mechanical loss/damping coefficient	3.3
	High specific natural flexural vibration frequencies	
Packaging	High Energy Absorption prior to densification	3.3
Shock Absorption	High Energy Absorption at very high strain rates	3.3
Ballistics	Low dynamic indentation	3.3
Electrodes	High Surface/Volume ratio	3.4
Catalysts	High surface/volume ratio	3.4
	High permeability	
Heat pipe wicks	High permeability	3.5
	High capillary performance	
Thermal Insulation	Low Thermal Conductivity	3.6
	Low Specific Heat	
Heat Exchanger	High Thermal Diffusivity	3.6
	Low Differential Thermal Expansion (Expansion limited)	
	High Failure Stress (Pressure Limited)	
Heat sink	High convective heat transfer	3.6
	Low thermal resistance	
Thermal control, hydrogen storage tanks	Controlled thermal conductivity	3.7
	High surface area	
Buoyancy	Low Density	3.8
	Good corrosion resistance	
Filtration	High Pore Size Control	3.8
	Adequate Pore Connectivity	
Acoustic Absorption	High sound-absorption coefficient	3.8
Soft hinges	Compliant mechanisms	3.8
Support structures and infill in additive manufacturing processes	Low-density	3.8
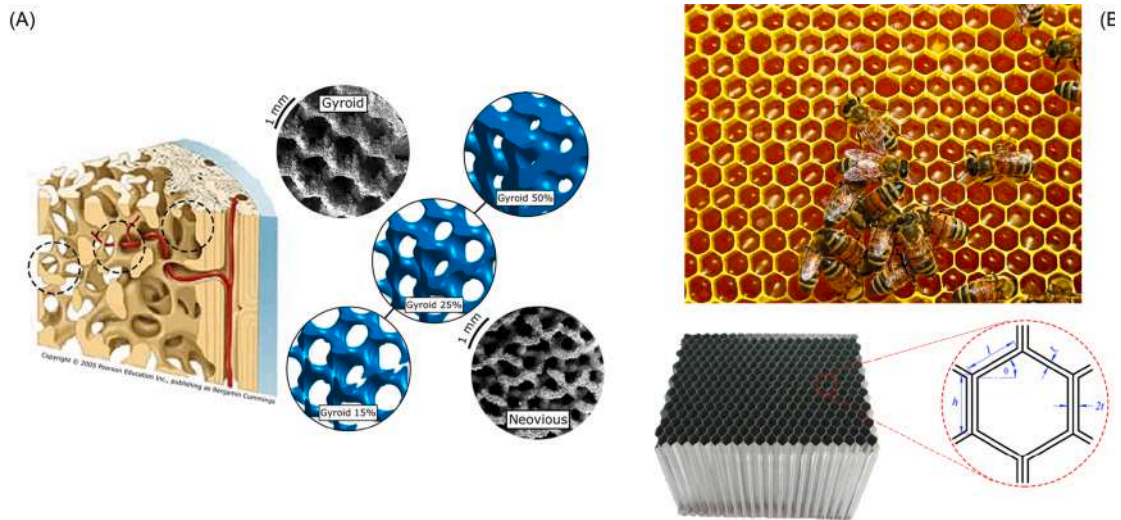
Fig. 1. (A) Porous cellular structure of bony tissue. (B) Triply periodic minimal surface (TPMS) artificial cellular material mimicking the structure of natural trabecular bone [32]. (C) natural [33] and (D) artificial honeycomb structure [34].

gaining more and more interest in the academic and industrial fields, generically termed as "architected metamaterials" or "cellular materials". The first definition outlines the fact that their extraordinary multifunctional properties mainly stem from their underlying architecture rather than only from the base material. The second one indicates the tessellation of a 3D space with a regular and un-distorted periodic pattern of identical cells. Their deterministic architecture distinguishes this class of materials from foams, in which the pores are distributed stochastically [37]. This difference makes the deterministic architecture of designed cellular structures more controllable, for individual or multifunctional properties to be achieved for specific engineering applications.

Most of the early investigations on the mechanical properties of architected cellular materials were summarized by Gibson and Ashby in their fundamental book "Cellular Solids: Structures and Properties" [38]. In the very commonly investigated strut-based lattices, nodes located at the vertices or edges of the unit cells are linked by slender members usually termed as struts (sometimes referred to as beams). The most important unit cells in strut-based metamaterials are summarized in Fig. 2, taken from our recent review on fatigue properties of this class of materials [29]. The most appealing property of such metamaterials is that their micro-architecture, namely the number and spatial arrangement of nodes and struts in the elementary unit cell, and their relative density (viz. the ratio of the density of the cellular material to the density of the base solid material) can be modulated in order to confer to the component the desired mechanical [39,40] (mainly stiffness, strength and energy absorption), thermal [41] and permeability prop-erties [42]. A general concept in porous materials is the term relative density which is used to describe the material fraction, while the total porosity value is the complementary value (Porosity = 1 – Relative Density). This "intentional" porosity value should not be confused with unintentional porosity that can be formed in struts or sheets. Cell topologies mentioned in Fig. 2 as "auxetic" are worthy to be explicitly mentioned, as they are a matter of intensive current research [43] due to their negative Poisson's ratio conferred by re-entrant arrangement of struts, which hold particular advantages.

Besides strut-based lattices, other architected cellular materials that are gaining increasing interest are based on triply periodic minimal surfaces (TPMS), some of them sketched in the last two rows of Fig. 2. TPMS are surfaces created mathematically such that they have a zero-mean curvature at each point [44]. The presence of TPMS in natural materials, like biological membranes [45] and crystals [44], has inspired researchers to consider TPMS architectures in tissue engineering and biomimetic material design, as exemplarily illustrated in Fig. 1B [32]. A recent review of TPMS is provided in [46] including a discussion of some of their applications. The shellular term has been recently used in the literature to represent thin TPMS cellular shells [47]. TPMS surfaces can be trigo-nometrically approximated using level surface equations [48].

2.2. Mechanical properties of cellular materials

This section introduces the background necessary to understand the mechanical properties of cellular structures. Fig. 3 illustrates examples of specimen geometries usually employed in mechanical tests. Due to the lack of appropriate standards specifically for evaluating the mechanical properties of additively manufactured cellular structures, ISO 13314:2011 [49] is often used as a guideline for mechanical testing. This standard was developed for stochastic porous materials but remains relevant to some extent for additively manufactured cellular materials as well. The prescribed geometry is illustrated in Fig. 3A, wherein the linear dimensions of the specimen must be at least 10 times d_a, viz. the unit cell size, so as to minimize edge effects.

When quasi-statically loaded in compression, cellular lattice structures initially show a linear elastic regime until the first struts fail, followed by a plateau regime during which the cells start to progressively collapse along preferential failure bands because of buckling, cracking or yielding depending on the material and the cellular architecture, and finally a densification phase that corresponds to the
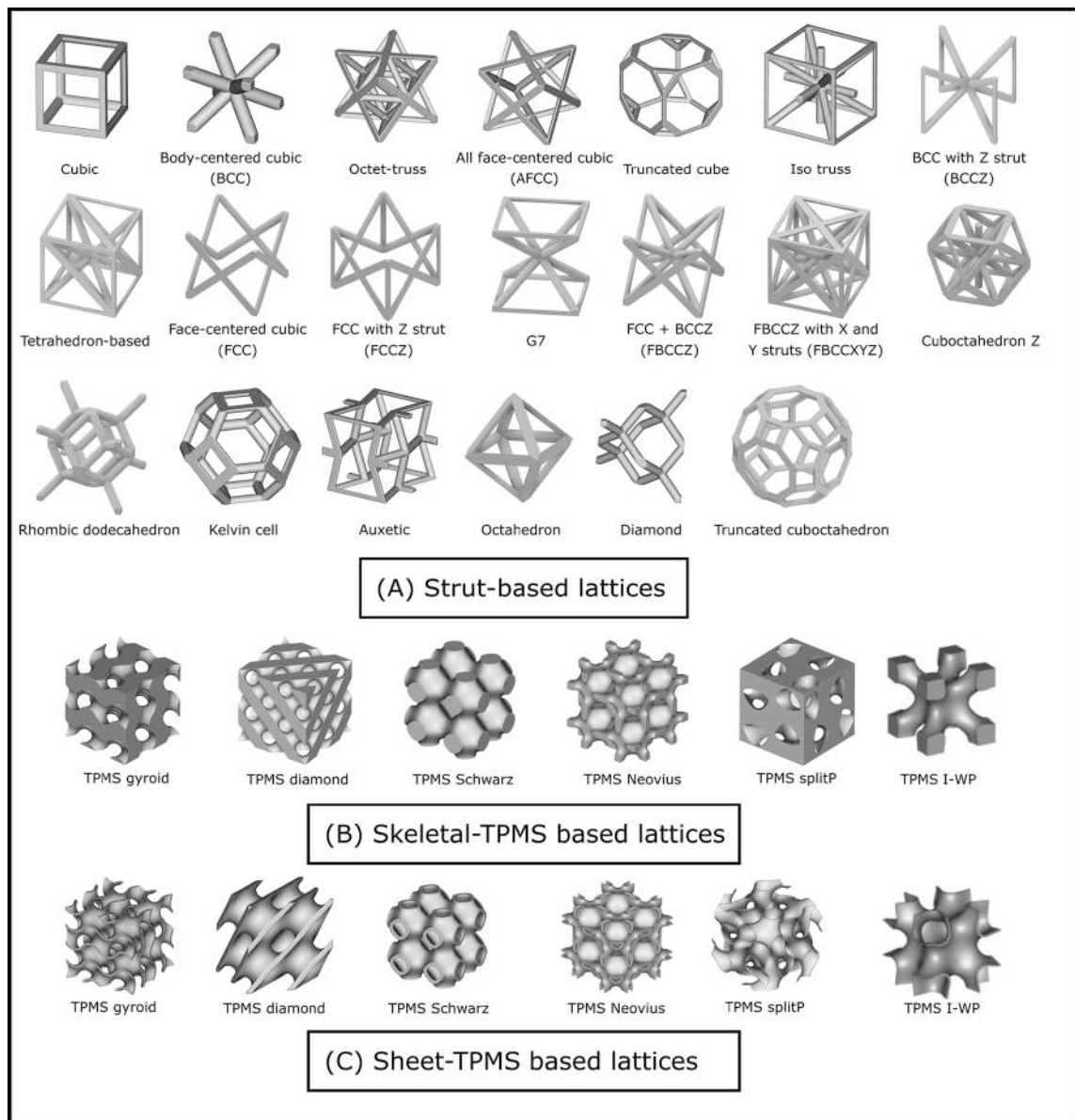
Fig. 2. Various architectures of lattice structures (A) Strut-based lattice cells are shown in the first three rows. (B) Skeletal- and (C) sheet-based triply periodic minimal surfaces (TPMS) [29].

full collapse of the cells one against the other. This is shown in Fig. 4A.

Different cellular architectures, densities, bulk/strut material properties and post processing regimens such as different heat treatments may influence the yielding behaviour and hence the plateau region may include larger variations or may not be horizontal (or may slope upwards or downwards), depending on the failure modes and associated response. The elastic modulus is usually measured in the first part of the force–displacement curve, or by unloading and reloading within the elastic regime, prior to yielding or plastic deformation. Following the above description of a typical cellular material's compressive stress–strain curve, it is important to note the influence of relative density on this curve. Fig. 4B shows four different densities of identical cellular design, showing that for denser structures there is a sharper rise in the initial (elastic) region indicating a higher stiffness, a higher yield strength (peak value prior to plastic deformation or failure) and a higher plateau region. This simplistic demonstration shows the complex relationship of lightweighting (reduced relative density) compared to other parameters such as energy absorption (total area under the curve).

As seen in Fig. 4B, the elastic modulus increases with density, which is well described by relationships developed for open-cell foams by Ashby and Gibson. The prediction of the mechanical properties of cellular materials is a matter of a vast scientific litera-ture, the interested reader can consult our recent review paper in this regard [29]. In brief, closed-form equations were proposed by Gibson et al. [50] to express elastic modulus and yield strength as a function of the relative density, which are still good approximations
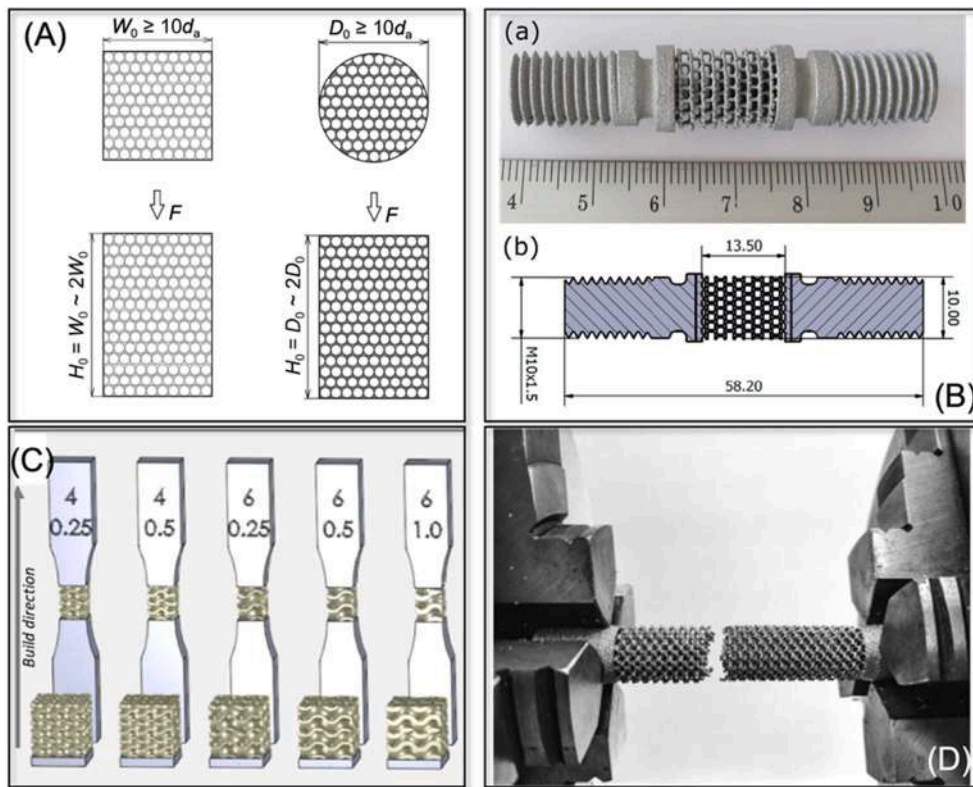
Fig. 3. (A) specimen geometry for compression-compression tests according to ISO 13314. Specimen geometry with threaded ends (B) [71] and solid flat ends (C) [64] proposed in the literature to carry out uniaxial tensile quasi-static and fatigue tests. (D) Specimen with solid cylindrical ends used for quasi-static torsion tests [70].

in most cases. They assume that the cell struts behave similar to slender and straight Euler-Bernoulli beams. Importantly, different equation constants were derived depending on the stretching or bending dominated behaviour of the unit cell type, or, equivalently, on the sign of the coefficient M of the Maxwell stability criterion [51]. This is defined as follows for 2D lattices: $M = b - 2j + 3$, where b is the number of struts and j is the number of nodes. For 3D lattices, $M = b - 3j + 6$ and for further information, the reader is referred to the recent work [29]. For M < 0, the structure is defined as bending-dominated and for M > 0, the structure is stretch-dominated with associated differences in failure modes. The elastic modulus as a function of relative density is shown in Fig. 5 for ideal bending and stretching dominated lattices.

The stress–strain curves of the stretching-dominated lattices are generally characterized by higher initial stiffness and yield strength (prior to the first yield) than a bending-dominated lattice of the same relative density (see Fig. 5). While stretching-dominated structures are more structurally efficient but prone to sudden failures and shear band failures, bending-dominated structures are more compliant and hence more effective in dissipating deformation energy [57]. Very recently, Liu et al. [58] succeeded in suppressing shear band formation in strut-based lattice structures by modifying the unit cell so as to eliminate associated stress fluctuations and enhance the energy absorption. Similarly, heat treatment which lead to precipitation in inconel lattices have been shown to change the behavior from bending dominated to stretch dominated, with associated differences in failure modes [59]. The Ashby equations are able to capture most of the trends displayed by experimental data as a function of the relative density. Interestingly, the majority of experimental data is in better agreement with the Gibson-Ashby predictions for bending-dominated behaviour, even though some of the cell architectures were nominally classified as stretch-dominated. This experimental evidence is often explained in terms of geometric inaccuracies [29,52], which can strongly affect additively manufactured cellular materials.

Typically, compression tests of cellular structures are performed with enough unit cells in each direction to evaluate the effective material properties without boundary effects playing a leading role, which according to the ISO 13314 standard requires 10 unit cells in each direction [28,29,53]. The difficulty with this requirement is that quite often the required sample size – for achieving a $10 \times 10 \times 10$ unit cell design in 20 mm cube for example – requires a 2 mm unit cell size, which at 20 % density approaches very small strut or wall thickness values. Therefore, sometimes fewer unit cells are used such as 5–7 unit cells in each direction, as the effective material properties converge toward a constant value as the number of unit cells increase, due to less influence from the edges. This is shown in Fig. 6 for aluminium foams of two types, showing the trend that for 7 or more cells across the sample width, the effective elastic modulus and yield strength reach constant values [54].

Also important to keep in mind is the recommended dimensions of coupon test samples – they should be cubic or cylindrical with
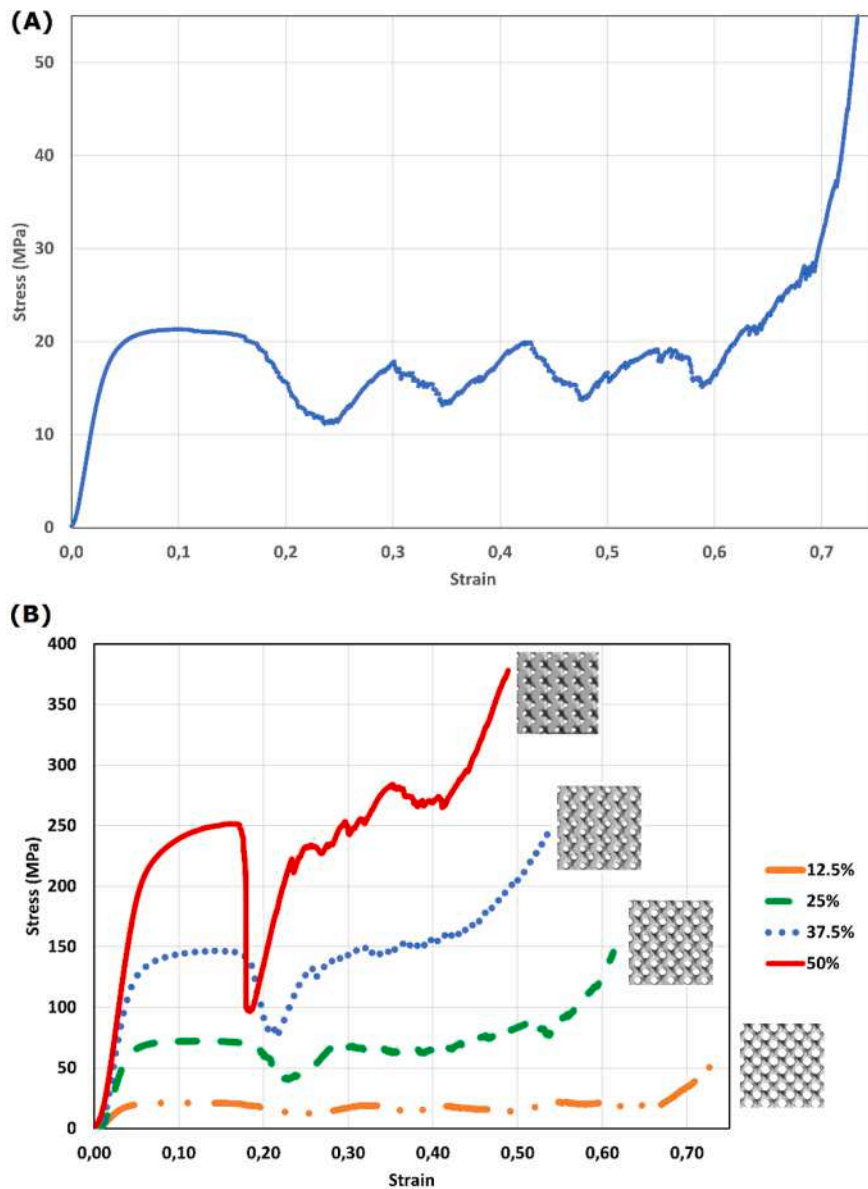
Fig. 4. (A) Typical experimental stress–strain curve for compression testing of a metallic cellular material, in this case a Ti6Al4V skeletal gyroid lattice manufactured by L-PBF, with 12.5 % density. The initial elastic response is followed by a first yielding point at 20 MPa, after which a plateau region with near constant stress around 15 MPa which continues up to high strains, with a final full densification and stress increase. (B) Stress–strain curves for cellular structures with varying density: higher lattice density results in increased initial stiffness in elastic region, with a higher yield strength and correspondingly higher plateau stress. Full densification occurs at smaller strains for higher density samples due to more material present. This experimental data is from Ti6Al4V skeletal gyroid structures manufactured by L-PBF, insets show sample front views.

height (in loading direction) between 1 and 2 times the diameter perpendicular to the loading direction. The two surfaces should be parallel to prevent irregular initial loading conditions. It is also important to note the conversion from force and displacement to stress and strain, which considers the total applied area as an effective material area. The obtained stress and strain are therefore the effective "meta-material" properties.

The comprehension of the fatigue properties of cellular materials is even more complicated and highly influenced by local defectiveness and geometrical inaccuracies that lead to the initiation of the fatigue damage [60]. In general, the reduction in fatigue strength with reducing relative density is more pronounced with respect to the yield stress, which is, in contrast, a phenomenon occurring at the scale of the whole lattice. Typically, structurally optimized lattices display the highest fatigue properties, especially if fabricated with base metals having high ductility, like Cr-Co alloys and stainless steels [29].

Very few papers in the literature report mechanical tests with more complex loading conditions in quasi-static [56,61,62] and
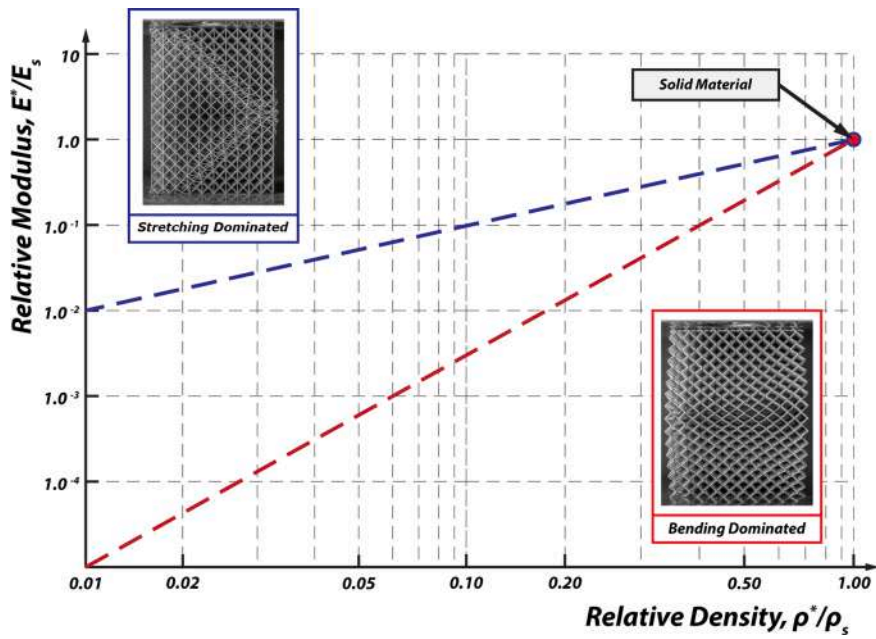
Fig. 5. Ashby plot showing relative elastic modulus as a function of relative density, with upper (blue) line indicating ideal stretching-dominated behaviour and lower (red) curve showing ideal bending-dominated behaviour. Note the logarithmic axes, and the intersection with fully dense material at (1;1). Insets show failure modes typically associated with these behaviours. (For interpretation of the references to colour in this figure legend, the reader is referred to the web version of this article.)
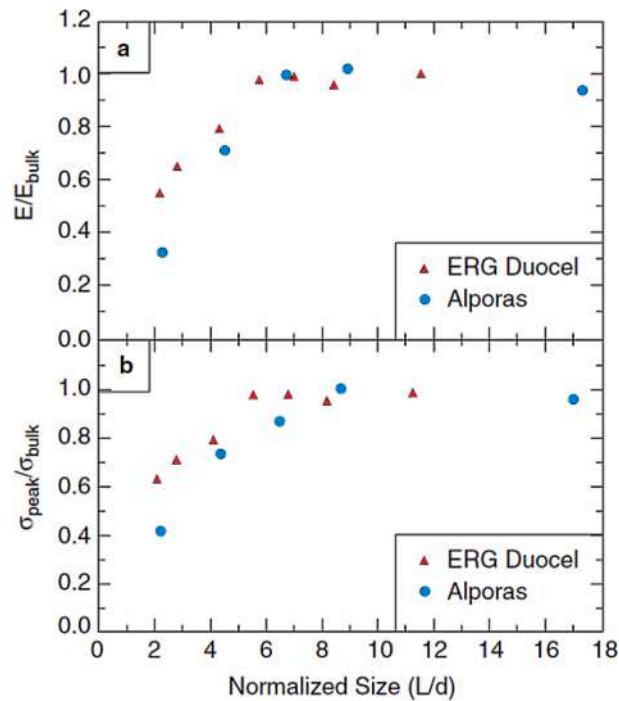

Fig. 6. Effective elastic modulus as a function of unit cell size, from the work of Andrews et al [55] and Ashby et al [54]. This case is for two types of aluminium foams, where the elastic modulus and strength become independent of cell size when there are 7 or more cell widths in a sample width. Below this value, the edge effects become more important. In this image L refers to the size length of the sample and d the unit cell size – the ratio L/d is therefore equivalent to the number of unit cells across the sample in one direction.

cyclic [63,64] loading. In the very recent literature, there is a rising interest in performing quasi-static and fatigue tests under uniaxial tensile loading conditions. Clearly, this poses a considerable experimental challenge as the specimen geometry must be designed to make it possible to transfer tensile loading from the machine to the sample and to locate specimen failure in the sample's central gauge section where edge effects are minimized. Examples of specimen provided with solid ends that can be either connected to threaded joints or gripped by hydraulic grips are provided in Fig. 3B and C, respectively. Typically, the load (stress)-versus-elongation (strain) curve, obtained in quasi-static uniaxial tensile tests, starts with an elastic zone (cells respond elastically to the applied load), followed by a small yielding regime, culminating in brittle fracture (no necking and very fast separation of cell walls or breakage of a large number of metallic arms in each section of the structure once a crack initiates, then propagation throughout the specimen). This loss in ductility with respect to quasi-static compression tests can be imputed to the more detrimental effect exerted by internal porosity and surface defectiveness in the presence of tensile global stresses. In addition, investigations performed in [56] attested to an asymmetry in the mechanical response under compression and tension loading. This was imputed to the difficulty of exactly orienting the cells with the loading axis in compression tests due to parallelism issues between compression plates and specimen. On the contrary, the application of tensile loads tends to orient the cells along the loading axis, thus making the experimentally measured mechanical behavior closer to the numerically predicted behavior on the basis of CT reconstruction of the actual lattice geometry [65].

Flexural tests are practically challenging due to the necessity of applying concentrated loads (to reproduce 3- or 4- point bending loading conditions) that may lead to indentation of the lattice material which is softer than the rollers used for bending fixtures. Therefore, flexural tests are limited almost exclusively to sandwich structures [66-68], wherein a porous core is comprised between fully dense face sheets thus able to resist the application of concentrated loads. To conclude, a few papers have been published so far reporting quasi-static torsional tests on cellular materials [69], as shown exemplarily in Fig. 3D for TPMS cellular materials [70].

Something that is reaching increasing attention in recent years is the simulation and prediction of mechanical properties of such cellular structures and metamaterials. Historically, this has been a significant computational challenge, and it remains the case today for typical design engineers, despite advances in computational resources. Often simplifications are used that allow the structure to be estimated as comprising of connected beam elements, for example. However, the actual geometry may be required for more accurate representation of the material distribution and to highlight problematic areas, for example using microCT scan data. Despite the computational expense involved, this brings added value to understanding the structure's response, and may highlight possible crack initiation locations as shown in [72]. Recently, the progressive damage in lattice structures could be modelled accurately, considering the changes in stress distributions after damage occurs, matching well with experimental data [73]. Additional simulations may be useful for prediction of angular responses of lattices, variations in their manufacturing quality and the impact of this on the predicted performance, or even for permeability [74] and for other properties such as thermal conductivity. Besides the prediction of lattice performance, simulations are also used to improve the design of lattice structures, for example through topology optimization approaches [75,76].

2.3. Additive manufacturing technologies and materials

Additive manufacturing comprises of seven process categories, with different technologies, materials and capabilities for each process. Despite diverse naming, different metal AM processes share a similar approach for fabrication, starting with a 3D CAD model. This model is then virtually sliced into thin layers with a typical layer thickness of 20 μm to 1 mm, depending on the AM process [3,30,77]. This model is then used as input for the software linked to the AM machine and the physical part is fabricated by repetitive deposition of single layers and locally melting/sintering the feedstock material using a heat source. This paper focusses on metal AM cellular structures, for which the categories of powder bed fusion (PBF) and directed energy deposition (DED) are most relevant. Depending on the type of heat source (e.g. laser beam, electron beam) in either of these two categories, different commercialized AM systems are available. Leading vendors and their specific process names are listed in Table 2.

In the laser powder bed fusion (L-PBF) process, the feedstock material in the form of metal powder is spread in thin layers of 20 μm-100 μm across the build stage with dimensions ranging from 50 mm × 50 mm up to 800 mm × 400 mm at present [4], with larger systems being custom developed. The spread powder is then selectively exposed to the laser beam in planes parallel to the build stage according to the geometry of the slice. These steps are iterated by layer by layer material deposition on the powder bed and selective melting of the cross sections until the part is completed. The residual powder in the build chamber can then be recycled and used in a subsequent L-PBF process. The presence of powder around the fabricated part during the AM process provides some level of support for the overhanging features such as surfaces of high angles with respect to the deposition direction, however, it is common to design and

Table 2
Metal AM equipment manufacturers and their specific process names [78].

Acronym	Commercial name in wide use	Manufacturer (examples)	ASTM process category
SLM	Selective Laser Melting	SLM solutions	L-PBF
DMLS	Direct Metal Laser Sintering	EOS	L-PBF
DMP	Direct Metal Printing	3D Systems	L-PBF
LaserCUSING	LaserCusing	Concept Laser	L-PBF
EBM	Electron Beam Melting	Arcam AB	EB-PBF
LENS	Laser Engineered Net Shaping	Optomec	L-DED
DMD	Direct Metal Deposition	DM3D Technology LLC	L-DED
EBAM	Electron Beam Additive Manufacturing	Sciaky Inc.	EB-DED

employ supporting structures on geometrically complex components to prevent excessive deformation of the part or even failure in the fabrication process. These supporting structures should eventually be removed from the final part after the AM process. Due to high temperatures and subsequent rapid cooling during L-PBF, the presence of residual stresses in the fabricated parts is unavoidable. Different solutions such as stress-relief heat treatment of the fabricated parts and pre-heating of the build stage prior and during the fabrication have shown to reduce the level residual stress in L-PBF parts [79,80].

Electron beam PBF (EB-PBF) employs a similar procedure to L-PBF for the fabrication of metallic parts by use of a powder bed. The powder layer thickness in this process commonly amounts to 50 μm – 200 μm. Unlike the L-PBF process which is carried out in a controlled inert gas atmosphere (nitrogen or argon), the operational atmosphere for the EB-PBF process is a vacuum of $< 10^{-2}$ Pa [81]. The powder bed is repeatedly pre-heated by a defocused electron beam, resulting in an elevated temperature of the powder bed during the subsequent melting process by high power electron beam. Due to the higher operational temperature and cyclic pre-heating of the powder bed, the fabricated parts show a negligible level of residual stresses [82]. Furthermore, the pre-heating process results in slight sintering of the powder in the build chamber which provides an improved support for the overhanging surfaces of the part and allows for stacking the fabricated parts in the build chamber [83].

Similar to PBF, both laser and electron beam can be used as the heat source in DED processes. In powder based DED, a part is built by melting a surface and simultaneously supplying the metal powder into the melt pool by means of a coaxial or multi-jet nozzle [84]. The melt pool is typically protected against oxidation by supplying a shielding gas (argon or helium). Different from PBF technologies, DED provides a high build rate with a typical layer thickness range of 40 μm to 1 mm and allows for fabrication of larger build volumes [79]. This process can be used for both fabrication and repair of damaged components such as turbine blades, shafts, and gear mechanisms [84]. Compared to PBF, DED is used for fabrication of parts with a lower level of geometrical complexity, making it a lower priority process for fabrication of lattice structures.

The most relevant and most widely used method for AM fabrication of lattice structures is L-PBF, due to its industrial adoption and widespread availability. This technology allows the manufacture of detailed and complex structures in many alloys including Ti6Al4V, AlSi10Mg and various steel grades, amongst others. New alloys are also constantly being developed through mixing of powders and in-situ alloying [4]. Table 3 represents the common alloys used for AM and their various applications in additive manufacturing. Further details about different AM processes can be found in [3,79,84].

2.4. Manufacturing constraints, errors, defects

Metal additive manufacturing is a complex process, with hundreds of variables that may affect the outcome of the process and the quality of the manufactured parts [3,85,86]. In L-PBF, there are now well defined approaches to finding optimal process parameters and various in-situ monitoring and quality control tools are available to maintain the required quality of parts produced. Different types of major defects may occur, including porosity formation, formation of unwanted microstructure, residual stress, rough surfaces or microcracking, amongst others. These may reduce the mechanical performance of the produced parts and therefore create a need for careful monitoring and quality control, to ensure reliable parts are manufactured. Post-processing methods are important for quality improvement, reducing the influence of some of these defect types [87,88], and post-process inspection may identify such defects [89-91]. This is now well understood and leads to processes and parts being qualified for use in critical applications such as rocket engines in aerospace or bone implants in medical industries; the qualification processes and requirements are discussed in more detail in [92-95].

In lattice structures, due to the small feature sizes, with short scan tracks, complex relationships may exist between the process parameters and obtained material, due to different pore formation mechanisms and unique microstructure formation that can occur, different than that in bulk material. Due to the fine feature sizes, only a few tracks alongside one another are needed in any single layer of the build process, with very short track lengths. The typical contouring and hatching scan strategies may lead to some areas not sufficiently melted and some gaps between contour and hatch tracks, and in some cases contouring or hatching cannot both be employed. The scale of individual track widths and short track lengths, combined with the choices of scan strategies, may lead to porosity formation inside struts especially for small-scale cellular structures. Additionally, the scan strategies and the different

Table 3
Common additive manufacturing alloys and their applications areas [78].

Application area	Aluminum	Maraging steel	Stainless steel	Titanium	Cobalt chrome	Nickel super alloys	Precious metals
Aerospace	X		X	X	X	X	
Medical			X	X	X		X
Energy, oil and gas			X				
Automotive	X		X	X			
Marine			X	X		X	
Machinability and weldability	X		X	X		X	
Corrosion resistance			X	X	X	X	
High temperature			X	X		X	
Tools and molds		X	X				
Consumer products	X		X				X

overhang angles may lead to differences in strut thickness and surface roughness in different locations. Similarly, the thermal conduction of heat away from the meltpool is different in cellular materials than in solid material. The lower thermal conductivity may cause higher local temperatures resulting in residual stresses and thin features may warp easily, especially near the top of the build. The repeated thermal cycles may influence the microstructure formation with differences expected compared to bulk materials. All of the above influences may vary depending on the material and process parameters used, the scan strategy, the cellular design and feature sizes involved (strut or sheet thickness).

This means that the optimal process parameters and scan strategy for cellular structures may be different than that for bulk material, and this may be different depending on the cellular structure involved. This has been demonstrated in [64], with specially optimized process parameters yielding less strut microporosity and improved mechanical properties. The existing quality controls and optimizations needed are therefore more important for lattice structures, to ensure their reliability and performance. Design may play a key role here, in the context of ensuring lattice architectures are selected and lattices are designed with the best possible manufacturability [15] (considering the strut/wall thickness, overhang angle, lack of supports, large connected pore sizes to allow powder removal, etc.). Coupon sample testing will play a further role in this improvement, as well as optimization of the post-processing to improve the surface finish, the microstructure and to remove microporosity. The mismatch between mechanical properties of macroscopic bulk specimens and sub-millimetric struts in lattice structures point out the necessity for their experimental characterization using miniaturized coupons so as to capture the effect of strut morphology [96,97].

2.5. Inspection

Cellular structures, by the nature of the wide variety of designs, materials and sizes of such structures, do not have any well-defined or standard testing approaches. As described in the previous section, the manufacturability of these structures is limited by the process parameters, scan strategy and more and require validation of the following physical conditions that influence their performance:

- Conformance to design geometry, e.g. strut thickness as expected
- Lack of extensive sheet/strut (micro-)porosity
- No warping or missing struts
- No powders or other material stuck inside [98]
- No irregular surface features / indentations
- Microstructure similar in all parts
- Lack of residual stress

The above conditions are important because they influence the expected performance of the structures, most importantly their mechanical properties but also their thermal properties, fluid flow/permeability properties, their appropriateness for the application (e.g. implants cannot have loose powders stuck inside), etc. Many of these conditions can be checked and quantified using X-ray computed tomography, as described in [99]. X-ray computed tomography is today widely used for evaluating AM metals as reviewed in [90]. It is important to realize that its use for process optimization is especially useful as it might indicate the specific combination of design, material and process parameters causing errors and assist in finding optimized parameters for the required cellular structure, prior to further manufacturing of large parts incorporating such structures. It is also important to realize that the listed conditions above do not have well defined thresholds for "good" or "bad" states and the relative influence of each point might vary depending on the application. It is therefore important to consider all of these and fully characterize the manufactured structures.

Besides non-destructive testing, physical testing is often required to validate the mechanical performance of the structures, using coupon samples. This was discussed in Section 2.2 in more detail, but effectively the use of coupon-scale samples for compression testing are most common due to the simplicity of this test.

3. Unique properties and their applications

In this section is summarized and explained how specific properties are obtained by cellular materials, including the main concepts and background of each. Applications are mentioned and referenced in the context of the properties obtained, so that there is a clear property-application link in each case.

3.1. Precisely tuned or locally optimized stiffness

One of the simplest yet most useful applications of cellular structures is to tailor or tune the mechanical properties, especially the effective stiffness of the structure. This can be done not only on the bulk part scale as homogenous latticing, but also with locally varied properties utilizing local density variations or architecture modifications (thickening of struts, etc.). As a well-known fact, the porosity and stiffness of lattice structures are interrelated. The relation between these two properties is well described by the models of Ashby-Gibson [12,54] developed for foams. By using those relations, the stiffness of a lattice can generally be predicted from the porosity of the structure. In addition to the porosity level in the structure, the unit cell designs can also alter the stiffness. This has been well studied in the literature for a wide variety of unit cell designs and porosity levels [53,74,100-104].

As mentioned in the introduction, one of the main applications of cellular structures so far is in medical implants. The global market for AM lattice structures in the biomedical industry is expected to grow to 147 billion US dollars by 2027 [105]. These complex
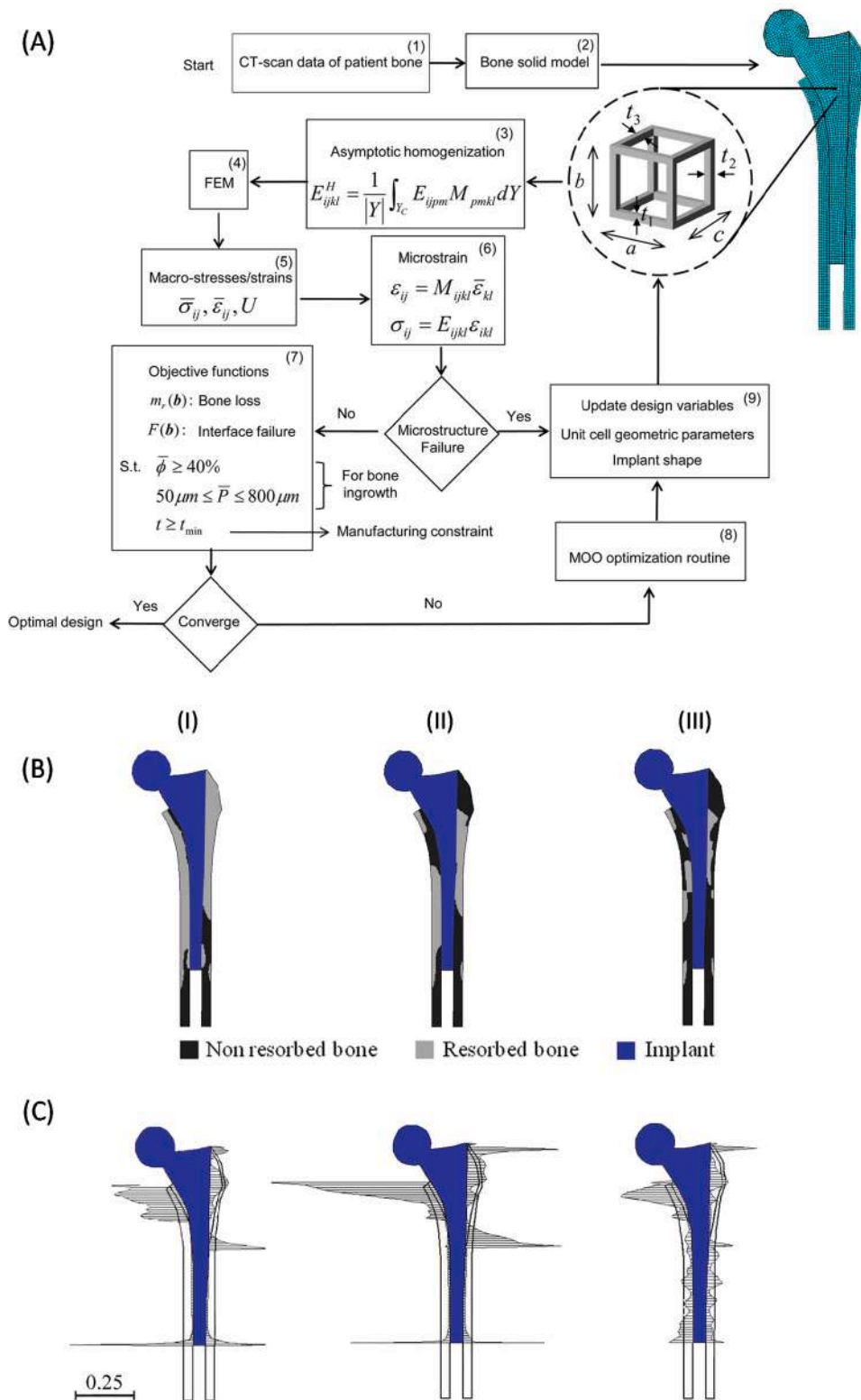
Fig. 7. (A) Flow chart illustration of the proposed methodology by Khonaki and Pasini [110] for a graded lattice hip implant with minimized resorption and interface failure; (B) distribution of bone resorption and (C) local interface failure around the implants. (I) Fully dense titanium implant, (II) uniform lattice implant with relative density of 50%, (III) graded lattice implant.

structures can have patient-specific designs with stiffness closer to that of bone which makes them a perfect choice for biomedical applications [27]. The specific requirements for design and fabrication of lattice structures for bone replacement implants have been discussed in detail in a number of recent reviews [19,20,22,24,106]. The primary aims for bone replacement implants are to have good strength, with the latticing to allow the bulk metal to match the elastic modulus of bone. This eventually results in minimized stress shielding around the implant and allows in-growth of new bone, which consequently leads to longer term operational life of the implant. In addition to stiffness, bone growth is strongly dependent on the available surface area and permeability of the lattice structure. The available surface area determines the quality of initial cell seeding and good permeability would guarantee effective bone growth by allowing nutrients to flow through the structure.

The significant potential of AM lattice structures for orthopedic implants has been well identified in recent literature on the topic. Yang et al. [107] performed a study on the mechanical properties of L-PBF Ti6Al4V gyroid specimens. Specimens of different bulk size, unit cell size, surface thickness, and isovalues were numerically modeled and the results were validated by experimental results obtained from compression tests. According to their analyses, the effect of different geometric factors based on their influence on the stiffness and strength can be ranked with the following order: number of unit cells, surface thickness, bulk size, and isovalue.

Ataee et al. [108] evaluated the mechanical properties of EB-PBF gyroid structures for bone implant applications using specimens of 2, 2.5 and 3 mm unit cell size. The results indicated an elastic modulus and yield strength comparable to that of trabecular bone. By altering the loading direction, the observed modulus and yield strength were reported to vary by approximately 70% and 49%, respectively. This anisotropy was higher in the samples with smaller unit cell size and can potentially be tuned to match that of trabecular bone for orthopedic applications. Near homogenous behavior for gyroid samples was reported by Yanez et al. [70] when the gyroid specimens were loaded at 45° angle to build direction. By altering the design and axially alongating the lattice architecture, the authors reported a relatively higher compression stiffness and strength compared to the standard gyroid samples. A smaller effect of this alteration was observed for samples of higher density (75%). Yanez et al. [109] reported an increase of structural strength by decreasing the associated strut angle in EB-PBF Ti6Al4V diamond and gyroid lattice samples. An optimized strength-to-weight-ratio was then reported for strut angles below 35°. They obtained a high correlation between the stiffness and compressive strength and the associated strut angle. Based on their findings, gyroid specimens were fabricated to imitate the stiffness of human trabecular bone.

Considering the mentioned influencing factors, the optimum implant that fulfils the complex design criteria should have a gradient of porosity that provides bone-level stiffness at the bone-implant interface for better bone in-growth and permeability and higher density in the areas where bone ingrowth is irrelevant to maintain a higher overall strength and structural integrity. Khanoki and Pasini [110] developed a design methodology based on multiscale mechanics and design optimization to synthesize graded lattice
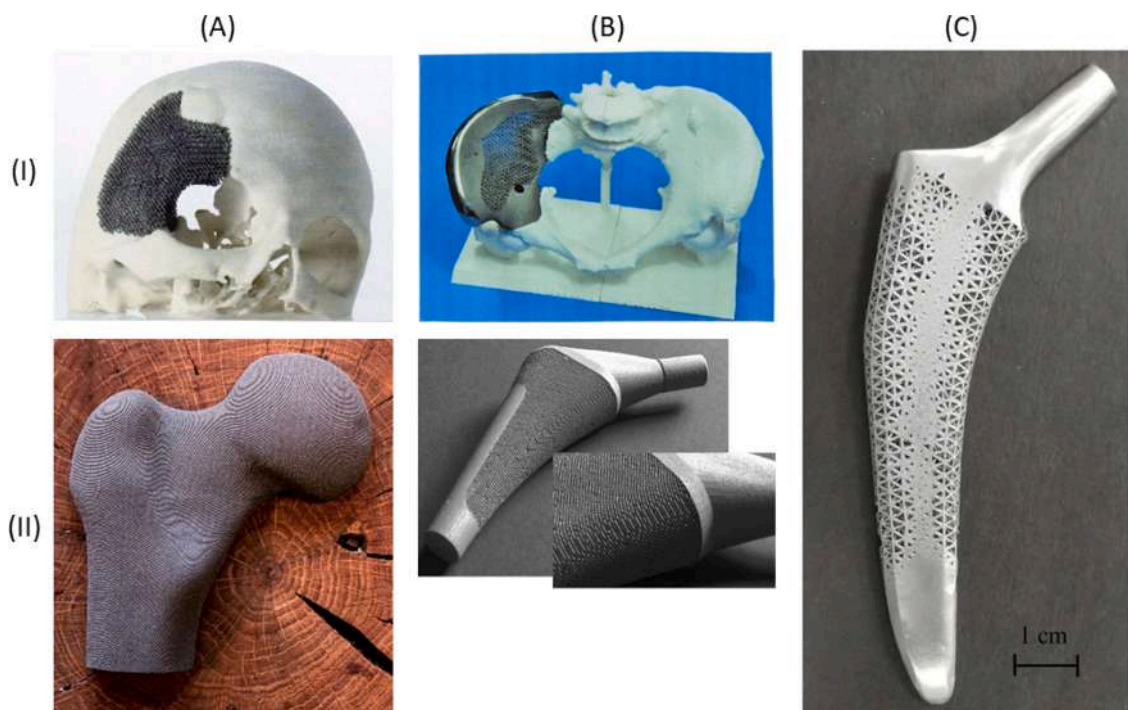

Fig. 8. Demonstrative Ti6Al4V biomedical implants incorporating lattice structures; (A.I) rhombic dodecahedral element reticulated mesh skull replacement prototype fabricated via EB-PBF [20], (A.II) L-PBF porous femur [112], (B.I) hybrid pelvic girdle, right wind iliac bone replacement implant fabricated via EB-PBF and fitted to skeletal model, Courtesy of Dr. S.J. Li, Institute of Metals Research (IMR), Shenyang, China. [20], (B.II) hybrid hip implant that combines solid regions with rationally designed porous parts in a single piece fabricated in a single-step additive manufacturing process [112], (C) geometrically optimized and functionally graded lattice hip implant fabricated via L-PBF with 41.9% of that of a fully solid implant [113].

implants with simultaneously minimized bone resorption and implant interface failure using 2D numerical analysis (see Fig. 7). Using this design methodology, the optimized relative density distribution of the porous implant is determined by using a gradient-free topology optimization scheme under several constraints imposed by implant micromotion, porosity, pore-scale, and the minimum thickness of the unit cells. This tool was then used to design a titanium femoral implant and the results were compared to that of a solid implant and a uniform lattice implant. Based on their findings, the bone resorption and the maximum value of interface stress of the lattice implant are found to be over 70% and 50% less than the solid implant while being 53% and 65% less than the uniform lattice implant. The proposed methodology was further modified by them for design of functionally graded lattice implant against fatigue loading [111]. Several research studies have been recently published proposing various design techniques for AM of implants, examples of some are shown in Fig. 8. The current designs are commonly in the form of the application of uniform lattice structures (with constant relative density) (Fig. 8a), hybrid design of implants incorporating both solid regions and lattice structures (Fig. 8b), and functionally graded lattice implants (Fig. 8c).

3.2. Light-weighting

Design based on light-weighting can typically be performed by replacement of the non- or less load carrying parts of the component with lattice structures. Due to the porous architecture of lattices, their application in the design will reduce the weight of the part and its fabrication time. Reduction of the mass of any parts of vehicles directly influences their fuel consumption, which is increasingly in demand for higher fuel efficiency and lower carbon footprint. In this scenario, it is an essential task to take full advantage of AM as a fabrication technique which provides a wide degree of freedom in design for light weighting. It should be noted that design for light-weighting is widely used in applications where the low weight of the fabricated part is a key factor (e.g. aerospace and automotive industries), however, from a sustainable production point of view, a wider range of industries can benefit from this design technique. In conventional subtractive manufacturing techniques, a block of material is machined to the final geometry. In this setting, by adding geometrical complexity to the part, the required volume of material in its initial stage would almost remain the same and the fabrication time increases. On the contrary, when using AM as a fabrication technique, an increased complexity in the component would not necessarily increase the build time and if the added complexity is with the aim of weight reduction, less feedstock would be required for fabricating the part. By requiring a lower amount of feedstock material for AM fabrication, the users can afford to use a higher grade alloy that can provide better fatigue resistance, corrosion resistance and eventually an extended lifetime of the fabricated part.

Although lattice structures offer a significantly high stiffness-to-weight ratio, however, their relatively low stiffness compared to the solid parts needs to be considered in the design process. In this context, research studies have been performed by combining solid skins and lattice core in the form of a sandwich panel. Those skins can have a variable thickness with thicker parts in locations with higher applied stresses and thinner regions elsewhere to keep the overall weight of the structure low. This solution has the potential to meet the need for the aerospace industry for stiff and lightweight frameworks. The leading edge of the wing is a key component for both onboard subsystems and construction characteristics. This part must withstand the aerodynamic forces and possible bird-strikes, integrating also anti-ice system functions. Currently this part is fabricated by bonding several components such as external skin, internal passageways, and feeding tubes. In this context, Bici et al. [114] proposed an innovative solution for design and fabrication of optimized multifunctional sandwich panels based on aeronautical performances, technological limitations, and sustainability. Fig. 9 shows a schematic representation of panel section with the focus on the cellular core providing light-weighting and heat exchange performance (de-icing), while the combined structure fabricated as a single-piece with AM has good stiffness. The panel uses and distributes the hot air bled from the engine compressor to the cellular core through incorporated channels for de-icing porpuses and the exhaust cooled air enters the wing structure to the end of the curved panel.

Bühring et al. [115] investigated the potential of AM sandwich structures with pyramidal lattice cores as load bearing members in small aircrafts. For this purpose, numerical and analytical models were derived for describing the mechanical properties of the sandwich and the models were then experimentally validated by performing bending and shear testing on AlSi10Mg test specimens. The validated models were then employed to analyze and optimize a small aircraft wing and the results were compared to that of an equivalent wing using a conventional structure. Based on their findings, considerable weight saving was reached using the new light
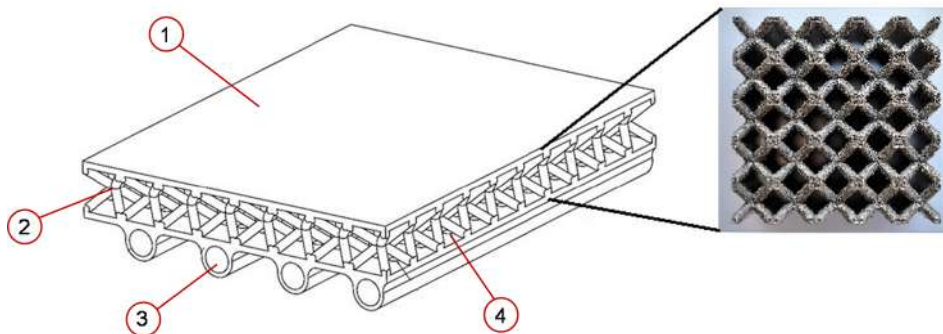

Fig. 9. Multifunctional panel for aerospace use; (1) outer layer of the sandwich panel which also acts as an aerodynamic surface, (2) cellular core, (3) hot air conveyance tubes connected to the area of the cellular core through holes (4) [114].

weighted component, however, it was reported that with the choice of AlSi10Mg as the model material, no sufficient qualities can be reached to fulfill the required structural performance. Further research studies have been performed on mechanical properties of AM sandwich panels with various cell architectures, details of which can be found in [116-119].

As stated earlier, functionally graded lattice structures can provide a range of stiffness values in a single component. This design technique has also been widely used recently for lightweighting purposes. In this case, the density of lattice and not necessarily the thickness of solid regions is considered as the design variable. In this context, Cheng et al. [120] proposed a homogenization-based topology optimization method to optimize the design of graded lattice structure with the aim to achieve lightweight design and overcome some of the fabrication difficulties in additive manufacturing. Fig. 10 illustrates the flowchart of the proposed method. According to this method, first, by performing homogenization the effective mechanical properties of lattice structures is obtained by use of the scaling law as a function of the relative density of lattice. In this step, the material type, lattice architecture, and AM process are determined as input parameters for the material model function to obtain the required material table for the optimization process and post-design numerical analyses. Then, the scaling law is directly used in the topology optimization algorithm to obtain the optimal density distribution of the component. Lastly, by use of a novel proposed technique, the CAD model of the optimal graded density lattice structure is reconstructed. The proposed methodology was validated through full-scale simulation and experimental testing of the additively manufactured optimized part and the results revealed the efficiency and accuracy of the method. This method was used in another work of the authors to compare the mechanical strength of two beam models with uniform and graded lattice structures. The experimental results revealed higher strength of the topology optimized lattice part (by 37%) compared to the beam with uniform density distribution of lattice [121]. The effect of influencing factors on the uncertainty of mechanical properties which are used as input in this method is yet to be studied. A similar concept was later studied by Garner et al. [122] where the geometrical connectivity between the adjacent unit cells were considered as a key factor in the topology optimization of graded lattices. In a recent research
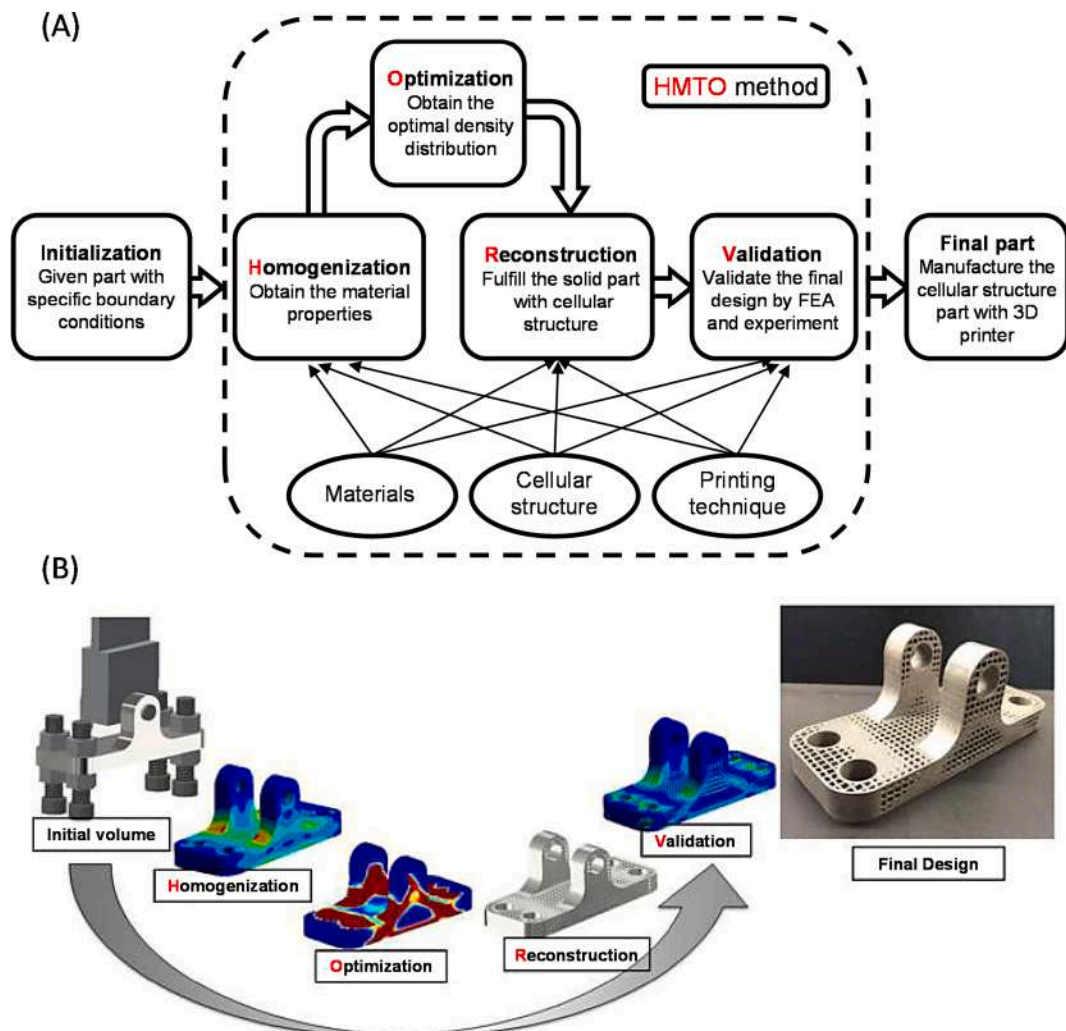

Fig. 10. (A) Flowchart of the lattice structure design optimization methodology, (B) illustrative steps for design of a Ti6Al4V pillow bracket [120].

article, Li et al. [123] presented a new anisotropic lattice structure design and multi-scale optimization method used for generating conformal gradient lattice structures. The key goal in their work was to achieve the highest mechanical stiffness. Unlike the previous proposals, this optimization method provides a lattice structure with the unit cells oriented along the principal stress direction. This feature results in the maximum mechanical properties of the designed lattice. In addition, a variable unit cell size can be obtained in different density regions of the part, which in turn enhances the overall stiffness of the structure. The proposed method was then used to design several lattice structures and extensive numerical and experimental analyses were performed on the designed parts. The
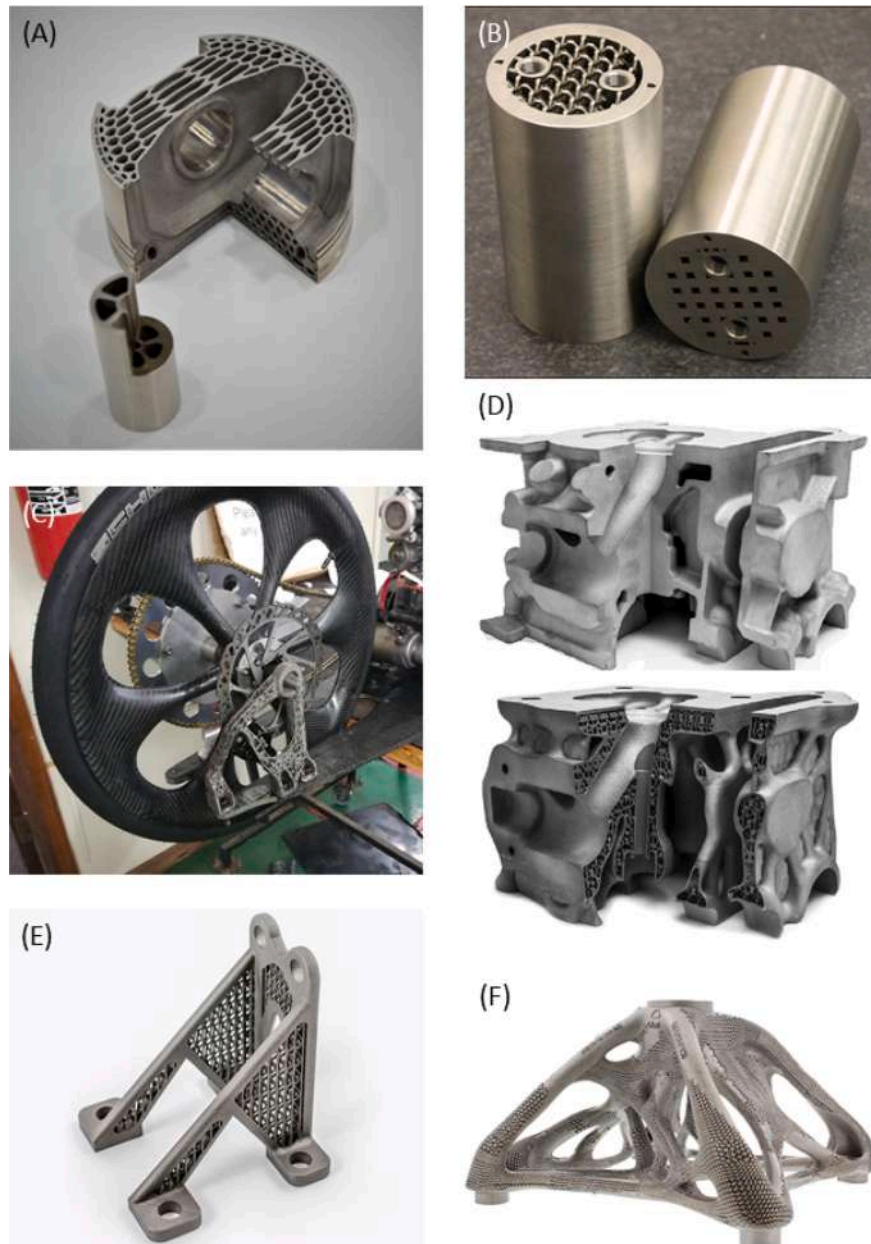

Fig. 11. (A) Cutaway of AM gasoline piston and pin incorporating honeycomb lattice with 25% reduced mass and improved cooling of critical areas (courtesy of IAV automotive engineering) [127]. (B) Oil and gas Inconel 718 component for downhole applications fabricated via L-PBF with 42.4% mass reduction. This component pumps fluid up and down an oil well by use of two "snaky" internal channels [128]. The designed component has a diameter of 81.3 mm and height of 135.9 mm. (C) Ti6Al4V lightweight lattice bracket manufactured by L-PBF implemented in an experimental vehicle [129]. (D) light weight design of racing car cylinder head with lattice core fabricated via L-PBF with 63% lower weight and more than 11 times larger internal cooling surface (courtesy of SLM solutions) [130]. The top and bottom images represent the conventional and light weight designs. (E) Titanium aero-bracket designed by Materialise team with 63% reduced weight and fabricated by GE aviation for aerospace application [131]. (F) the Renishaw spider bracket first demonstrated in 2017 fabricated by L-PBF in Ti6Al4V [132].

findings revealed that in contrast to uniform lattice structures, the new designs not only present higher stiffness (around 3.5 times), but also have robust structure for damage tolerance and buckling resistance ability.

By combining the density gradient from topology optimization and a size optimization, Daynes et al. [124] designed functionally graded truss structures in which the beams align with the principal stresses during loading. An initial topologically optimized design is automatically obtained and then substituted by pre-defined unit cells before a size optimization confirms that the overall target density is realized. The authors developed a MATLAB subroutine based on the information on the in-plane stresses and principal orientations in the structure extracted from the software to create a functionally graded mesh. This functionally graded mesh was then fed back into the software for further analysis. This design method was used to design prisms for three point bending tests and a series of test specimens with graded and uniform lattice structures were fabricated from jetting of ABS-like material. The resulting graded lattice by substituting the domain with body centered cubic (BCC) unit cells conformal with the isostatic lines presented twice the stiffness and about 2.75 times higher strength compared to the lattice design with uniform density. Later on, the authors [125] further studied the importance of latticing for reducing support structures by ensuring manufacturability of lattice features using definition of an upper and lower density thresholds and a minimum truss member size in the design process.

The mentioned light weighting design methods focused on combining uniform lattice structures with solid shells (sandwich panel) and functionally grading the lattice structure to obtain high strength parts with promising stiffness. In a recent research, Dong et al. [126] presented a design method in which a combination of the previously mentioned design categories is employed to fabricate hybrid structures. This design algorithm is capable of generating a functionally graded heterogeneous lattice structure which is connected to solid parts in the component. First, functional analysis are performed to determine the design space (lattice and solid parts) and non-design space (solid parts in the constraint areas). Then, topology optimization is performed on the design space to differentiate the solid spaces and lattice spaces. In this stage, the density threshold is adjusted based on the requirements of weight reduction and stiffness. High relative density areas are kept as connected solid space for load transmission purposes. These solid spaces are then combined with non-design space to form a uniform solid region. In the next step, the lattice structure is designed by selection of topology of lattice structure, modifying the lattice wireframe, and optimizing the strut thickness. Ultimately, the lattice structure is merged into the solid space to generate a solid lattice hybrid structure. The proposed design and optimization method was then experimentally validated. Experimental analysis on a three point bending beam revealed 4% and 38% higher stiffness of the hybrid specimen compared to fully solid and pure graded lattice specimens, respectively. Furthermore, the critical load of hybrid specimens was 40% and 35% higher than that of fully solid part and pure graded lattice, respectively.

Other applications of lightweight metal cellular structures are shown in Fig. 11, including a diesel piston, a fluid pump, racing car cylinder head, and three brackets, in all cases to reduce the mass of the structure while fulfilling mechanical performance requirements. The car piston is an example demonstrating lightweighting by 25% while also optimizing the cooling of critical areas, reducing friction and parasitic losses compared with traditional pistons. The lighter weight of this new design by IAV would directly influence the counterweights on the crankshaft and eventually results in lower applied loads to the bearings and less friction in the motor [127]. Additionally, further adjustments such as incorporating cooling channels in the piston head have been made by the designing company. It should be stated that depending on the surface and clearance requirements of the part, hybrid fabrication techniques (i.e. a combination of AM and other production processes) may be required to obtain the final geometry. For instance, Fig. 11b shows a lightweight design where the initial geometry of the part has been fabricated with L-PBF and finishing features such as hole treads and the smooth outer surface were created by machining.

Fig. 12. Aluminum honeycomb energy absorber under a rotorcraft seat [136]. The image to the right is a zoom section of the aluminum honeycomb.

3.3. Energy and impact absorption

Energy absorption refers to the ability of a material to withstand loads without catastrophic failure, while impact absorption refers to the same concept, but specifically at high strain rates. The area under the stress strain curve represents the absorbed energy, prior to final catastrophic failure (or in the case of compression, full densification). The energy and impact absorption of cellular materials is well known, with sandwich panels adopted for decades in industry in the form of aluminium foams sandwiched between solid plates for crash protection in vehicles. The concept of sandwich panels with various foam types also been used for impact protection for packaging and for thermal insulation and protection in construction, in all cases the lightweight construction is particularly beneficial. They are also good for vibration damping as the vibrations are absorbed due to the nature of the energy absorptive capability.

There are some commercial examples of polymer-AM based cellular structures suitable for impacts and cushioning for individuals in sports equipment, viz. at effectively low velocity impact. This includes football helmet liners and shoe soles manufactured with lattice geometries [6,133,134]. For higher velocity impact, or blast protection, a metal lattice might be more suitable, with energy absorbed irreversibly and accompanied with buckling, plastic deformation and/or fracture. Situations where a metal based lattice would be more useful for impact protection is in automobiles, airplanes, rotorcrafts (see Fig. 12), and spacecraft, due to the durability of metals compared to polymers, as well as the higher impact strength achievable. For impact protection, the impact event typically imparts an impulse rather than transmitting energy, and it is more typical to leverage heavy face plates to absorb this impact with similar requirements as described for the ideal energy absorber [54]. However, emphasis has also been places on lightweight structures for weight-sensitive applications, which is where lattice materials have the potential for application. Studies of energy absorbing structures usually begin with quasi-static analysis and testing, the majority of which is done in compression, which is followed by studies at impact velocities more relevant to the application of interest [135].

Generally, the energy absorption can be tuned by the design and density of the cellular structure. It has been shown recently that the Poisson's ratio is inversely proportional to the damping properties, with the best damping properties found for lattices with near-zero Poisson's ratio [137]. Cellular structures with tunable Poisson's ratio have unique potential applications and negative Poisson's ratio (auxetic) structures are currently widely studied [138].

3.3.1. Energy absorption under quasi-static compression

At quasi-static strain rates, the key variables that influence energy absorption behaviour are the properties of the base material, the relative density of the lattice structure, and the geometry of the cells that constitute it. A typical force–displacement response for a metallic lattice material under low strain rate compression is shown in Fig. 13a, showing a large plateau region of near-constant load, book-ended by rises in load on either end – the first due to the elastic response of the structure, the second due to densification. An ideal energy absorber has a long, flat plateau that is just below the peak stress that will damage the object being protected – and it must absorb all the energy needed from it prior to reaching densification. Hollow tubes [139-143], honeycombs [144-148], and metal foams [149-151] have been used for these applications since their behaviour approaches that of an ideal energy absorber.

Once the force–displacement curve shown in Fig. 13a is converted into an effective stress–strain curve, several metrics may be defined to enable comparison across different energy absorber designs and materials. In addition to the peak and plateau stress, the metric of most interest for comparative purposes is the Specific Energy Absorption (SEA), which is a measure of the amount of energy absorbed per unit mass (typical units: J/g) and is given by:

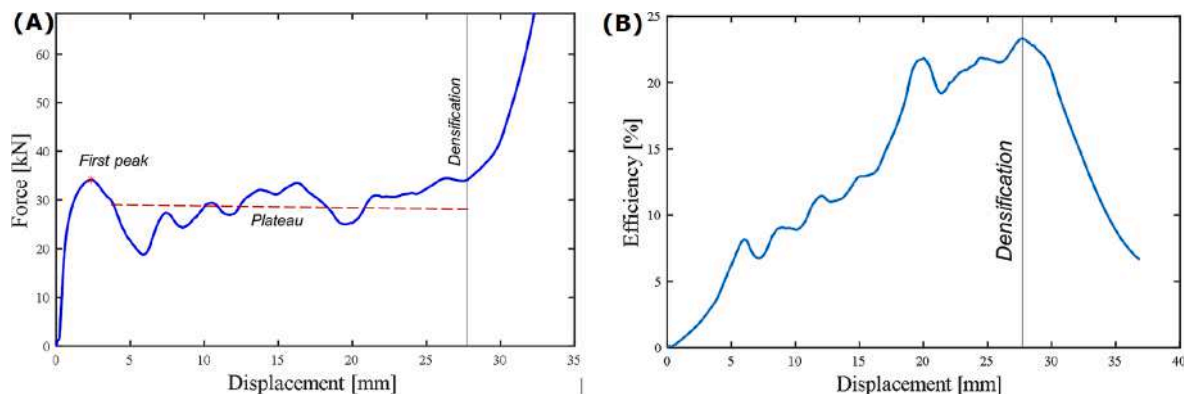$$SEA = \frac{\int_0^{\varepsilon_D} \sigma d\varepsilon}{\rho}$$

Fig. 13. (a) A typical compression load–displacement response of a metallic lattice material, showing the first peak (load), the plateau region, and the densification point on the graph up to which the energy absorbed (area under the curve) is typically estimated. (b) Energy absorption efficiency graphed against displacement, with the peak used to identify the onset of densification. The onset of densification correlates with maximum energy efficiency.

where the numerator is the area under the stress strain curve integrated up to the densification strain ε_D (this area itself yields an energy absorbed per unit volume), and ρ represents the density of the lattice structure. This measure could also be arrived at by dividing the area under the force displacement curve by the measured mass of the lattice structure under compression. Another metric of interest is the energy absorption efficiency η, which enables a comparison of a lattice material's energy absorption behaviour to an ideal energy absorber for an allowable maximum transmitted stress σ_{peak} as:

$$\eta = \frac{\int_0^{\varepsilon_D} \sigma d\varepsilon}{\sigma_{peak} * 100\%}$$

A key metric utilized in both these equations is the densification strain ε_D. The densification strain (more correctly, the onset strain of densification [152]) is important because it defines the strain up to which energy may be absorbed usefully in most applications before stresses rise at a rate significantly higher than that in the plateau. From a designer's perspective, any energy absorbed beyond the peak allowable transmitted stress is not useful, which may be interpreted as using the peak stress value to define the onset of densification [153].

Another approach to defining densification strain is to plot energy efficiency as a function of strain as shown in Fig. 13b, and use the maximum energy efficiency as an indicator of the onset strain of densification, which has been argued to be a more consistent method, especially for structures that show little hardening in their compressive response [152].

Prior to the adoption of metal additive manufacturing, metallic energy absorbers were constructed primarily using honeycomb (including pre-crushed honeycomb), and foam materials, details on the behaviour of these cellular materials at both quasi-static and impact strain rates can be found in the review in [149]. The additional design freedom afforded by AM has enabled the exploration of cross-cutting design concepts such as gradients [154] and bio-inspired design approaches [155]. With regard to the key metrics of interest in energy absorption, the following insights have emerged in recent research studies:

A. First maximum/peak stress: The first maximum stress for a given cellular material shape is determined by the relative density of the cellular material and generally follows the Gibson-Ashby power-law relationship of the form $\varnothing^* = C(\rho^*/\rho_s)^n$, where $\varnothing^*$ is the effective property of the cellular material, ρ^*/ρ_s is its relative density, and C and n are fitting constants, derived empirically [12]. While this relationship is borne out for all metallic cellular structures, the fitting constants differ by unit cell geometry [156], depending on the relative contribution of stretch- and bending-dominated deformation modes [51].

B. Plateau slope: The plateau slope is an indicator of hardening or softening phenomena in the cellular structure of interest. For a given shape, relative density (or volume fraction) of the cellular solid significantly affects plateau slope: the higher the relative density, the harder the plateau compressive response will be and the higher the plateau will be (see Fig. 4). From a designer's perspective, a hardening response results in the plateau stress exceeding the first maximum prior to densification, which is not ideal. An ideal energy absorber has a flat plateau, and further, the slope is not sensitive to changes in relative density which are needed to achieve maximum transmitted stress targets while maximizing energy absorption. While the sensitivity of the plateau slope to relative density has not received much attention, the plateau slope of the P-type TPMS geometry has been shown to be less affected by changes in relative density in comparison to other shapes [156,157]. Recent work has also demonstrated the ability to generate two distinct plateaus by developing a novel shape inspired by crystal structure of the C15 Laves phase [158].

C. Plateau undulation: The undulation, or waviness, of the plateau (see Fig. 4 for example) is strongly determined by the mechanisms of failure within the cellular structure, which in turn depend on the unit cell shape, including any variations in shape across the structure such as gradients. With regard to lattices, bending dominated lattices tend to have smoother plateaus, with stretch dominated lattices typically associated with greater undulation [159]. A drop in load is typically associated with a buckling, folding or a fracture event, and these events could be localized in failure bands and influence bulging or barreling of the cellular structure accordingly, as shown in Fig. 14. Relative density also plays a role in the degree of undulation with higher relative density structures tending to have larger undulations on account of thicker beams or walls that have a tendency for fracture by localized shear. Finally, it has been shown for Stainless Steel 316L double gyroid lattices that heat treatment had a significant impact on the waviness of the plateau [160]. This was attributed to a shift in the failure mechanism from brittle shear fractures (in the non-heat
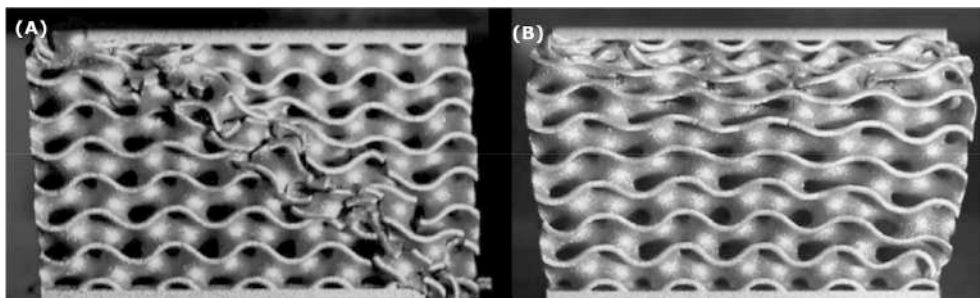

Fig. 14. Differences in failure mechanisms for a TPMS gyroid under compression: (a) Fracture of walls and a diagonal or shear failure band, (b) folding of walls and layerwise collapse also leading to bulging of the structure.

treated specimen) to a more controlled collapse, followed by bulging in the heat treated specimen, similar to that shown in Fig. 14a and 14b, respectively.

D. Onset Strain of Densification: The onset strain of densification (ε_D) is a metric not consistently defined or specified across literature, and yet is important for the computation of energy absorption, and also vital in its own right as a quality characteristic. Generally speaking, four different approaches are used to define ε_D: the first is the use of a specific strain value at which all values are specified, typically 40% [156] or 50% [145] strain – this approach has the advantage of enabling comparisons between different studies, but disregards the nature of the stress plateau at the specific strain value. The second is the use of the energy efficiency method, where the strain at the maximum energy efficiency point defines ε_D [157,161,162] – this approach works well in particular when the plateau shows little hardening behaviour prior to a change in slope associated with densification. The third approach is to use the first maximum stress as a threshold – when stress exceeds this threshold (after the first maximum), that is where ε_D is defined [163,164]. The fourth approach is to use the intersection of the slopes of the plateau and the densification region to define ε_D [54,158]. These differences in definition make it challenging to compare onset strain of densification and energy absorption values across different research studies.

E. Specific Energy Absorption (SEA): SEA is essentially a normalized (by mass) measure of energy absorbed. Its volumetric counterpart is often called energy absorption capacity (W_v), and has the units of J/cm^3. Since both metrics depend on the definition of ε_D, which defines the limit of usable energy absorption, comparisons across the literature are difficult. Further, since SEA and W_v both typically increase with increasing relative density along with a higher transmitted stress, a comparison across shapes is only relevant in the context of one or both of these measures. From a designer's perspective, the goal is to maximize SEA for an allowable transmitted stress, and a property chart of SEA versus maximum transmitted stress, as shown in Fig. 15, is often used to identify optimum design choices across different relative densities [164].

3.3.2. Impact and blast energy absorption

The key phenomenological difference in energy absorption behaviour of cellular materials from quasi-static to high strain rate impact and shock is that at higher strain rates the properties that start to matter are the rate dependence of the base materials, micro-inertia, trapped and flowing gases in the cellular material and the macro-inertia and wave transmission properties [149], all of which are not very significant at low strain rate regimes in metallic cellular materials [165]. While highly ductile metallic foams have been implemented in sandwich structures for impact and blast protection, many of these early structures had irregular responses, requiring overly conservative designs, and lattice structures have been proposed as alternatives with potentially higher strength- and stiffness-to-weight ratios than traditional foams [166].

High strain rate testing approaching impact velocities are typically conducted using the split Hopkinson pressure bar (SHPB) technique (or Kolsky bar), and this approach has also been applied to study the behaviour of cellular materials fabricated with metal AM processes over strain rate regimes approaching $10^3 \, \text{s}^{-1}$ [145,167-169]. The SHPB approach has several challenges when applied to cellular structures primarily arising from the limited diameter of the pressure bar versus known size effects in cellular materials, an inability to generate sufficient crushing throughout the plateau stage, and low wave impedances for cellular materials making it challenging to generate sufficiently strong signals when using metallic bars [149]. Alternatives like the pendulum and drop hammer test have additional limitations, and the SHPB test method is generally accepted as the best approach to obtain dynamic behaviour of cellular materials as long as the data is interpreted with caution and sufficient replications are conducted to quantify experimental uncertainty. Even higher strain rates can be obtained with a light gas gun [166]. Blast response of cellular materials is typically studied using a ballistic pendulum and an explosive, which sandwich the specimen of interest [170,171].

A key point of interest in high strain rate testing of cellular materials is to examine the difference between quasi-static and dynamic test results, and some studies have explored the compressive response of cellular materials under these widely varying strain rates. For example TPMS sheet-based cellular structures were studied at varying strain rates and with different designs, showing strain hardening behaviour in all cases at high strain rates [172]. In general, higher impact velocities are associated with higher peak stresses [145], but
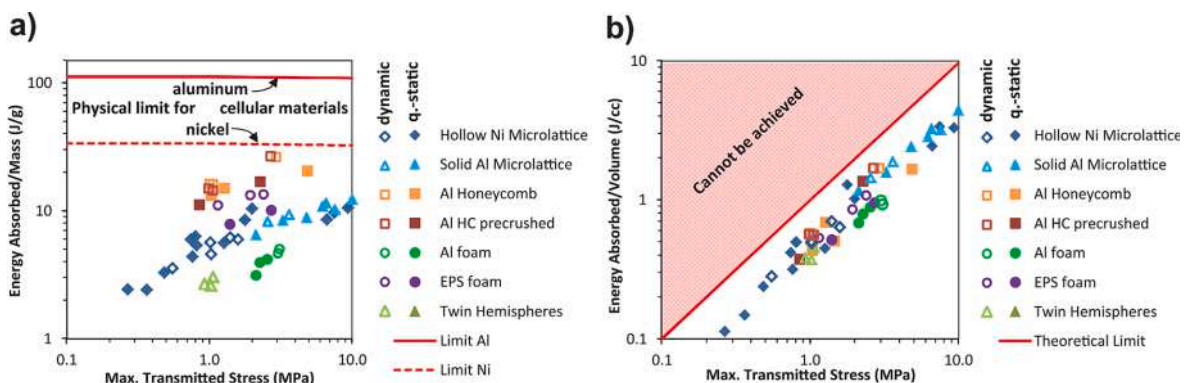

Fig. 15. Energy absorption in the context of maximum transmitted stress: (a) Specific Energy Absorption (SEA); and (b) Energy absorption capacity (W_v) for microlattices, honeycomb and foam – solid markers are from quasi-static tests, hollow markers from dynamic tests [164].

the degree of this dependence is a function of cellular material composition and topology [164]. This results in the fact that quasi-static data cannot be reliably used to estimate absorbed energy in dynamic loading conditions, though comparisons between cell topologies may still be valid. It has also been suggested that differences between quasi-static and dynamic flow stresses are reduced after heat treatment, in studies conducted on beam-based inconel 718 lattice specimens before and after solution aging [169]. Increases in the yield strength of lattices at higher strain rates was also reported in blast testing, which results in higher energy absorption and increased performance when withstanding blast loads [170]. Higher blast impulses also increase the degree of crush [170,171] but limited data suggests that deformation modes remained unchanged from quasi-static and intermediate strain rates [170,171].

In addition to characterizing quasi-static and high strain rate loading responses of metallic cellular materials, there are also opportunities to leverage these materials for reducing vibrations and mass, as demonstrated for a mechanical gear where the body of the gear was infilled with a lattice structure [173], and in a different iteration also infilled with a polymer, which was shown to further reduce vibration amplitudes [174]. Another use of metallic cellular materials is in the context of mitigating the effects of projectile penetration, or dynamic indentation [166] in armor and ballistics applications, in military vehicles, passenger aircraft, and spacecraft and satellites. In one study, interwoven Ti6Al4V cellular rings were used as inserts between aramid fabric for use in bullet proof vests and showed lower indentations than those required by body armor standards [175]. A review of the methods of evaluating cellular materials, primarily focused on honeycombs and aerospace applications, is provided in [176]. Crashworthiness applications of metamaterials in general are reviewed in some depth in [177].

3.4. High surface area & surface roughness

Lattices are porous with highly interconnected pore spaces, creating inherently a very high surface area to volume ratio. This is one of a series of morphological parameters that can be used to characterize lattices and compare them for different applications. For example, in the study reported in [74], a series of strut-based and sheet-based cellular structures were compared showing significant differences in surface area for different designs, when all densities are set equal. In the same way, it was also shown in this study that despite total porosity being similar, pore sizes are different and dual or multiple pore sizes can be found in some designs. This type of morphological comparison of designs is useful when designing for a specific application requiring one such parameter, such as high surface area.

In addition to high surface area, high surface roughness is also prevalent in additively manufactured metallic cellular structures. This roughness further increases the available surface area compared to the idealized geometry, which can be useful for some applications. For example, it may be beneficial for bone growth on implants, where it has been shown that the roughness is beneficial to bone cell attachment and initial stages of bone growth [18]. Other applications where the increased surface area may be beneficial include thermal conductivity or heat transfer, catalysts, battery electrodes [178,179] or materials intended for chemical reactions or corrosion. Any changes to the morphology over time may however influence the subsequent performance, which is something that needs to be considered for these applications. For example, gyroid sheet-based cellular structures may be highly efficient for application as catalyst materials, but the thin sheet material might degrade faster than thicker strut-based equivalent systems.

Related to the high surface area are the permeability and thermal conductivity properties as discussed in other sections in more detail. Here it is important to highlight that the surface roughness adds to the available surface area and impacts the fluid flow and thermal conductivity performance. For example, surface roughness might induce more turbulent flow especially near the surface, which reduces the fluid flow rate. Fluid flow rates are influenced primarily by the pore size and hence the available space between struts, but the influence of the strut surfaces start to play a role for small spaces, as this may induce turbulent flow locally at the interface with the material. As the surface roughness increases and as pore spaces become smaller, this influence is expected to be higher.

Surface roughness is important for fatigue performance of additively manufactured parts [180-182] and especially so for cellular structures [29]. One can intuitively understand that the relative roughness value compared to the strut or sheet thickness of the cellular structure is much larger than the same ratio for roughness and thickness of bulk parts, dictating a larger influence on mechanical performance. For this reason post-processing methods for surface smoothing has been studied for cellular structures, including etching and abrasive flow methods [183], with the caveat that the processing removes a layer of material with a thickness depending on the processing conditions and which needs to be controlled.

3.5. Permeability to fluids

Permeability is a property of paramount importance for porous specimens, such as architected cellular materials. It can be defined as the ability of a fluid, i.e., liquid or gas, to flow through porous media under a pressure gradient. It is usually determined, within the laminar region, by applying the Darcy's law:

$$\kappa = \frac{Q*\mu*L}{A*\Delta P}$$

where κ is the permeability coefficient [m^2], Q is the inlet fluid flow rate [m^3/s], μ is the dynamic viscosity coefficient of the fluid [kg/m s], L is the model length [m], A is the inlet cross section area [m^2] and ΔP is the pressure difference [Pa]. It is trivial to consider that porosity is one of the main parameters dictating the permeability of a lattice structure [53,184-187]. Hence, as reported by Timercan et al. [185], it can be correlated to the absolute permeability by the Kozeny-Carman equation, typically used to approximate the

(A)

(B)

a) *b)* *c)* *d)*

e) *f)* *g)* *h)*
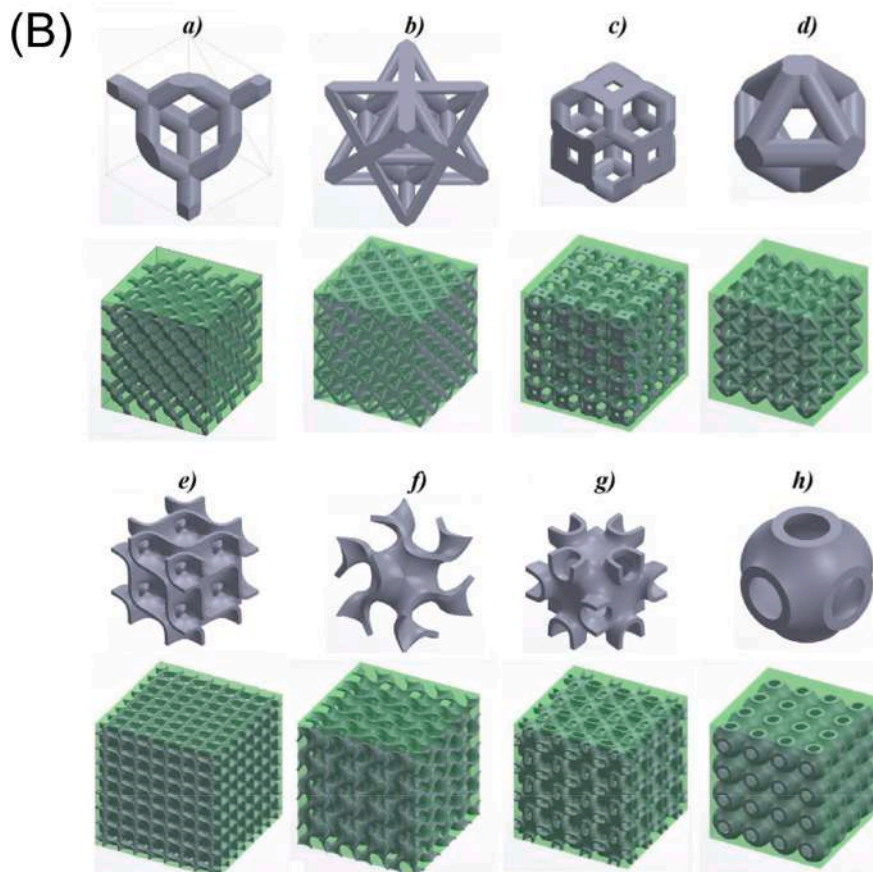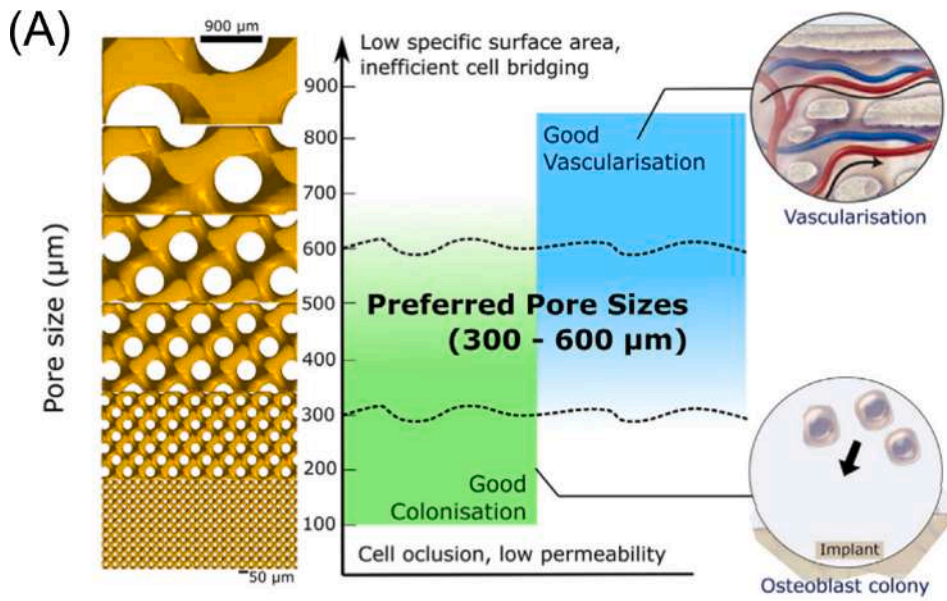
(caption on next page)

Fig. 16. Pore size and scaffold porosity strongly influence the permeability of a prosthetic device, which influences the cell colonisation and bone formation as well as vascularisation (from Barba et al. [187]). B) Unit cells and their scaffold (grey) and fluid domain (green) investigated in the work of Ali et al. [192]. The reported cellular designs are the following: (a) Lattice-diamond, (b) Octet, (c) Truncated-octahedron, (d) Optimized-lattice, (e) Double-diamond, (f) Gyroid, (g) FR-D, and (h) Schwarz primitive. (For interpretation of the references to colour in this figure legend, the reader is referred to the web version of this article.)

absolute soil permeability in earth science [188] and reported below:

$$\kappa = \frac{\varphi^3}{c^*(1-\varphi)^2 * S^2}$$

where φ is the porosity (as percentage and calculated as the ratio of volumes of voids with respect to the total volume of the structure), c is the Kozeny-Carman constant and S is the specific surface area.

As mentioned in the previous sections, architected cellular materials find a major application in the biomedical field, as orthopaedic prosthetic devices or as scaffolds for bone tissue engineering [29,189,190]. In this context, to properly mimic the target bone tissue, it is necessary to promote an optimization of opposing requirements, particularly mechanical versus biological needs. Among the main biological parameters to be optimized, fluid permeability has a crucial role in the design of a biologically efficient device. Indeed, a permeable scaffold allows a proper transport of cells, nutrients, and growth factor, guaranteeing a correct bone formation once the device is implanted (Fig. 16a). For instance, Kemppainen et al. [191] pointed out that low permeability architected structures are more prone to form cartilaginous tissue rather than healthy bone tissue. Additionally, it has also been stated that cell nutrition and their oxygenation are diffusion-based mechanisms, strongly influenced by the scaffold/implant permeability and its porous morphology [53]. These processes are fundamental for a correct angiogenesis of the newly formed bone tissue.

In this scenario, a consistent body of work on the assessment of the permeability of additively manufactured lattice scaffolds is available in the literature. As reported in refs [53,74,186,192-194], not only porosity (%) but also several other parameters, such as lattice unit architecture, pore size and morphology as well as lattice geometrical features play a crucial role to properly tune the structure. For instance, Bobbert et al. [53] investigated the permeability of four different TPMS L-PBF Ti6Al4V structures, namely primitive (P), I-WP (I), gyroid (G) and diamond (D). The authors experimentally performed tests on sixty-four samples (four samples for each TPMS geometry with four different density values ranging from about 30% up to 60%), revealing a decrease in permeability (water flow under pressure) with an increase of the apparent density and a dependency on the lattice unit geometry at a given density value. In addition, an inverse dependency with respect to the surface area of the specimens was also noticed, related to the rise of frictional forces. Nonetheless, high surface areas are usually associated with high values of porosity and, consequently, also with high permeability. This suggests that the porosity effect is more dominant with respect to the surface area-induced frictional forces. In the work of Ali et al. [192], a thorough comparison among different lattice structure configurations, suitable for bone scaffold applications, has been addressed by Computational Fluid Dynamics (CFD). In particular, the authors investigated and compared the permability behaviour of strut-based and sheet-based TPMS lattice structures, as reported in Fig. 16b. Two main geometrical parameters have been involved to describe the effect of the different lattice unit architectures on the overall structure's permeability. Firstly, the authors considered the channel size variation by adopting the ratio (D/d) between the widest and the narrowest pore size. This parameter is of extreme importance since a narrowing of channel size can lead to an increase of flow tortuosity and hence a decrease of permeability. Secondly, permeability is also affected by the presence or absence of straight-gaps between the inlet and outlet streamline flow location, depictable by the ratio (A/A$_0$) between the area without obstacles versus the total inlet area. Among the main outcomes of this work, the authors noticed that, for a comparable lattice porosity, the TPMS structures exhibit a lower permeability with respect to the strut-based lattices. This result is also in agreement with other works reported in literature [74,185]. Additionally, although all the analysed configurations show permeability values in the range of the human trabecular bone permeability, the most promising lattice structure seems to be the lattice-diamond configuration, due to its highest permeability, wall shear stress and the presence of convex surfaces. Moreover, as discussed by Du Plessis et al. [74], high tortuosity is another main requirement to be considered in the design of a bone implant. Indeed, a more complex flow guarantees that more areas of the lattice device can be reached by nutrients, further enhancing cell seeding and bone growth.

To this extent, the discussion has been only addressed to uniform porous lattice structures, nevertheless graded lattice structures are gaining increasing attention in the biomedical field, due to the possibility of locally tuning porosity and pore shape according to specific needs [195,196]. In a recent study of Zhianmanesh et al. [194], CFD simulations and permeability analysis have been performed on TPMS radially graded lattice structures. The authors discovered that, in the peripheral regions, the sensitivity of permeability to porosity is almost double with respect to the one in the central regions and that, also in this case, the cellular unit topology and the pore morphology play a major role in a proper tuning of the structure fluid flow and mass transport. The possibility of tailoring the permeability between the outer and inner regions of a medical device is of extreme interest to locally boost the bone growth along the desired direction. For instance, in orthopaedic prosthetic devices, cell growth should usually occur from the peripheral (bone-implant interface) to the central regions, thus higher peripheral porosity (hence permeability) should be required.

Permeable lattice structures find application in several other industrial fields, particularly when thermal management issues should be addressed. In this context, permeability to fluids and air plays a critical role and, for instance, it is fundamental for the design of heat exchangers, cooling systems or even for catalytic convertors [197]. These devices found increasing interest in several sectors, most notably in the aerospace, automotive and electronics industries. For a deeper discussion of these applications, please refer to the subsequent section on thermal conductivity and heat transfer applications.

Another application area of interest with regard to permeability is in the development of wicks used in heat pipe applications. Recent work using L-PBF to create porous wicks based on lattice geometries [198] has shown promise with regard to obtaining large permeability and capillary performance (the latter assessed as the ratio of permeability to effective pore radius). Some of the opportunities and challenges that need to be resolved for incorporation of wicks fabricated with metal AM into heat pipe fabrication and integration include selecting the optimum design approach, and in the case of structured wicks, the appropriate lattice shape, reliably controlling pore dimensions [199], and accounting for dependency on print orientation [200]. An experimental test example is shown in Fig. 17, where ethanol uptake in a L-PBF manufactured Inconel lattice was studied.

3.6. Convective heat transfer

Among the thermal- and fluid-dynamic applications, metal additive manufacturing has established itself as a ground-breaking technology potentially able to revolutionize the field of heat transfer devices, specifically in the design of heat exchangers [197], heat sinks [201], cooling systems [202] and catalytic converters [203], as also visible in Fig. 18. The thermal management of electronic devices arises as one of the most important industrial challenges, due to the device miniaturization trend of the last decades, coupled with an abrupt request of performance increment and an increase of their power density. The possibility of AM to manufacture thermally efficient structures with an extremely complex and miniaturized design, in a one-stage fast process, can be an effective solution to this open issue. Therefore, in this scenario, metal hierarchical cellular materials are considered as cutting-edge architectures suitable for these industrial fields.

Among the most common lattices involved, applications with woven meshes [209], Kagome trusses [210], octet-truss lattices [211] and TPMS unit cells [212] are reported. Stochastic structures (i.e., metal foams) are increasingly being replaced by periodic lattices, because the first architectures report a less controllable manufacturing process, the generation of larger pressure drops and poor load-bearing capabilities [213]. Concerning the latter issue, their design versatility, i.e. the possibility of topology-optimizing and multi-functionalizing periodic lattices (e.g., coupling load bearing/structural integrity, heat transfer, electrical damping, or acoustic functionalities) can be considered one of the main reasons for their attractiveness [213]. Additionally, the high surface-to-volume ratio, an intrinsic characteristic of AM lattice structures, is a key parameter to enhance the heat transfer coefficient and to promote an effective fluid mixing at a small scale. For instance, in the work of Ekade et al. [214], the authors studied the combined fluid flow and thermal behaviour of octet truss lattice geometries, considering these lattice units as potential applications for multifunctional heat exchangers or heat sinks. In particular, they compared the effective thermal conductivity, friction factors, inertial coefficients, and permeability in comparison with stochastic metal foams by numerical simulations. The authors reported an increase in permeability ranging from 20% to 80%, a decrease of 50% of the inertial coefficient at a fixed porosity value and lower or comparable friction factors with respect to the metal foams. These outcomes, combined with the stretch-dominated failure behaviour of octet truss lattices - ideal for load-bearing applications – lead the authors to state that these units might be suitable for multifunctional lightweight heat exchangers or heat sinks, in which robust mechanical properties are also required. Recently, Broughton et al. [215] compared the single-phase convection of traditional commercial Aluminium ERG foams with respect to an additively manufactured lattice counterpart. Upon a preliminary screening, they chose the rhombic dodecahedron-based unit cell, exhibiting better performances over the ERG foam. Particularly, the heat transfer performances and the heat transfer rate through the finning surface are remarkably larger for the AM lattice components. According to the authors, this might be related to the absence of a thermal interface material and the more favourable rhombic window geometries in the developed heat transfer model. Zhao et al. [209] investigated 3D copper woven lattices. Their choice was mainly related to the material high thermal conductivity that, combined with a periodic micro-scale pattern with increased specific surface area, can lead to improved heat transfer capabilities. They investigated two design topologies - standard and optimized weaves - and their thermal and fluidic response under different flow patterns (axial, focused and full bifurcated) and cooling media (air and water). From the authors' outcomes, while these structures have room for further optimization, they can already be suitable for applications where high heat dissipation and uniform temperature distribution are required.
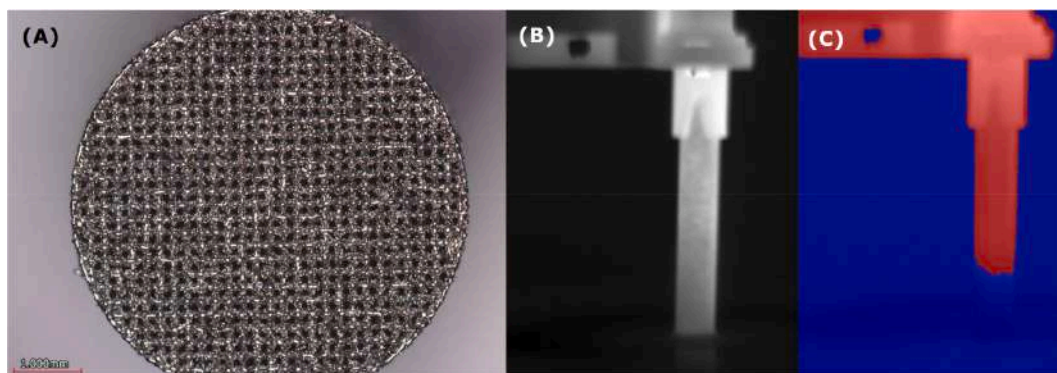

Fig. 17. (a) Inconel 718 wick made with cubic lattices; (b) Optical and (c) IR thermal images showing uptake of ethanol in the wick via capillary action.
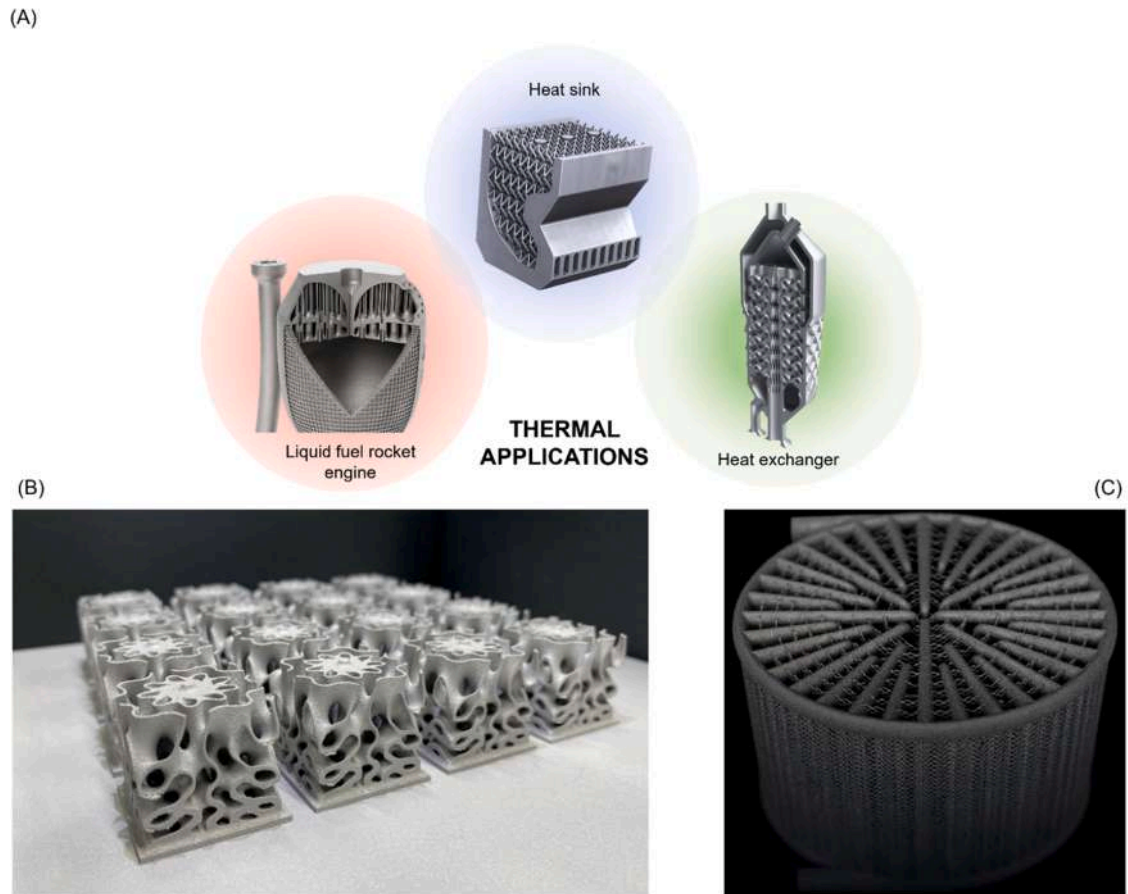
Fig. 18. Examples of lattice structures involved in the design of thermal management applications. More in detail, a monolithic thrust chamber, fabricated from Inconel 718 via L-PBF with lattice walls, aimed to enhance the fluid transport simultaneously acting as a cooling system (realized by Cellcore and SLM Solutions [204]). A topology-optimized lattice heat sink device, which guarantees the flow recirculation (realized by Purdue University [205]). A heat exchanger infilled with Triply Periodic Minimal Surface lattices, for applications in aerospace turbine (realized by nTopology [206]). B) Additional examples of TPMS structures adopted for heat sinks suitable for electronic applications (realized by nTopology [207]). C) Ultralight alluminum alloy AM heat exchanger for F1 racecar (realized by Betatype and Progressive Technologies [208]).

Another interesting work on lattice application for heat exchanger devices is reported by Son et al. [216]. They studied lattice frame materials (LFM) in a tetrahedral ligament configuration with a porosity ranging from 75% to 95%. They carried out a characterization of LFM thermal and hydraulic performances as a function of the porosity by means of simulation tools further supported by experimental results (Fig. 19a). Interestingly, the authors provided a series of metrics useful for a designer to properly tune the lattice structure in order to fulfil the main requirements and requested constraints of a heat exchanger for a specific practical application. Among these, a particular focus was drawn to the "area goodness", "volume goodness" and efficiency index parameters [216]. Tetrahedral lattices have also been employed to possibly solve the increasing issue of thermal management of batteries in unmanned aerial vehicles (UAVs) - commonly known "drones". Indeed, as reported in a recent work of Son et al. [202], these porous structures can be employed as fillers of cold plates of lithium-ion batteries. According to the authors, the lattice introduction can enhance the thermal management and cooling system efficiency of these batteries, particularly affected by an abrupt increase of temperatures and consequent dramatic capacity losses due to their fast charge/discharge (Fig. 19b). Additionally, these porous periodic structures can also act as load bearing devices, avoiding any structural degradation (hence irreversible capacity loss) of the battery itself.

Among the reviewed literature works, TPMS lattice structures are also reported in the context of convective heat transfer. For instance, in the work of Catchpole-Smith et al. [212], the authors compared the thermal conductivity behaviour of three TPMS lattices, namely gyroids, diamond and Schwarz primitive units. These lattices can be adopted for compact heat sink devices or thermal insulation layers, in several fields, varying from aerospace or automotive industries to the electronics industry. From this comparative work, the authors pointed out that lattice units with the lower minimum wall thickness exhibit a lower thermal conductivity, but a better convective heat transfer. Additionally, also the unit cell size plays an important role, since too small units might hinder the natural convective heat transfer. A recent study also indicated a significant effect of wall thickness on thermal efficiency for Schwarz-lattice heat exchanger design [217]. Surface roughness (particularly in samples with high surface area-to-volume ratio) can also
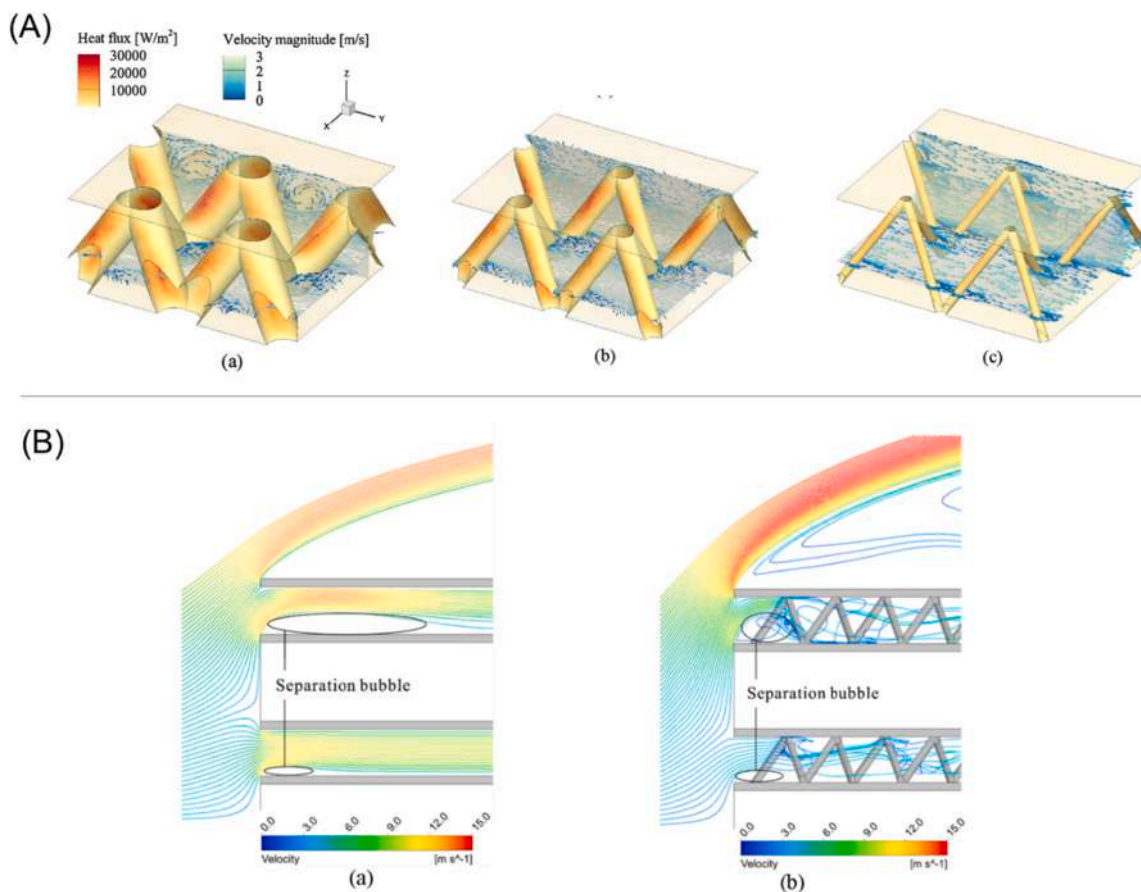
Fig. 19. (A) Heat flux contours on the solid–fluid interface displayed together with the velocity vectors along x- and z- plane slices. Reynolds number is set equal to Re = 620. Figure (a), (b) and (c) reports three different levels of porosity of the lattices, Namely, 75%, 90% and 96%. Image adapted from [216]. (B) shows a simulation comparison (performed by Son et al. [202]) between lithium-ion batteries cold plates without (a) and with (b) the lattice structure introduction. Reported streamlines for the leading edge are referred to as a forward flight mode simulation at u∞ = 33 km/h. (~9.1 m/s).

decrease the lattice thermal conductivity.

Another potential thermal application of lattice structures concerns the field of catalytic convertors, due to the great design flexibility of lattice structures and the high heat conduction with respect to traditional foams [218,219]. Ambrosetti et al. [203] investigated the use of Ti6Al4V and AlSi10Mg lattices (cubic, diamond and tetrakaidekahedron unit cells) for this purpose. They showed that these structures might be adopted as intensifiers of the catalytic processes, due to their capability of increasing the transfer heat rate of tubular reactors, in the presence of conventional industrial catalyst pellet, thus without the need of their downsizing, a drawback of recently proposed alternatives exploiting packed foams. This was further supported by a computational fluid dynamics study [220] indicating correlations of strut diameter and cell porosity with heat and mass transfer properties.

3.7. Thermomechanical applications of architected metamaterials

The possibility of tuning architected metamaterials does not only concern the mechanical but also the thermal and thermo-mechanical properties. At present, the thermal applications of cellular materials are still in their initial stages, with limited industrial adoption. However, looking at the applications of their stochastic porous counterparts, viz. metallic foams, we can have an outlook on promising applications of periodic architected cellular materials in high-performance thermal management applications. Since in such applications, dissimilar materials are exposed to pronounced stress gradients, thermal mismatch strains can produce elevated thermal stresses. The possibility of tuning also the coefficient of thermal expansion by modulating the metamaterial microarchitecture to accommodate differential thermal expansion will be reviewed in this section as well. Specifically, we will consider here applications wherein thermal conductivity is of primary concern. This typically occurs when the cellular material is manufactured by a highly-conductive matrix, like metals, and voids which are empty or filled with stagnant less-conductive gases or liquids. In this case, conductive and convective contributions of such inclusions are deemed negligible [221,222].

Typical examples of metal foams as thermal conductivity enhancers are illustrated in Fig. 20A. This shows the layout of a hydrogen

storage tank [223] (HST), where the hydrogen is under moderate temperature and pressure in solid solution in the form of metal hydrides. Hydrogen is stored (charging phase) or released (discharging phase) by removing or supplying heat. Clearly, the performance of such devices mainly depend on the speed of this transient heat transfer [225]. For this reason, the thermal management of HST plays a crucial role in their efficiency. To facilitate the heat exchange with the outer environment, finned enclosures and heat exchanger tubes can be employed, while the thermal conductivity of the metal hydride bed can be enhanced through the insertion of a metallic foam. Investigations carried out in [226] showed that the use of Al foam allowed the reactor diameter to be increased by 7.5 times, without losing its performance.

Fig. 20B shows a similar application of a metallic foam as a thermal conductivity enhancer in phase change materials (PCM) used for thermal energy storage [224]. PCMs store thermal heat in the form of sensible and principally latent heat. They change state from solid to liquid or liquid to gas or vice versa at almost constant temperature during latent heat storage. Commonly chosen PCMs are paraffin wax [224] and sodium nitrate (NaNO3) [227]. However, such PCMs display a low thermal conductivity, ranging from 0.1 to 1.0 W/(m K) [228]. This low thermal conductivity limits the performance of the thermal management systems, since thermal energy can only be slowly transferred into the heat sink. The effect of embedding metal foams into the PCM reported in the literature [224,227,229-231] is remarkable, especially during the discharging process when the PCM is in the solid state, viz. when conduction is the prevalent heat transfer mechanism. Conversely, during the charging process in the liquid state, the presence of the metal foams weakens the contribution of natural convection and therefore limited the process [230].

The advantages of metal foams lie in their low-density, large surface area in a limited volume and high-strength structure. Their stochastic architecture makes their thermal behaviour quasi-isotropic, and mostly dictated by porosity, conductivity of the base metal and tortuosity of the struts composing the foam structure [232]. For this purpose, the scientific community is currently addressing research efforts towards the possibility of tuning the deterministic architecture of cellular metamaterials in order to redirect the heat flux, for instance towards heat sinks for a more efficient thermal management, and improved fluid/structure interaction of the cell struts/walls [233]. In addition, such architected cellular materials display superior structural characteristics [41] thanks to increased nodal connectivity which lend themselves well to topology optimization and integration of multiple functions enabling a high degree of tailorability and superior performance benefits.

To exploit the multifunctional potentials of cellular materials, a mathematical model capable of accurately predicting their effective properties is of crucial importance. Specific to heat transfer design, the first approaches devised to predict the thermal properties of cellular materials relied on the thermal-circuit method based on the analogy between electrical and thermal conductivities [234]. This method was particularly valuable to identify the upper and lower bounds of the effective thermal conductivity of cellular materials [221]. More recently, advanced computational models, like Monte Carlo analyses [235] and asymptotic homogenization techniques have been conceived to predict the effect of the architecture of cellular materials on their effective thermal properties [236]. In essence, the energy balance equation, viz, the energy equation combined with Fourier heat conduction, is solved over a representative volume element (RVE) using the finite element method. The effective thermal conductivity is calculated by averaging the heat flux over the RVE [237]. In this way, it is possible to estimate the effective thermal conductivity tensor $\overline{K}_{eff}$ governing the linear Fourier's relationship between heat flux $\vec{q}$ and temperature gradient ∇T:

$$\vec{q} = -\overline{K}^{eff} \nabla T$$

$$\overline{K}^{eff} = \begin{bmatrix} k_{xx}^{eff} & k_{xy}^{eff} & k_{xz}^{eff} \\ k_{yx}^{eff} & k_{yy}^{eff} & k_{yz}^{eff} \\ k_{zx}^{eff} & k_{zy}^{eff} & k_{zz}^{eff} \end{bmatrix}$$

where $\overline{K}_{eff}$ is a 3x3 symmetric tensor. The diagonal terms k_{ii} are always positive, as they relate the temperature gradient to the heat flux
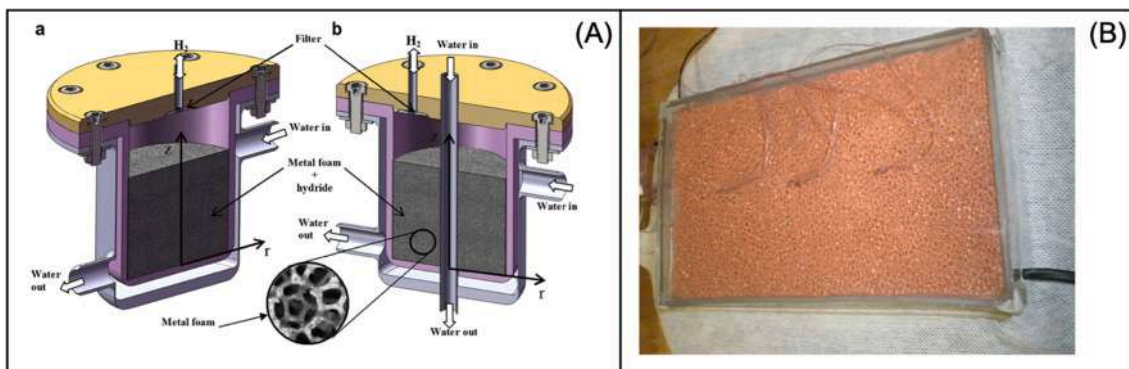

Fig. 20. (A) Schematic view of a hydrogen storage tank wherein metal hydrides are embedded in a metal foam for enhanced thermal conductivity [223]. (B) A separate example of energy storage where paraffin was used as phase change material (PCM) in a thermal energy storage system, in this case paraffin is embedded in a copper foam [224].

along the same direction.

The trace of the tensor is an invariant (independent of the orientation of the coordinate system) and obeys the following summation law in case of cellular lattice structures made of the same base material of conductivity k_m and of porosity p [238]:

$$k_{xx} + k_{yy} + k_{zz} = (1-p)k_m$$

Moreover, for isotropic materials the summation law reduces to:

$$k_{xx} = k_{yy} = k_{zz} = \frac{1-p}{3}k_m$$

This predicts very well the conductivity of stochastic open-cell porous media. In the case of cellular materials, the effective thermal conductivity is generally anisotropic and depends on the cell microarchitecture [239,240]. Interestingly, looking at these equations it can be noted that one can make the thermal conductivity component in a particular direction higher only at the expense of those in the other two directions. The summation law has been generalized in [238] in terms of the thermal conductivity tensor in order to identify the conditions for orthotropic thermal conductivity. This condition in general coincides with the condition of structural symmetry about a Cartesian coordinate. Off-diagonal terms k_{ji} of the conductivity tensor represents the most interesting thermal feature of cellular materials. Indeed, they control the coupling effect between the temperature gradient and the heat flux along an orthogonal direction. Depending on the orientation of the coordinate system, k_{ji} elements can be negative, zero, or positive. In a similar way to stress or strain tensorial notation, thermal conductivity can be graphically represented in terms of Mohr's circles to determine the orientation of the reference frame that nullifies the off-diagonal terms. The resulting diagonal terms are the principal thermal conductivities.

Mirabolghasemi et al. [41] have recently presented a fundamental investigation on the thermal conductivities of architected metamaterials. In this regard, Fig. 21A shows an annular domain subjected to thermal loading in the inner contour. The disk is composed of a regular pattern of square cells carrying a central elliptical pore variously oriented with respect to the cell symmetry axis. The same thermal problem was also solved through a homogenized anisotropic material (central columns in Fig. 21A). It can be noted that the thermal flux spreads from the inner to the outer surface following a distorted path dictated by the orientation of the elliptical holes as a result of the variation in the components of the thermal conductivity tensor (graphically by the Mohr's circles shown in the right column of Fig. 21A). Given the crucial role played by the off-diagonal terms k_{ij} in the redirection of the heat flux, the same authors investigated the possibility of tuning k_{ij} by acting on the pore shape. For this purpose, they utilized the mathematical tool devised in [241] to define the pore shape in the form of Lamé curves (denoted as "supershapes"), as exemplarily shown in Fig. 21B. Fig. 21C shows the off-diagonal term for different supershapes as a function of the relative density of the 2D cellular material. It can be noted that a wide range k_{ij} can be obtained, ranging from -0.1 to 0.4 times the thermal conductivity of the solid matrix k_m. In an attempt to
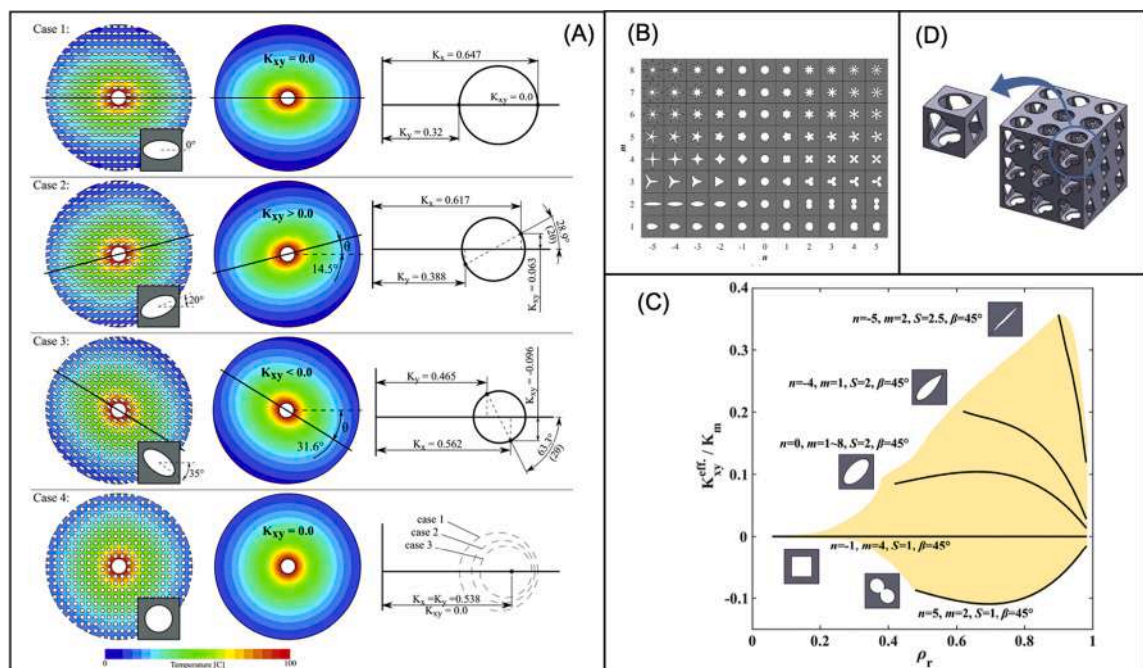

Fig. 21. (A) Effect of changing the pore angle on temperature contours of a cellular disk under thermal loading. (B) 2D architected cellular metamaterials with different pore supershapes. (C) Effective off-diagonal term in the thermal conductivity tensor for 2D supershape pores as a function of the relative density r_r. (D) 3D architected metamaterial composed of thin-walled cubic cells provided with supershape pores. Image readapted from [41].

extend these analyses to 3D cellular materials, Mirabolghasemi et al. [41] investigated the thermal properties of TPMS shellular materials. They concluded that these metamaterials only cover a narrow region of thermal conductivity versus relative density chart and display a rather isotropic thermal behaviour, as also found in [242]. To overcome this drawback, they proposed to provide the faces of thin-walled cubic cells with supershape pores, as illustrated in Fig. 21D, in order to exploit their high tunability of thermal properties. Finally, to explore the effect of tailoring the pore architecture across the cellular metamaterials on tuning the heat flow, they modulated topology and cell relative density of supershape pores according to the concept of functionally graded cellular materials.

This concept took inspiration from the work of Park et al. [243], among the first to investigate thermal metamaterials to manipulate heat flux at a continuum level [244,245]. The basic idea is to discretize a 2D domain with an assembly of discrete unit-cell thermal shifters representing discretized heat flux lines in local spots. As schematically shown in Fig. 22, the designed assemblies of thermal shifters as unit-cells enables the manipulation of the local heat flux for multiple functions: thermal shifter, concentrator, diffuser, and rotator. The authors proposed to achieve the functions of thermal metamaterial by layering structures of high thermal conductivity materials and low thermal conductivity materials, but the same idea could be potentially applied in the future to architected cellular materials.

A material physical property closely connected to thermal conductivity is the coefficient of thermal expansion. It is reasonable to expect that architected metamaterials employed in thermal insulation and heat exchangers are exposed to intense thermal gradients and therefore to high thermal strain gradients. In addition, materials with low coefficient of thermal expansion (CTE) are less sensitive to temperature changes and thus sought in several applications, like precision instruments, satellite antennas, flexible electronics, biomedical sensors, thermal actuators, and MEMS [246,247].

If the cellular materials are composed of a single solid material, their effective thermal expansion will be identical to that of the matrix. This might be problematic when such strains are impeded because mismatch stresses arise with consequent risk of mechanical failure. A frontier application of cellular materials is in the fabrication of hybrid carbon fibre reinforced composite to metal junctions [248]. A metal cellular lattice structure provides the mechanical anchoring to the long fibres of the composite and reduces the mismatch in elastic properties between metal and composite at the interface, thus attenuating parasitic stresses arising from the strain incompatibility at the junction. The two adherends are however affected by very dissimilar coefficient of thermal expansion (by a factor of more than 2) and this poses serious concerns about the structural integrity of the joint.

Recent works on metamaterials have shown that when two solid materials with positive, but dissimilar, thermal expansions are
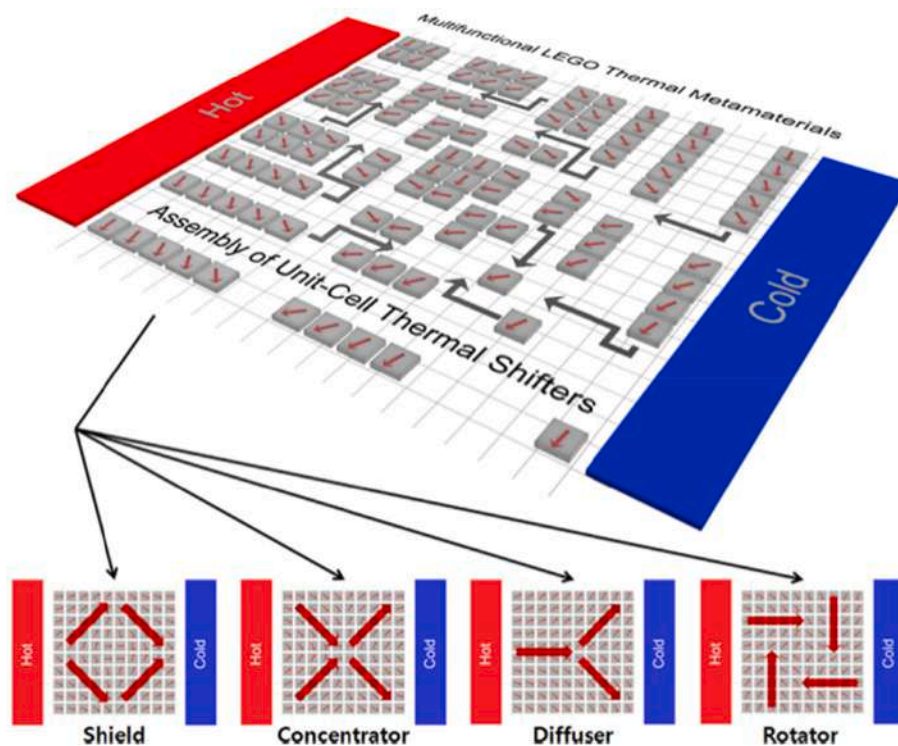

Fig. 22. Scheme of tunable multifunctional thermal metamaterials. The designed assemblies of thermal shifters as unit-cells enables the manipulation of the local heat flux for multiple functions: thermal shifter, concentrator, diffuser, and rotator. The differently inclined thermal shifters induce the discretized heat flux lines, inspired by two-dimensional digital images. The grey arrows indicate that the specific assembly of unit-cell thermal shifters enables a certain function for local heat flux manipulation. The red arrows show that such assembled design can carry out the diverse functions [243]. (For interpretation of the references to colour in this figure legend, the reader is referred to the web version of this article.)

arranged into a cellular material, the effective thermal expansion can be substantially less than or greater than the thermal expansion of either constituent material [249]. As a result, thermal expansion can be controlled using a variety of constituent materials, and all the other benefits of periodic cellular materials can be simultaneously achieved.

A number of bimaterial cellular designs for zero or negative thermal expansion have been proposed so far. Accordingly, the material composition of individual struts or cell walls varies within each unit cell. Materials with mismatched thermal expansions are arranged such that a change in temperature causes structural elements to rotate or bend into the interior void space of the unit cell, compensating for or exceeding the positive thermal expansion of the constituent solids. Fig. 23A-B show the two mechanisms of thermal deformation in a bimaterial tetrahedron analyzed by Xu and Pasini [250]. The first one results in stationary-nodes (Fig. 23A) and can be used in an Octet cell to generate thermal expansion isotropy. The second mechanism resorts to stationary-lines that appear in a bi-material tetrahedron upon thermal expansion (Fig. 23B). This mechanism can be applied to obtain an Octet lattice with zero CTE in a specific direction. Xu and Pasini [250] generated more complex 3D unit cells based on octet truss topology, either with isotropic or anisotropic thermal expansion. The prototype shown in Fig. 23C was obtained by laser cut pieces from Al6061 and Ti–6Al–4 V alloy sheets with pretension snap-fit joints and demonstrated a tunable CTE along one direction ranging from 0.17 to 9.83×10^{-6} $°C^{-1}$. A similar approach was adopted in [251] to design bimaterial lattice structures based on pyramidal and tetrahedral cells.

In a more recent work, Ai and Gao [252] observed that *iso*-octet and aniso-octet lattice structures do not display isotropic thermal expansion. To overcome this drawback, they proposed four types of 3-D bi-material lattice metamaterials with both negative Poisson ratio and non-positive CTE by extending the 2-D re-entrant lattice structures proposed in a previous work of the same authors [253]. They are illustrated in Fig. 23D, where the red and blue struts represent the materials with the higher and lower CTEs, respectively. Each of them can be described by using two length parameters and two angle parameters. Parametric FE analyses have been carried out
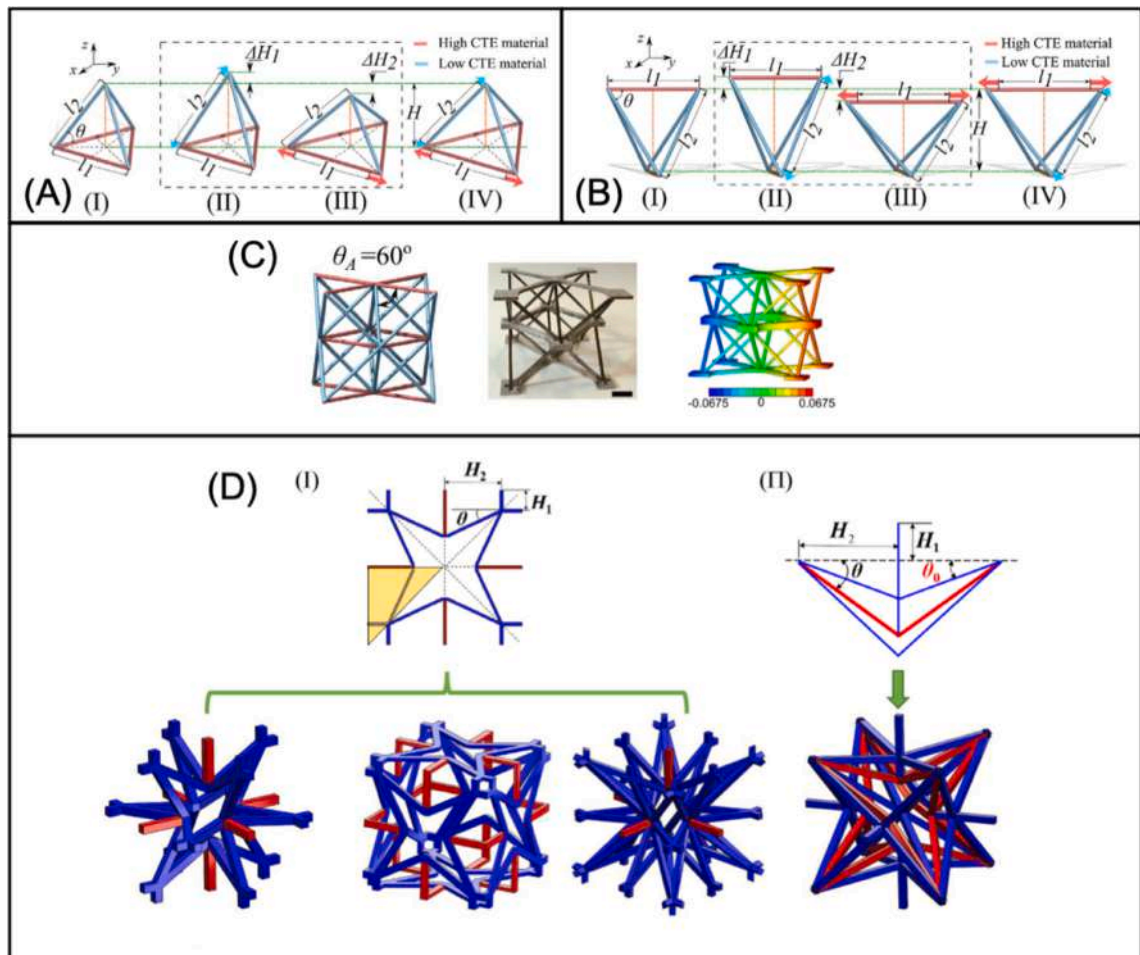

Fig. 23. Thermal mechanisms a bi-material tetrahedron featuring either a stationary-node (A) or stationary- lines (B). II and III show visually uncoupled thermal expansions, one for the low-CTE material and the other for the high-CTE material. (C) Prototype of aniso-octet truss cell manufactured from Al6061 (high-CTE) and Ti-6Al-4 V (low-CTE) [250]. (D) Four types of 3-D bi-material metamaterials proposed by Ai and Gao as 3D extension of re-entrant 2D lattice structures with auxetic properties [252].

to find relationships between design parameters and Poisson's ratio, CTE, Young's modulus and shear modulus.

Parsons [254] observed that applications of these materials is severely limited because the proposed designs are very difficult to manufacture robustly at useful scales. From metals, samples have been fabricated primarily by cutting individual elements or sections from plates and manually joining the separate pieces with pins [255], bolts [256], interference [246] and snap [250] fits, adhesives [257], brazing or welding [255], but the mechanical properties allowed by these manufacturing techniques are often not compliant with the requirements of aerospace structural applications. A notable potential exception is the work of Ding et al. [258], who devised a directed energy deposition (DED) technique to fabricate 2D bimaterial lattice proposed by Ai and Gao [253]. They used a robot arm equipped with a laser head and two powder feeders supply two different powders independently, as needed. Recently, Parsons [254] devised an ultrasonic additive manufacturing technique to fabricate 2D hexagonal lattice structures made of Al and Ti alloys.

3.8. Other properties and new applications

This section briefly discusses some other applications, some of which have been investigated for metallic cellular structures manufactured by additive manufacturing, while some are still promising concepts. Electromagnetic and acoustic wave properties are of particular interest in metamaterials, for new devices for wave absorption (damping), propagation (waveguides), or for focusing or directing waves in particular ways. The field covering electromagnetic and acoustic properties and possible applications was reviewed in [259]. Though the theoretical concepts are well developed, manufacturing and testing such devices are still limited in terms of metallic cellular structures, which is a significant opportunity.

A relatively new application is the use of metallic cellular structures for filtration – the design of porous materials with specific designed pore sizes and permeability allowing the interaction of the fluid with the cellular material. This interaction can be to block particles above a specific size range (using pore size control in design), or it may be by chemical interaction, for example incorporating copper into the lattice struts (by in situ alloying during L-PBF [260]) which provides anti-microbial properties [261]. Filtration is strongly dependant on interaction between the fluid and the material, while allowing sufficient flow through the cellular structure.

One well known use of lattice structures is as support materials for metal additive manufacturing [262], whereby overhang regions of a complex part requires some form of support material to attach it to the build plate. Lattice is beneficial here due to the relative ease of removal compared to thicker bulky supports, and their low material use, leaving more powder to be re-used.

Since the manufacturing process typically uses a powder bed, additively manufactured metallic lattice structures need to be open-cellular design, since closed-cell designs would contain the unmelted powder. Closed-cell designs are beneficial for some applications areas, such as in buoyancy applications, thermal insulation and reduced permeability requirements. Therefore new approaches to implement this using non-powder bed AM methods, or through the use of powder release holes which are closed after powder removal (by post processing) might be promising for selected applications.

A recent example of a vacuum chamber design manufactured by additive manufacturing, incorporated a gyroid cellular design as seen in Fig. 24 [263]. The advantage of the lattice design here is primarily light-weighting, but also holds some advantages for heat exchange and vibration isolation, which are highly sought after in such systems.

Multi-functionality is a concept that is inherent in cellular design, as the use of a cellular structure implies combinations of functions such as light-weighting and other properties. The use of multi-functional properties in a cellular design can be implemented through combined simulation approaches [264], by rational design based on property-function principles [25] or by biomimetic design approaches, since multifunctionality is prevalent in natural structures [6].

An interesting application utilizing multifunctionality is the demonstration of stretchable electrical conductors using cellular designs [265]. This approach is promising for architected electronics circuits and might be later combined with 4D printing approaches [266]. 4D printing refers to the manufacturing of 'smart materials' by additive manufacturing which can respond to some stimulus to change their geometry and function as required. This is being investigated for medical applications (e.g. stents which inflate once inserted to correct location) and in space applications (e.g. deployment of antennae once satellite is in orbit). Ultra-stretchable materials made using cellular designs may also be promising for wearable electronics, soft robotics and more [267].
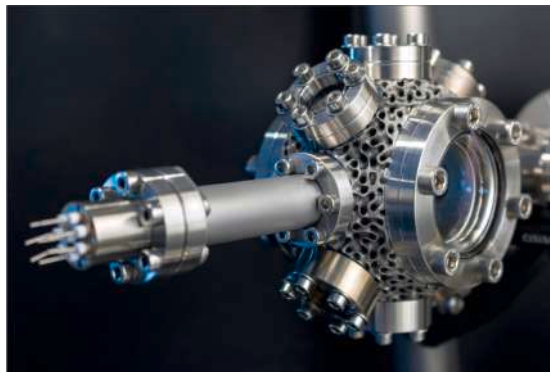

Fig. 24. Additively manufactured vacuum system incorporating cellular design for lightweighting and heat transfer [263].

Compliant mechanisms are another area of future growth due to their high potential as discussed in demonstrations of such systems in [268,269]. These mechanisms allow mechanical operations with reduced parts and less friction and wear and they may be implemented by architected cellular designs, for example for soft hinges or to locally adapt to surroundings.

An interesting application is the use of cellular design for artistic or visual appeal (without a functional requirement), as shown in Fig. 25 for a ceremonial university mace, manufactured entirely of titanium using a lattice design geometry. The appeal may be partly linked to the unusual design and partly to the resemblance to natural porous structures.

4. Design for AM: Architected materials

The complexity and flexibility enabled by commercial metal AM systems allows for the manufacture of intricate lattice structures with high technical performance and complex designs not achievable with traditional manufacturing systems, with unique and many new potential applications, as reviewed in the last section. However, the complexity of AM lattices can induce new manufacturing challenges, whereby some AM structures are designed in a manner that is not synergistic with the AM manufacturing process (or the associated certification process) and that can compromise the properties and performance of the structures. To mitigate this potential for sub-optimal outcomes, numerous Design For AM (DFAM) strategies are emerging. These strategies exist on multiple technical and economic fronts of relevance to successful metal AM applications. This section provides a design guide for these strategies, specifically to guide design and manufacturing engineers.

Specific validated DFAM tools to support design and manufacturing decisions can be categorized according to:

- Data that characterizes **AM manufacturability constraints** – this data includes, for example manufacturability data (minimum strut thickness, lattice geometry, microstructural and mechanical attributes).
- Methods to **quantify design outcomes**, for example, topological optimization methods, predictive tools for metal AM build simulation, and other simulation and analytical approaches.
- Insights on the **economic implications** of the proposed manufacturing quantity, geometric complexity and methods of manufacture, for example build time and cost, required post processing costs, performance enhancement leading to economic advantages.

4.1. Lattice geometry definition, storage and optimization

Lattice structures typically consist of a series of strut elements that intersect at defined nodes. These elements may be defined by different methods – either explicit geometric definitions (e.g. traditional CAD design software) or by implicit mathematical functions (e.g. TPMS functions), examples of each are shown in Fig. 26. Explicit definition allows direct control of individual node locations and strut connectivity, as well as the local geometric attributes of these structures. These explicit methods are directly compatible with traditional CAD methodologies, specifically constructive solid geometry (CSG) and boundary representation (B-Rep) [270]. Despite
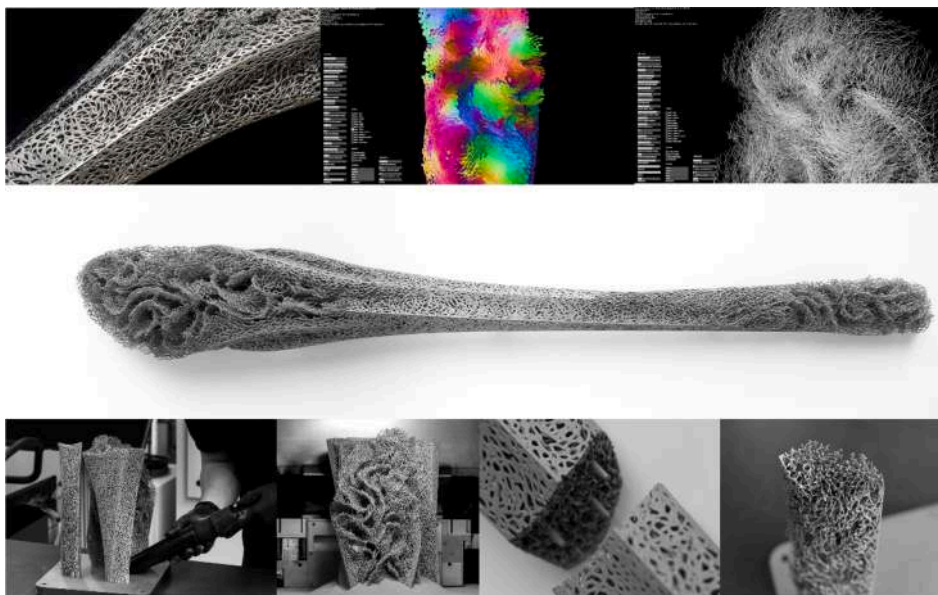

Fig. 25. Ceremonial mace with lattice design for artistic appeal, manufactured in titanium at RMIT. Total mace length is 1.2 m (full mace shown in middle). Top panels show design snapshots while bottom panels show manufacturing snapshots (L-PBF build plate with parts shown bottom left). The mace was printed in parts and welded together.

the advantages associated with the traditional implementation of explicit methods, they can be technically challenging due to the computational costs involved for lattice structures. The file sizes are large, making design modifications challenging and storage and export of these limit their wider use. These challenges are further exasercated for high complexity structures such as locally optimized and hierarchical lattices [271]. In response to this design challenge, implicit CAD design represents the intended geometry with a mathematically defined spatial field that is intersected with an isosurface to define the intended geometric volume. Using signed distance functions [272], a thicknesses can be applied to this isosurface, or its interior filled to create a solid representation. Implicit CAD representations provide several key advantages for applied lattice structure design: geometric representations are rapidly generated, including local optimization, with significantly reduced computational resources and file sizes. This allows more advanced design capabilities with the same available computing resources.

Both explicit and implicit CAD representations require transition from the design representation to a format that represents the intended geometry in an AM-compatible manner. Traditionally, this representation is the stereolithographic (STL) format, which represents the intended geometry with a series of triangular facets that represent the external component volume. This representation is technically robust, but fundamentally limited for lattice design scenarios. The fine feature sizes and many strut elements result in large numbers of unique facets – large file sizes and typically too bulky for typical AM computing resources. Alternate AM-specific representations are emerging, for example the 3MF consortium format that increases data storage efficiency and allows for specific "beam element" definitions as are appropriate for AM lattice applications [271,274]. Appropriate selection of file format can substantially reduce data size and associated computational overheads (Fig. 27).

4.2. Lattice manufacturability

Lattice manufacturability data is presented in terms of allowable cross-sectional diameter and associated inclination (Fig. 28). This data is typically reported in binary terms of "manufacturable" or "non-manufacturable" permutations, but increasingly the associated porosity, roughness and variabilitiy in cross-section is also being reported to improve lattice structure design decisions. This strongly influences the mechanical performance of the cellular structure, with differences even in the "manufacturable" domain. It is therefore ideal to optimize the manufacturability and reach the best possible quality by designing struts as thick as possible and with inclination angles as high as possible (closer to parallel to the build direction).

Related to manufacturing quality is the combined challenge of file size of typical lattice representations in STL files. Since the number of facets used in the surface representation strongly influences the file size, reduced facets are often used. This may however influence the accuracy of the representation, with an extreme example being a circular strut being represented by three or four facets, making it triangular or square. It is possible to utilize this simplication process if the resulting manufacturing quality is confirmed and its influence on the lattice performance is acceptable [275].

4.3. Lattice response prediction

Effective lattice design requires that the functional response of this arrangement be predictable. This prediction can be made by numerical analysis or by first-principles analysis. In typical lattice design practice it is likely that first-principles and numerical analysis provide embodiment and detail-level design insight, respectively.

The analysis proposed by Ashby and collaborators are highly regarded and cover a comprehensive range of intented lattice functions (energy absorption, heat transfer, load bearing) and associated failure modes (yield strength, ultimate strength, deflection) as described in previous sections [14,276]. These first-principles methods provide correlation of the relative material property of interest as a function of the relative lattice density. More precise correlation can be acquired according to lattice design variables, for example the specific AM manufacturing technology and material, or classified according to whether the structure exhibits a stretch-dominated or bending-dominated response [51].

Numerical analysis provides highly specific insight into the technical performance and critical failure modes for a specific lattice structure of interest. The complexity of AM lattices is a technical challenge for numerical analysis due to the large mesh sizes, as well as geometric variations and non-linear effects. To provide confidence in proposed simulation models, they typically should be validated against reported experimental data for coupon samples.

AM lattice structures include geometric and microstructural imperfections that deviate from the idealized CAD representation, and must ideally be accommodated for in the design. In response to this requirement, DFAM tools are emerging to quantify the implications of these imperfections. This is done by using high resolution microCT data and evaluating the extent and influence of the surface and internal defects [72]. These strategies have been applied to quantify as-manufactured lattice geometric imperfections [277] and their structural response, including effective stress concentrations of as-manufactured node elements [278]. These DFAM capabilities enable the generation of a robust digital twin of the as-manufactured AM component, as is becoming increasingly necessary for high value applications including medical and aerospace lattice applications [279].

4.4. Lattice architectures

Coupon samples comprising of regular periodic unit cells are commonly specified to acquire mechanical property data. However these are rarely optimal for real applications, where the local functional requirements vary throughout the component. Commercial DFAM design tools and data storage protocols are available that allow ready (generative) control of local lattice geometry and topology. This control allows for functionally graded lattice architectures (see Fig. 29) that are optimized or conformal to the local
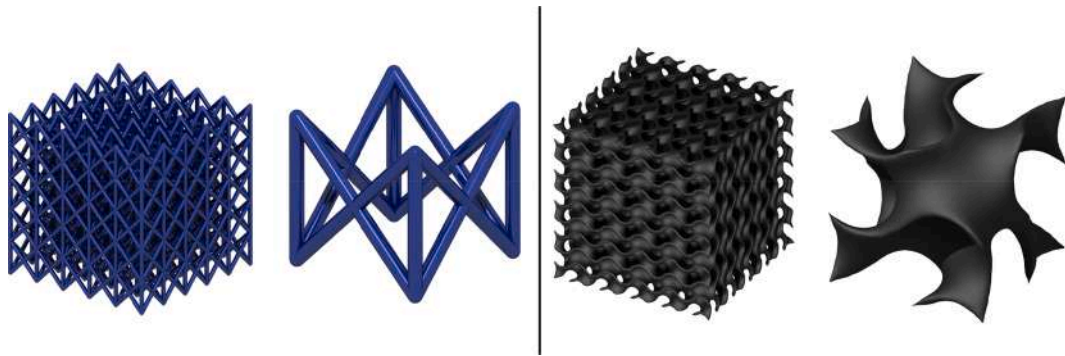
Fig. 26. Examples of explicit FCC-Z lattice generated using custom Matlab script [273] (left) and implicit gyroid-sheet lattice generated using commercial software nTopology (right). STL's for both lattices have been rendered using commercial CAD platform Catia v5.
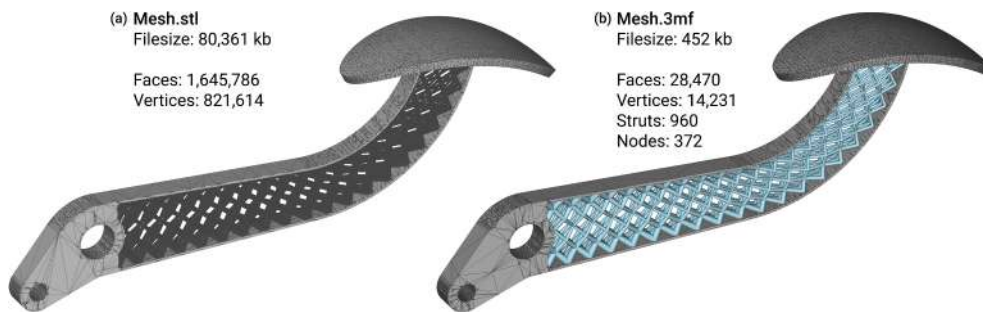

Fig. 27. Equivalent lattice geometry characterized by (A) stereolithographic (STL) and (B) 3D Manufacturing Format (3MF) [271].
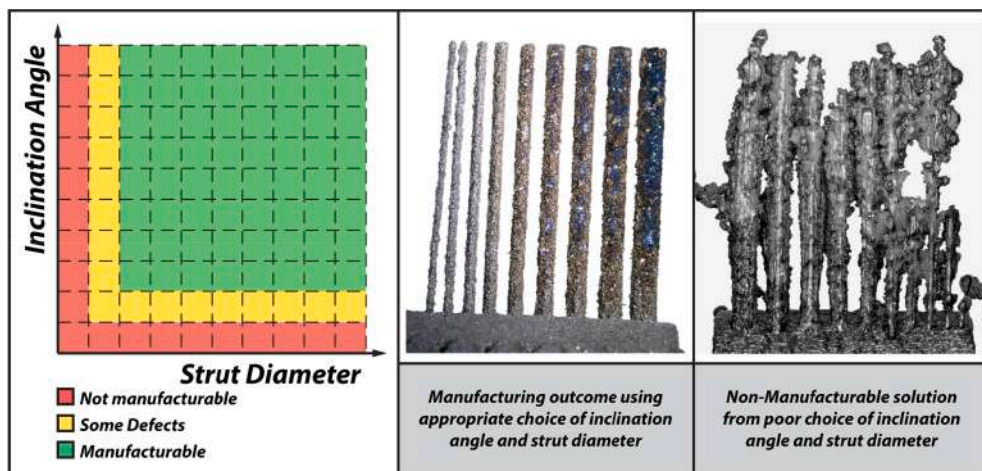

Fig. 28. Manufacturability data: strut elements as a function of diameter and inclination angle. Shown here are coupon strut-level manufacturing for different strut thickness and build angles as examples.

functional requirements. This enables a range of lattice applications, for example:

- Patient-specific implant structures that are conformal to the patient geometry (customized) and load-bearing requirements [280] while allowing for variable cell size to promote bone ingrowth.
- Energy absorbing structures whereby the graded design can be tailored to optimize energy absorption for the given expected loading conditions.
- Damage tolerant design of fatigue loaded structures where simulation highlights high-stress regions and the lattice is locally optimized to minimize stress concentration and hence delay the onset of crack initiation [29].
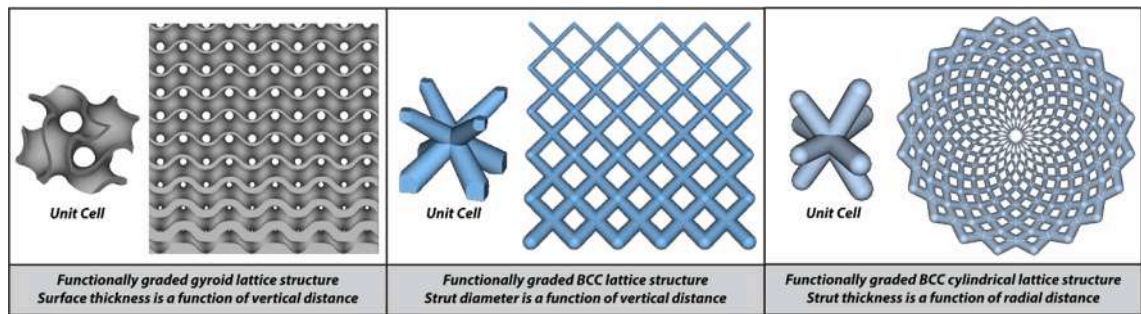
Fig. 29. Functionally graded lattice structures showing the linear variation of density and strut thickness in BCC strut-based lattice (left), sheet-based gyroid (middle) and radial variation of the same in a BCC strut-based lattice (right). The associated changes in pore size is visible in each case.

- Thermal systems that locally vary flow rate and thermal properties according to the predicted required thermal field.

4.5. Local design optimisation

Lattice architectures are typically designed and fabricated with circular strut cross-sections that are readily implemented but are not guaranteed to provide optimal functional response. New lattice design applications consider local optimization strategies for increasing the mass-specific performance, including hollow lattice structures [281,282] and tapered beam elements [283]. Hollow structures are recognised as providing efficient material distribution for bending-loaded structures and enables high-efficiency load bearing lattice structures. These structures however require that powder removal holes be accommodated. Similarly, variable cross-section beams are well understood within the civil engineering discipline to provide enhanced mechanical properties, and their application is beginning to be seen in optimized lattice applications to provide a more effective stress distribution in critical node elements [283]. These local design optimization strategies are relatively infrequently implemented so far in AM lattice design and provide a clear technical advantage for designers willing to understand and implement these opportunities.

Due to the highly complex nature of lattice structures, their design can be difficult and costly when utilising traditional techniques. In response to these challenges, generative design strategies have emerged which aim to utilise algorithmic tools to generate and optimise solutions to a problem that is well defined by the designer. Algorithmic tools such as shape grammars [284], topology optimisation [285], and programmatic lattice generation [273] can be used to generate the form that solutions should take. These generated forms can be further optimised with respect to design objectives and constraints using optimisation algorithms such as gradient descent [286] or metaheuristic techniques [287]. The coupling of form generation and optimisation algorithms allows for efficient management of the complexity inherent with the design of lattice structures, while reducing the cost required for traditional design techniques and simplifying documentation requirements for part certification; all while ensuring that generated solutions perform highly. The ceremonial mace depicted in Fig. 25 represents one such application of the generative design of lattice structures. Additionally, generative design strategies enable mass customisation of bespoke custom products by reducing the lead time required to progress from a problem definition to a manufactured solution greatly. The use of these techniques could enhance the use of lattices in mass customisation applications such as the design and manufacture of bespoke patient specific implants.

5. Conclusions and outlook

Architected cellular structures manufactured by metal AM are providing an entirely new paradigm with properties and capabilities which are only now starting to be utilized. A huge untapped potential exists in new applications of these structures due to their many unique properties that can be adjusted and precisely controlled, including low mass, designed mechanical properties, high surface area, permeability, energy and impact absorption, thermal insulation and thermomechanical properties and much more. This review has provided some insight into the design capabilities and achievable properties in this context while discussing relevant applications. A comprehensive coverage of the property-application links was therefore presented.

Some words of caution are important here. Despite all the potential benefits of metallic AM lattice structures, they may not be suitable for some situations or applications and may yield worse results than stochastic foams in some cases. These include cases where the load directions are not known beforehand – architected lattices have superior performance in specific directions but are often highly anisotropic, for example. The manufacturing limits for commercial metal AM systems have been discussed and these may cause unexpected errors or problems. In some applications, such as in medical implants, the entrapment of powder in the pore spaces is a key problem that has been identified, amongst many others. As with all new technologies and engineering approaches, the design and manufacturing of cellular structures requires careful consideration and quality control. In this context, a section was also devoted to the design and manufacturing considerations.

By providing an overview of the manufacturing challenges in addition to the property-application space, this paper provides a comprehensive resource for design and manufacturing engineers, for inspiring and further driving new advances utilizing these types of structures for new parts and products in a wide variety of application areas.

Declaration of Competing Interest

The authors declare that they have no known competing financial interests or personal relationships that could have appeared to influence the work reported in this paper.

Acknowledgements

References

[1] ISO/ASTM, ISO/ASTM 52900-2015: Additive manufacturing – General principles – Terminology, 2015. https://www.iso.org/obp/ui/#iso:std:iso-astm:52900: ed-1:v1:en (accessed April 18, 2020).
[2] Bourell D, Kruth JP, Leu M, Levy G, Rosen D, Beese AM, et al. Materials for additive manufacturing. CIRP Ann 2017;66(2):659–81.
[3] DebRoy T, Wei HL, Zuback JS, Mukherjee T, Elmer JW, Milewski JO, et al. Additive manufacturing of metallic components – Process, structure and properties. Prog Mater Sci 2018;92:112–224. https://doi.org/10.1016/j.pmatsci.2017.10.001.
[4] Yadroitsev I, Yadroitsava I, du Plessis A, MacDonald E. Fundamentals of laser powder bed fusion of metals - 1st edition, Elsevier, 2021. https://www.elsevier. com/books/fundamentals-of-laser-powder-bed-fusion-of-metals/yadroitsev/978-0-12-824090-8 (accessed November 25, 2020).
[5] Yadroitsev I, Yadroitsava I, Du Plessis A, MacDonald E, editors, Fundamentals of laser powder bed fusion of metals - 1st edition, Elsevier, 2021. https://www. elsevier.com/books/fundamentals-of-laser-powder-bed-fusion-of-metals/yadroitsev/978-0-12-824090-8 (accessed November 20, 2020).
[6] du Plessis A, Broeckhoven C, Yadroitsava I, Yadroitsev I, Hands CH, Kunju R, et al. Beautiful and functional: a review of biomimetic design in additive manufacturing. Addit Manuf 2019;27:408–27. https://doi.org/10.1016/j.addma.2019.03.033.
[7] Lewandowski JJ, Seifi M. Metal additive manufacturing: a review of mechanical properties. Annu Rev Mater Res 2016;46(1):151–86. https://doi.org/ 10.1146/annurev-matsci-070115-032024.
[8] Fatemi A, Molaei R, Simsiriwong J, Sanaei N, Pegues J, Torries B, et al. Fatigue behaviour of additive manufactured materials: An overview of some recent experimental studies on Ti-6Al-4V considering various processing and loading direction effects. Fatigue Fract Eng Mater Struct 2019;42:991–1009. https://doi. org/10.1111/FFE.13000.
[9] Ye C, Zhang C, Zhao J, Dong Y. Effects of post-processing on the surface finish, porosity, residual stresses, and fatigue performance of additive manufactured metals: a review. J Mater Eng Perform 2021;30(9):6407–25.
[10] Molaei R, Fatemi A, Razavi SMJ, Berto F. Fatigue and fracture of additively manufactured metallic materials. Ref Modul Mater Sci Mater Eng 2021. https://doi. org/10.1016/B978-0-12-822944-6.00010-4.
[11] Gibson LJ, Ashby MF, Harley BA. Cellular materials in nature and medicine. 1st ed. Cambridge University Press; 2010.
[12] Gibson L, Ashby M. Cellular solids: structure and properties. Cambridge University Press; 1999.
[13] Ashby M, Evans T, Fleck N, Hutchinson J. Metal foams: a design guide, 2000. https://books.google.co.za/books? hl=en&lr=&id=C0daIBo6LjgC&oi=fnd&pg=PP1&ots=RzdRpOQWLh&sig=Qn3nc7WmcuuoFa7fl4QUxiACMHk (accessed May 15, 2018).
[14] Ashby MF. The properties of foams and lattices. Philos Trans R Soc A Math Phys Eng Sci 2006;364(1838):15–30. https://doi.org/10.1098/rsta.2005.1678.
[15] Dallago M, Raghavendra S, Luchin V, Zappini G, Pasini D, Benedetti M. The role of node fillet, unit-cell size and strut orientation on the fatigue strength of Ti- 6Al-4V lattice materials additively manufactured via laser powder bed fusion. Int J Fatigue 2021;142:105946. https://doi.org/10.1016/j. ijfatigue.2020.105946.
[16] Han Lu, Che S. An overview of materials with triply periodic minimal surfaces and related geometry: from biological structures to self-assembled systems. Adv Mater 2018;30(17):1705708. https://doi.org/10.1002/adma.v30.1710.1002/adma.201705708.
[17] Bhate D, Penick C, Ferry L, Lee C, Bhate D, Penick CA, et al. Classification and selection of cellular materials in mechanical design: engineering and biomimetic approaches. Designs 2019;3:19. https://doi.org/10.3390/designs3010019.
[18] Yadroitsava I, du Plessis A, Yadroitsev I. Bone regeneration on implants of titanium alloys produced by laser powder bed fusion: A review, 2019. Doi: 10.1016/ B978-0-12-815820-3.00016-2.
[19] Tan XP, Tan YJ, Chow CSL, Tor SB, Yeong WY. Metallic powder-bed based 3D printing of cellular scaffolds for orthopaedic implants: A state-of-the-art review on manufacturing, topological design, mechanical properties and biocompatibility. Mater Sci Eng C 2017;76:1328–43. https://doi.org/10.1016/J. MSEC.2017.02.094.
[20] Murr LE. Open-cellular metal implant design and fabrication for biomechanical compatibility with bone using electron beam melting. J Mech Behav Biomed Mater 2017;76:164–77. https://doi.org/10.1016/J.JMBBM.2017.02.019.
[21] Murr LE. Strategies for creating living, additively manufactured, open-cellular metal and alloy implants by promoting osseointegration, osteoinduction and vascularization: An overview. J Mater Sci Technol 2019;35(2):231–41. https://doi.org/10.1016/j.jmst.2018.09.003.
[22] Wang X, Xu S, Zhou S, Xu W, Leary M, Choong P, et al. Topological design and additive manufacturing of porous metals for bone scaffolds and orthopaedic implants: A review. Biomaterials 2016;83:127–41.
[23] Zhang XZ, Leary M, Tang HP, Song T, Qian M. Selective electron beam manufactured Ti-6Al-4V lattice structures for orthopedic implant applications: Current status and outstanding challenges. Curr Opin Solid State Mater Sci 2018;22(3):75–99. https://doi.org/10.1016/j.cossms.2018.05.002.
[24] Zhang X-Y, Fang G, Zhou J. Additively manufactured scaffolds for bone tissue engineering and the prediction of their mechanical behavior: a review. Materials (Basel) 2017;10:50. https://doi.org/10.3390/ma10010050.
[25] Zadpoor AA. Mechanical performance of additively manufactured meta-biomaterials. Acta Biomater 2019;85:41–59. https://doi.org/10.1016/J. ACTBIO.2018.12.038.
[26] Chen H, Han Q, Wang C, Liu Y, Chen B, Wang J. Porous scaffold design for additive manufacturing in orthopedics: a review. Front Bioeng Biotechnol 2020;8: 609. https://doi.org/10.3389/fbioe.2020.00609.
[27] Maconachie T, Leary M, Lozanovski B, Zhang X, Qian Ma, Faruque O, et al. SLM lattice structures: Properties, performance, applications and challenges. Mater Des 2019;183:108137. https://doi.org/10.1016/j.matdes.2019.108137.
[28] Mirzaali MJ, Azarniya A, Sovizi S, Zhou J, Zadpoor AA. Lattice structures made by laser powder bed fusion, in: Fundam. Laser Powder Bed Fusion Met., Elsevier, 2021: pp. 423–465. Doi: 10.1016/B978-0-12-824090-8.00020-2.
[29] Benedetti M, du Plessis A, Ritchie RO, Dallago M, Razavi SMJ, Berto F. Architected cellular materials: A review on their mechanical properties towards fatigue- tolerant design and fabrication. Mater Sci Eng R Reports 2021;144:100606. https://doi.org/10.1016/j.mser.2021.100606.
[30] Gu D, Shi X, Poprawe R, Bourell DL, Setchi R, Zhu J. Material-structure-performance integrated laser-metal additive manufacturing. Science 2021;372(6545). https://doi.org/10.1126/science.abg1487.
[31] Zhang Q, Yang X, Li P, Huang G, Feng S, Shen C, et al. Bioinspired engineering of honeycomb structure - Using nature to inspire human innovation. Prog Mater Sci 2015;74:332–400. https://doi.org/10.1016/j.pmatsci.2015.05.001.
[32] Alabort E, Barba D, Reed RC. Design of metallic bone by additive manufacturing. Scr Mater 2019;164:110–4. https://doi.org/10.1016/j. scriptamat.2019.01.022.

[33] Bees on honeycomb, (n.d.). https://www.informatoreagrario.it/news/miele-italiano-un-2018-ripresa/attachment/api-su-favo/ (accessed June 26, 2021).

[34] Wang Z. Recent advances in novel metallic honeycomb structure. Compos Part B Eng 2019;166:731–41. https://doi.org/10.1016/j.compositesb.2019.02.011.

[35] Robling AG, Castillo AB, Turner CH. Biomechanical and molecular regulation of bone remodeling. Annu Rev Biomed Eng 2006;8(1):455–98. https://doi.org/10.1146/annurev.bioeng.8.061505.095721.

[36] Mistry Y, Anderson D, Bhate D. Bio-inspired design, in: Fundam. Laser Powder Bed Fusion Met., Elsevier, 2021: pp. 467–489. Doi: 10.1016/B978-0-12-824090-8.00010-X.

[37] Gibson LJ. Mechanical behavior of metallic foams. Annu Rev Mater Sci 2000;30(1):191–227. https://doi.org/10.1146/annurev.matsci.30.1.191.

[38] Gibson LJ, Ashby MF. Cellular solids: Structure and properties, second edition, 2014. Doi: 10.1017/CBO9781139878326.

[39] Vigliotti A, Pasini D. Stiffness and strength of tridimensional periodic lattices. Comput Methods Appl Mech Eng 2012;229–232:27–43. https://doi.org/10.1016/j.cma.2012.03.018.

[40] Köhnen P, Haase C, Bültmann J, Ziegler S, Schleifenbaum JH, Bleck W. Mechanical properties and deformation behavior of additively manufactured lattice structures of stainless steel. Mater Des 2018;145:205–17. https://doi.org/10.1016/j.matdes.2018.02.062.

[41] Mirabolghasemi A, Akbarzadeh AH, Rodrigue D, Therriault D. Thermal conductivity of architected cellular metamaterials. Acta Mater 2019;174:61–80. https://doi.org/10.1016/j.actamat.2019.04.061.

[42] Arjunan A, Demetriou M, Baroutaji A, Wang C. Mechanical performance of highly permeable laser melted Ti6Al4V bone scaffolds. J Mech Behav Biomed Mater 2020;102:103517. https://doi.org/10.1016/j.jmbbm.2019.103517.

[43] Babaee S, Shim J, Weaver JC, Chen ER, Patel N, Bertoldi K. 3D soft metamaterials with negative poisson's ratio. Adv Mater 2013;25(36):5044–9. https://doi.org/10.1002/adma.201301986.

[44] Mackay AL. Periodic minimal surfaces. Nature 1985;314(6012):604–6. https://doi.org/10.1038/314604a0.

[45] Deng Y, Mieczkowski M. Three-dimensional periodic cubic membrane structure in the mitochondria of amoebae Chaos carolinensis. Protoplasma 1998;203(1-2):16–25. https://doi.org/10.1007/BF01280583.

[46] Al-Ketan O, Abu Al-Rub RK. Multifunctional mechanical metamaterials based on triply periodic minimal surface lattices. Adv Eng Mater 2019;21(10):1900524. https://doi.org/10.1002/adem.v21.1010.1002/adem.201900524.

[47] Han SC, Lee JW, Kang K. A new type of low density material: shellular. Adv Mater 2015;27(37):5506–11. https://doi.org/10.1002/adma.201501546.

[48] Maskery I, Sturm L, Aremu AO, Panesar A, Williams CB, Tuck CJ, et al. Insights into the mechanical properties of several triply periodic minimal surface lattice structures made by polymer additive manufacturing. Polymer (Guildf) 2018;152:62–71. https://doi.org/10.1016/j.polymer.2017.11.049.

[49] ISO - ISO 13314:2011 - Mechanical testing of metals — Ductility testing — Compression test for porous and cellular metals, (n.d.). https://www.iso.org/standard/53669.html (accessed July 1, 2021).

[50] Gibson LJ, Ashby MF, Schajer GS, Robertson CI. The mechanics of two-dimensional cellular materials. Proc R Soc A Math Phys Eng Sci 1982;382:25–42.

[51] Deshpande VS, Ashby MF, Fleck NA. Foam topology: bending versus stretching dominated architectures. Acta Mater 2001;49(6):1035–40. https://doi.org/10.1016/S1359-6454(00)00379-7.

[52] Seiler PE, Li K, Deshpande VS, Fleck NA. The influence of strut waviness on the tensile response of lattice materials. J Appl Mech 2021;88. https://doi.org/10.1115/1.4049140.

[53] Bobbert FSL, Lietaert K, Eftekhari AA, Pouran B, Ahmadi SM, Weinans H, et al. Additively manufactured metallic porous biomaterials based on minimal surfaces: A unique combination of topological, mechanical, and mass transport properties. Acta Biomater 2017;53:572–84. https://doi.org/10.1016/j.actbio.2017.02.024.

[54] Ashby MF, Evans AG, Fleck NA, Gibson LJ, Hutchinson JW, Wadley HNG. Metal foams : a design guide. Butterworth Heinemann; 2000.

[55] Andrews EW, Gioux G, Onck P, Gibson LJ. Size effects in ductile cellular solids. Part II: Experimental results. Int J Mech Sci 2001;43(3):701–13. https://doi.org/10.1016/S0020-7403(00)00043-6.

[56] Raghavendra S, Molinari A, Fontanari V, Dallago M, Luchin V, Zappini G, et al. Tension-compression asymmetric mechanical behaviour of lattice cellular structures produced by selective laser melting. Proc Inst Mech Eng Part C J Mech Eng Sci 2020;234(16):3241–56. https://doi.org/10.1177/0954406220912786.

[57] Leary M. Design of titanium implants for additive manufacturing. In: Titan. Med. Dent. Appl., Elsevier, 2018: pp. 203–224. Doi: 10.1016/B978-0-12-812456-7.00009-3.

[58] Liu X, Wada T, Suzuki A, Takata N, Kobashi M, Kato M. Understanding and suppressing shear band formation in strut-based lattice structures manufactured by laser powder bed fusion. Mater Des 2021;199:109416. https://doi.org/10.1016/j.matdes.2020.109416.

[59] Banait S, Jin X, Campos M, Pérez-Prado MT. Precipitation-induced transition in the mechanical behavior of 3D printed Inconel 718 bcc lattices. Scr Mater 2021;203:114075. https://doi.org/10.1016/j.scriptamat.2021.114075.

[60] Dallago M, Winiarski B, Zanini F, Carmignato S, Benedetti M. On the effect of geometrical imperfections and defects on the fatigue strength of cellular lattice structures additively manufactured via selective laser melting. Int J Fatigue 2019;124:348–60. https://doi.org/10.1016/j.ijfatigue.2019.03.019.

[61] Aly MS. Effect of pore size on the tensile behavior of open-cell Ti foams: Experimental results. Mater Lett 2010;64(8):935–7.

[62] Gümrük R, Mines RAW, Karadeniz S. Static mechanical behaviours of stainless steel micro-lattice structures under different loading conditions. Mater Sci Eng A 2013;586:392–406. https://doi.org/10.1016/j.msea.2013.07.070.

[63] de Krijger J, Rans C, Van Hooreweder B, Lietaert K, Pouran B, Zadpoor AA. Effects of applied stress ratio on the fatigue behavior of additively manufactured porous biomaterials under compressive loading. J Mech Behav Biomed Mater 2017;70:7–16. https://doi.org/10.1016/j.jmbbm.2016.11.022.

[64] Kelly CN, Francovich J, Julmi S, Safranski D, Guldberg RE, Maier HJ, et al. Fatigue behavior of As-built selective laser melted titanium scaffolds with sheet-based gyroid microarchitecture for bone tissue engineering. Acta Biomater 2019;94:610–26. https://doi.org/10.1016/j.actbio.2019.05.046.

[65] Raghavendra S, Molinari A, Dallago M, Zappini G, Zanini F, Carmignato S, et al. Uniaxial static mechanical properties of regular, irregular and random additively manufactured cellular materials: Nominal vs. real geometry. Forces Mech 2021;2:100007. https://doi.org/10.1016/j.finmec.2020.100007.

[66] Bellini C, Borrelli R, Di Cocco V, Franchitti S, Iacoviello F, Mocanu LP, et al. Failure energy and stiffness of titanium lattice specimens produced by electron beam melting process. Mater Des Process Commun 2021;3(6). https://doi.org/10.1002/mdp2.v3.610.1002/mdp2.268.

[67] Bellini C, Borrelli R, Di Cocco V, Franchitti S, Iacoviello F, Sorrentino L. Bending properties of titanium lattice structures produced by electron beam melting process. Fatigue Fract Eng Mater Struct 2021;44(7):1961–70.

[68] Queheillalt DT, Murty Y, Wadley HNG. Mechanical properties of an extruded pyramidal lattice truss sandwich structure. Scr Mater 2008;58(1):76–9. https://doi.org/10.1016/j.scriptamat.2007.08.041.

[69] Imwinkelried T. Mechanical properties of open-pore titanium foam. J Biomed Mater Res Part A 2007;81A(4):964–70. https://doi.org/10.1002/jbm.a.31118.

[70] Yánez A, Cuadrado A, Martel O, Afonso H, Monopoli D. Gyroid porous titanium structures: A versatile solution to be used as scaffolds in bone defect reconstruction. Mater Des 2018;140:21–9. https://doi.org/10.1016/j.matdes.2017.11.050.

[71] Dallago M, Fontanari V, Torresani E, Leoni M, Pederzolli C, Potrich C, et al. Fatigue and biological properties of Ti-6Al-4V ELI cellular structures with variously arranged cubic cells made by selective laser melting. J Mech Behav Biomed Mater 2018;78:381–94. https://doi.org/10.1016/j.jmbbm.2017.11.044.

[72] du Plessis A, Yadroitsava I, Yadroitsev I. Ti6Al4V lightweight lattice structures manufactured by laser powder bed fusion for load-bearing applications. Opt Laser Technol 2018;108:521–8.

[73] Drücker S, Schulze M, Ipsen H, Bandegani L, Hoch H, Kluge M, et al. Experimental and numerical mechanical characterization of additively manufactured Ti6Al4V lattice structures considering progressive damage. Int J Mech Sci 2021;189:105986. https://doi.org/10.1016/j.ijmecsci.2020.105986.

[74] du Plessis A, Yadroitsava I, Yadroitsev I, le Roux SG, Blaine DC. Numerical comparison of lattice unit cell designs for medical implants by additive manufacturing. Virtual Phys Prototyp 2018;13(4):266–81. https://doi.org/10.1080/17452759.2018.1491713.

[75] Pan C, Han Y, Lu J. Design and optimization of lattice structures: a review. Appl Sci 2020;10:6374. https://doi.org/10.3390/app10186374.

[76] Vilardell AM, Takezawa A, du Plessis A, Takata N, Krakhmalev P, Kobashi M, et al. Topology optimization and characterization of Ti6Al4V ELI cellular lattice structures by laser powder bed fusion for biomedical applications. Mater Sci Eng A 2019;766:138330. https://doi.org/10.1016/j.msea.2019.138330.

[77] Gu DD, Meiners W, Wissenbach K, Poprawe R. Laser additive manufacturing of metallic components: materials, processes and mechanisms. Int Mater Rev 2012;57(3):133–64. https://doi.org/10.1179/1743280411Y.0000000014.

[78] Milewski JO. Additive Manufacturing of Metals, Springer International Publishing. Cham 2017. https://doi.org/10.1007/978-3-319-58205-4.

[79] Herzog D, Seyda V, Wycisk E, Emmelmann C. Additive manufacturing of metals. Acta Mater 2016;117:371–92. https://doi.org/10.1016/j.actamat.2016.07.019.

[80] Bartlett JL, Li X. An overview of residual stresses in metal powder bed fusion. Addit Manuf 2019;27:131–49. https://doi.org/10.1016/j.addma.2019.02.020.

[81] Murr LE, Gaytan SM, Ramirez DA, Martinez E, Hernandez J, Amato KN, et al. Metal fabrication by additive manufacturing using laser and electron beam melting technologies. J Mater Sci Technol 2012;28(1):1–14. https://doi.org/10.1016/S1005-0302(12)60016-4.

[82] Raghavan S, Nai MLS, Wang P, Sin WJ, Li T, Wei J. Heat treatment of electron beam melted (EBM) Ti-6Al-4V: microstructure to mechanical property correlations. Rapid Prototyp J 2018;24(4):774–83. https://doi.org/10.1108/RPJ-05-2016-0070.

[83] Ameen W, Mohammed MK, Al-Ahmari A, Ahmed N, Mian SH. Investigation of support structure parameters and their affects during additive manufacturing of Ti6Al4V alloy via electron beam melting. Proc Inst Mech Eng Part L J Mater Des Appl 2020. https://doi.org/10.1177/1464420720981668.

[84] Frazier WE. Metal additive manufacturing: a review. J Mater Eng Perform 2014;23(6):1917–28. https://doi.org/10.1007/s11665-014-0958-z.

[85] Yadroitsev I, Yadroitsava I. A step-by-step guide to the L-PBF process. In: Fundam. Laser Powder Bed Fusion Met., Elsevier, 2021: pp. 39–77. Doi: 10.1016/B978-0-12-824090-8.00026-3.

[86] Oliveira JP, LaLonde AD, Ma J. Processing parameters in laser powder bed fusion metal additive manufacturing. Mater Des 2020;193:108762. https://doi.org/10.1016/j.matdes.2020.108762.

[87] Maleki E, Bagherifard S, Bandini M, Guagliano M. Surface post-treatments for metal additive manufacturing: Progress, challenges, and opportunities. Addit Manuf 2021;37:101619. https://doi.org/10.1016/j.addma.2020.101619.

[88] Bagherifard S, Guagliano M. Post-processing. In: Fundam. Laser Powder Bed Fusion Met., Elsevier, 2021: pp. 327–348. Doi: 10.1016/B978-0-12-824090-8.00001-9.

[89] Sanaei N, Fatemi A, Phan N. Defect characteristics and analysis of their variability in metal L-PBF additive manufacturing. Mater Des 2019;182:108091. https://doi.org/10.1016/j.matdes.2019.108091.

[90] du Plessis A, Yadroitsev I, Yadroitsava I, Le Roux SG. X-ray microcomputed tomography in additive manufacturing: a review of the current technology and applications. 3D Printing and Additive Manufacturing 2018;5(3):227–47.

[91] Du Plessis A, MacDonald E, Waller JM, Berto F. Non-destructive testing of parts produced by laser powder bed fusion. Fundam Laser Powder Bed Fusion Met 2021:277–300. https://doi.org/10.1016/b978-0-12-824090-8.00016-0.

[92] Yadroitsev I, Krakhmalev P, Yadroitsava I, Du Plessis A. Qualification of Ti6Al4V ELI alloy produced by laser powder bed fusion for biomedical applications. JOM 2018;70(3):372–7. https://doi.org/10.1007/s11837-017-2655-5.

[93] Romano S, Brandão A, Gumpinger J, Gschweitl M, Beretta S. Qualification of AM parts: Extreme value statistics applied to tomographic measurements. Mater Des 2017;131:32–48. https://doi.org/10.1016/j.matdes.2017.05.091.

[94] Seifi M, Salem A, Beuth J, Harrysson O, Lewandowski JJ. Overview of materials qualification needs for metal additive manufacturing. JOM 2016;68(3):747–64. https://doi.org/10.1007/s11837-015-1810-0.

[95] Seifi M, Gorelik M, Waller J, Hrabe N, Shamsaei N, Daniewicz S, et al. Progress towards metal additive manufacturing standardization to support qualification and certification. JOM 2017;69(3):439–55. https://doi.org/10.1007/s11837-017-2265-2.

[96] Murchio S, Dallago M, Zanini F, Carmignato S, Zappini G, Berto F, et al. Additively manufactured Ti–6Al–4V thin struts via laser powder bed fusion: Effect of building orientation on geometrical accuracy and mechanical properties. J Mech Behav Biomed Mater 2021;119:104495. https://doi.org/10.1016/j.jmbbm.2021.104495.

[97] Persenot T, Burr A, Martin G, Buffiere JY, Dendievel R, Maire E. Effect of build orientation on the fatigue properties of as-built Electron Beam Melted Ti-6Al-4V alloy. Int J Fatigue 2019;118:65–76. https://doi.org/10.1016/j.ijfatigue.2018.08.006.

[98] Hunter LW, Brackett D, Brierley N, Yang J, Attallah MM. Assessment of trapped powder removal and inspection strategies for powder bed fusion techniques. Int J Adv Manuf Technol 2020;106(9-10):4521–32. https://doi.org/10.1007/s00170-020-04930-w.

[99] du Plessis A, Razavi SMJ, Berto F. The effects of microporosity in struts of gyroid lattice structures produced by laser powder bed fusion. Mater Des 2020;194:108899. https://doi.org/10.1016/j.matdes.2020.108899.

[100] Ahmadi S, Yavari S, Wauthle R, Pouran B, Schrooten J, Weinans H, et al. Additively manufactured open-cell porous biomaterials made from six different space-filling unit cells: the mechanical and morphological properties. Materials (Basel) 2015;8(4):1871–96. https://doi.org/10.3390/ma8041871.

[101] Parthasarathy J, Starly B, Raman S, Christensen A. Mechanical evaluation of porous titanium (Ti6Al4V) structures with electron beam melting (EBM). J Mech Behav Biomed Mater 2010;3(3):249–59.

[102] Sallica-Leva E, Jardini AL, Fogagnolo JB. Microstructure and mechanical behavior of porous Ti–6Al–4V parts obtained by selective laser melting. J Mech Behav Biomed Mater 2013;26:98–108. https://doi.org/10.1016/J.JMBBM.2013.05.011.

[103] Ahmadi SM, Campoli G, Amin Yavari S, Sajadi B, Wauthle R, Schrooten J, et al. Mechanical behavior of regular open-cell porous biomaterials made of diamond lattice unit cells. J Mech Behav Biomed Mater 2014;34:106–15.

[104] Smith M, Guan Z, Cantwell WJ. Finite element modelling of the compressive response of lattice structures manufactured using the selective laser melting technique. Int J Mech Sci 2013;67:28–41. https://doi.org/10.1016/J.IJMECSCI.2012.12.004.

[105] Shinde S, Srivastava A, Sumant O. Medical Implant Market Size | Industry Forecast by 2027, 2020. https://www.alliedmarketresearch.com/medical-implants-market (accessed June 26, 2021).

[106] Dong G, Tang Y, Zhao YF. A survey of modeling of lattice structures fabricated by additive manufacturing. J Mech Des Trans ASME 2017;139:100906. https://doi.org/10.1115/1.4037305.

[107] Yang E, Leary M, Lozanovski B, Downing D, Mazur M, Sarker A, et al. Effect of geometry on the mechanical properties of Ti-6Al-4V Gyroid structures fabricated via SLM: A numerical study. Mater Des 2019;184:108165. https://doi.org/10.1016/j.matdes.2019.108165.

[108] Ataee A, Li Y, Fraser D, Song G, Wen C. Anisotropic Ti-6Al-4V gyroid scaffolds manufactured by electron beam melting (EBM) for bone implant applications. Mater Des 2018;137:345–54. https://doi.org/10.1016/j.matdes.2017.10.040.

[109] Yánez A, Herrera A, Martel O, Monopoli D, Afonso H. Compressive behaviour of gyroid lattice structures for human cancellous bone implant applications. Mater Sci Eng C 2016;68:445–8. https://doi.org/10.1016/j.msec.2016.06.016.

[110] Arabnejad Khanoki S, Pasini D. Multiscale design and multiobjective optimization of orthopedic hip implants with functionally graded cellular material. J Biomech Eng 2012;134. https://doi.org/10.1115/1.4006115.

[111] Khanoki SA, Pasini D. The fatigue design of a bone preserving hip implant with functionally graded cellular material. J Med Devices, Trans ASME 2013;7. https://doi.org/10.1115/1.4024310.

[112] Zadpoor AA, Malda J. Additive manufacturing of biomaterials, tissues, and organs. Ann Biomed Eng 2017;45(1):1–11. https://doi.org/10.1007/s10439-016-1719-y.

[113] Wang Y, Arabnejad S, Tanzer M, Pasini D. Hip implant design with three-dimensional porous architecture of optimized graded density. J Mech Des Trans ASME 2018;140:1–13. https://doi.org/10.1115/1.4041208.

[114] Bici M, Brischetto S, Campana F, Ferro CG, Seclì C, Varetti S, et al. Development of a multifunctional panel for aerospace use through SLM additive manufacturing. Procedia CIRP 2018;67:215–20. https://doi.org/10.1016/j.procir.2017.12.202.

[115] Bühring J, Nuño M, Schröder K-U. Additive manufactured sandwich structures: Mechanical characterization and usage potential in small aircraft. Aerosp Sci Technol 2021;111:106548. https://doi.org/10.1016/j.ast.2021.106548.

[116] Ferro C, Varetti S, Vitti F, Maggiore P, Lombardi M, Biamino S, et al. A robust multifunctional sandwich panel design with trabecular structures by the use of additive manufacturing technology for a new de-icing system. Technologies 2017;5(2):35. https://doi.org/10.3390/technologies5020035.

[117] Yazdani Sarvestani H, Akbarzadeh AH, Niknam H, Hermenean K. 3D printed architected polymeric sandwich panels: Energy absorption and structural performance. Compos Struct 2018;200:886–909. https://doi.org/10.1016/j.compstruct.2018.04.002.

[118] Monteiro JG, Sardinha M, Alves F, Ribeiro AR, Reis L, Deus AM, et al. Evaluation of the effect of core lattice topology on the properties of sandwich panels produced by additive manufacturing. Proc Inst Mech Eng Part L J Mater Des Appl 2021;235(6):1312–24. https://doi.org/10.1177/1464420720958015.

[119] Zaharia SM, Enescu LA, Pop MA. Mechanical performances of lightweight sandwich structures produced by material extrusion-based additive manufacturing. Polymers (Basel) 2020;12:1740. https://doi.org/10.3390/POLYM12081740.

[120] Cheng L, Zhang Pu, Biyikli E, Bai J, Robbins J, To A. Efficient design optimization of variable-density cellular structures for additive manufacturing: Theory and experimental validation. Rapid Prototyp J 2017;23(4):660–77. https://doi.org/10.1108/RPJ-04-2016-0069.

[121] Zhang Pu, Toman J, Yu Y, Biyikli E, Kirca M, Chmielus M, et al. Efficient design-optimization of variable-density hexagonal cellular structure by additive manufacturing: Theory and validation. J Manuf Sci Eng Trans ASME 2015;137(2). https://doi.org/10.1115/1.4028724.

[122] Garner E, Kolken HMA, Wang CCL, Zadpoor AA, Wu J. Compatibility in microstructural optimization for additive manufacturing. Addit Manuf 2019;26:65–75. https://doi.org/10.1016/j.addma.2018.12.007.

[123] Li D, Liao W, Dai N, Xie YM. Anisotropic design and optimization of conformal gradient lattice structures. CAD Comput Aided Des 2020;119:102787. https://doi.org/10.1016/j.cad.2019.102787.

[124] Daynes S, Feih S, Lu WF, Wei J. Optimisation of functionally graded lattice structures using isostatic lines. Mater Des 2017;127:215–23. https://doi.org/10.1016/j.matdes.2017.04.082.

[125] Daynes S, Feih S, Lu WF, Wei J. Design concepts for generating optimised lattice structures aligned with strain trajectories. Comput Methods Appl Mech Eng 2019;354:689–705. https://doi.org/10.1016/j.cma.2019.05.053.

[126] Dong G, Tang Y, Li D, Zhao YF. Design and optimization of solid lattice hybrid structures fabricated by additive manufacturing. Addit Manuf 2020;33:101116. https://doi.org/10.1016/j.addma.2020.101116.

[127] Future Powertrains | IAV Sees Huge Potential With 3D-Printed Pistons | WardsAuto, (n.d.). https://www.wardsauto.com/engines/iav-sees-huge-potential-3d-printed-pistons (accessed June 26, 2021).

[128] Kantareddy SNR, Roh BM, Simpson TW, Joshi S, Dickman C, Lehtihet EA. Saving weight with metallic lattice structures: Design challenges with a real-world example. Solid Free. Fabr. 2016 Proc. 27th Annu. Int. Solid Free. Fabr. Symp. - An Addit. Manuf. Conf. SFF 2016. (2016) 2139–2154.

[129] Hands CH, du Plessis A, Minnaar N, Blakey-Milner BA, Burger E. Can Additive Manufacturing Help Win the Race?, 2018. Doi: 10.20944/PREPRINTS201811.0040.V1.

[130] Design for additive manufacturing | Design | LLC Fitnik services, (n.d.). http://fitnik.tech/de/services/design/design_for_additive_manufacturing (accessed June 26, 2021).

[131] A 63% Lighter Titanium Aerospace Part | Materialise - Innovators you can count on, (n.d.). https://www.materialise.com/en/cases/a-63-lighter-titanium-aerospace-part (accessed June 26, 2021).

[132] Spider bracket: Mesh architectural Altair materialise, (n.d.). https://resources.renishaw.com/gen/details/spider-bracket–78295 (accessed June 14, 2021).

[133] Riddell Partners with Carbon® to Produce First-Ever 3D Printed Football Helmet Liner - Carbon, (n.d.). https://www.carbon3d.com/news/riddell-partners-with-carbon-to-produce-next-gen-football-helmet/ (accessed February 11, 2019).

[134] adidas Futurecraft: The Ultimate 3D-Printed Personalized Shoe | Materialise - Innovators you can count on, (n.d.). https://www.materialise.com/en/cases/adidas-futurecraft-ultimate-3d-printed-personalized-shoe (accessed February 11, 2019).

[135] Lu G, Yu TX. Energy absorption of structures and materials, 2003. Doi: 10.1533/9781855738584.268.

[136] Astori P, Zanella M, Bernardini M. Validation of numerical models of a rotorcraft crashworthy seat and subfloor. Aerospace 2020;7:1–17. https://doi.org/10.3390/aerospace7120174.

[137] Naghavi Zadeh M, Alijani F, Chen X, Dayyani I, Yasaee M, Mirzaali MJ, et al. Dynamic characterization of 3D printed mechanical metamaterials with tunable elastic properties. Appl Phys Lett 2021;118(21):211901. https://doi.org/10.1063/5.0047617.

[138] Kolken HMA, Zadpoor AA. Auxetic mechanical metamaterials. RSC Adv 2017;7(9):5111–29. https://doi.org/10.1039/C6RA27333E.

[139] Chen BC, Zou M, Liu GM, Song JF, Wang HX. Experimental study on energy absorption of bionic tubes inspired by bamboo structures under axial crushing. Int J Impact Eng 2018;115:48–57. https://doi.org/10.1016/j.ijimpeng.2018.01.005.

[140] Tang Z, Liu S, Zhang Z. Analysis of energy absorption characteristics of cylindrical multi-cell columns. Thin-Walled Struct 2013;62:75–84. https://doi.org/10.1016/j.tws.2012.05.019.

[141] Yang K, Xu S, Zhou S, Shen J, Xie YM. Design of dimpled tubular structures for energy absorption. Thin-Walled Struct 2017;112:31–40. https://doi.org/10.1016/j.tws.2016.12.003.

[142] Xiang Y, Wang M, Yu T, Yang L. Key performance indicators of tubes and foam-filled tubes used as energy absorbers. Int J Appl Mech 2015;7:1–20. https://doi.org/10.1142/S175882511550060X.

[143] Wu F, Xiao X, Yang J, Gao X. Quasi-static axial crushing behaviour and energy absorption of novel metal rope crochet-sintered mesh tubes. Thin-Walled Struct 2018;127:120–34. https://doi.org/10.1016/j.tws.2018.02.004.

[144] Yin S, Li J, Liu B, Meng K, Huan Y, Nutt SR, et al. Honeytubes: Hollow lattice truss reinforced honeycombs for crushing protection. Compos Struct 2017;160:1147–54. https://doi.org/10.1016/j.compstruct.2016.11.007.

[145] Harris JA, Winter RE, McShane GJ. Impact response of additively manufactured metallic hybrid lattice materials. Int J Impact Eng 2017;104:177–91. https://doi.org/10.1016/j.ijimpeng.2017.02.007.

[146] Sun G, Jiang H, Fang J, Li G, Li Q. Crashworthiness of vertex based hierarchical honeycombs in out-of-plane impact. Mater Des 2016;110:705–19. https://doi.org/10.1016/j.matdes.2016.08.032.

[147] Ha NS, Lu G, Xiang X. Energy absorption of a bio-inspired honeycomb sandwich panel. J Mater Sci 2019;54(8):6286–300. https://doi.org/10.1007/s10853-018-3163-x.

[148] Alantali A, Alia RA, Umer R, Cantwell WJ. Energy absorption in aluminium honeycomb cores reinforced with carbon fibre reinforced plastic tubes. J Sandw Struct Mater 2019;21(8):2801–15. https://doi.org/10.1177/1099636217727145.

[149] Sun Y, Li QM. Dynamic compressive behaviour of cellular materials: A review of phenomenon, mechanism and modelling. Int J Impact Eng 2018;112:74–115. https://doi.org/10.1016/j.ijimpeng.2017.10.006.

[150] Branch B, Ionita A, Patterson BM, Schmalzer A, Clements B, Mueller A, et al. A comparison of shockwave dynamics in stochastic and periodic porous polymer architectures. Polymer (Guildf) 2019;160:325–37. https://doi.org/10.1016/j.polymer.2018.10.074.

[151] Rakow JF, Waas AM. Size effects and the shear response of aluminum foam. Mech Mater 2005;37(1):69–82. https://doi.org/10.1016/j.mechmat.2003.12.002.

[152] Li QM, Magkiriadis I, Harrigan JJ. Compressive strain at the onset of densification of cellular solids. J Cell Plast 2006;42(5):371–92. https://doi.org/10.1177/0021955X06063519.

[153] Schaedler TA, Ro CJ, Sorensen AE, Eckel Z, Yang SS, Carter WB, et al. Designing metallic microlattices for energy absorber applications. Adv Eng Mater 2014. https://doi.org/10.1002/adem.201300206.

[154] Xu F, Zhang X, Zhang H. A review on functionally graded structures and materials for energy absorption. Eng Struct 2018;171:309–25. https://doi.org/10.1016/j.engstruct.2018.05.094.

[155] Ha NS, Lu G. A review of recent research on bio-inspired structures and materials for energy absorption applications. Compos Part B Eng 2020;181:107496. https://doi.org/10.1016/j.compositesb:2019.107496.

[156] Liang Y, Zhou W, Liu Y, Li Z, Yang Y, Xi H, et al. Energy absorption and deformation behavior of 3D printed triply periodic minimal surface stainless steel cellular structures under compression. Steel Res Int 2021;92(3):2000411. https://doi.org/10.1002/srin.v92.310.1002/srin.202000411.

[157] Zhang L, Feih S, Daynes S, Chang S, Wang MY, Wei J, et al. Energy absorption characteristics of metallic triply periodic minimal surface sheet structures under compressive loading. Addit Manuf 2018;23:505–15. https://doi.org/10.1016/j.addma.2018.08.007.

[158] Liu X, Suzuki A, Takata N, Kobashi M, Kato M. Dual plateau stress of C15-type topologically close-packed lattice structures additive-manufactured by laser powder bed fusion. Scr Mater 2021;202:114003. https://doi.org/10.1016/j.scriptamat.2021.114003.

[159] Leary M, Mazur M, Williams H, Yang E, Alghamdi A, Lozanovski B, et al. Inconel 625 lattice structures manufactured by selective laser melting (SLM): Mechanical properties, deformation and failure modes. Mater Des 2018;157:179–99. https://doi.org/10.1016/j.matdes.2018.06.010.

[160] Maskery I, Aboulkhair NT, Aremu AO, Tuck CJ, Ashcroft IA. Compressive failure modes and energy absorption in additively manufactured double gyroid lattices. Addit Manuf 2017;16:24–9. https://doi.org/10.1016/J.ADDMA.2017.04.003.

[161] Harris JA, McShane GJ. Metallic stacked origami cellular materials: Additive manufacturing, properties, and modelling. Int J Solids Struct 2020;185–186: 448–66. https://doi.org/10.1016/j.ijsolstr.2019.09.007.

[162] Ma Z, Zhang DZ, Liu F, Jiang J, Zhao M, Zhang T. Lattice structures of Cu-Cr-Zr copper alloy by selective laser melting: Microstructures, mechanical properties and energy absorption. Mater Des 2020;187:108406. https://doi.org/10.1016/j.matdes.2019.108406.

[163] Liu Y, Schaedler TA, Jacobsen AJ, Chen X. Quasi-static energy absorption of hollow microlattice structures. Compos Part B Eng 2014;67:39–49. https://doi.org/10.1016/j.compositesb.2014.06.024.

[164] Schaedler TA, Ro CJ, Sorensen AE, Eckel Z, Yang SS, Carter WB, Jacobsen AJ. Designing metallic microlattices for energy absorber applications **, (2014) 276–283. Doi: 10.1002/adem.201300206.

[165] Lam Q, Patil D, Le T, Eppley T, Salti Z, Goss D, et al. An examination of the low strain rate sensitivity of additively manufactured polymer, composite and metallic honeycomb structures. Materials (Basel) 2019;12(20):3455. https://doi.org/10.3390/ma12203455.

[166] Phani AS, Hussein MI. Dynamics of Lattice Materials. John Wiley @ Sons Ltd 2017. https://doi.org/10.1002/9781118729588.

[167] Sadeghi H, Bhate D, Abraham J, Magallanes J. Quasi-static and dynamic behavior of additively manufactured metallic lattice cylinders. In: 20th Bienn. Conf. APS Top. Gr. Shock Compression Condens. Matter, 2018. Doi: 10.1063/1.5044838.

[168] Ozdemir Z, Hernandez-Nava E, Tyas A, Warren JA, Fay SD, Goodall R, et al. Energy absorption in lattice structures in dynamics: Experiments. Int J Impact Eng 2016;89:49–61. https://doi.org/10.1016/j.ijimpeng.2015.10.007.

[169] Hazeli K, Babamiri BB, Indeck J, Minor A, Askari H. Microstructure-topology relationship effects on the quasi-static and dynamic behavior of additively manufactured lattice structures. Mater Des 2019;176:107826. https://doi.org/10.1016/j.matdes.2019.107826.

[170] Smith M, Cantwell WJ, Guan Z, Tsopanos S, Theobald MD, Nurick GN, et al. The quasi-static and blast response of steel lattice structures. J Sandw Struct Mater 2011;13(4):479–501. https://doi.org/10.1177/1099636210388983.

[171] McKown S, Shen Y, Brookes WK, Sutcliffe CJ, Cantwell WJ, Langdon GS, et al. The quasi-static and blast loading response of lattice structures. Int J Impact Eng 2008;35(8):795–810. https://doi.org/10.1016/j.ijimpeng.2007.10.005.

[172] Novak N, Al-Ketan O, Krstulović-Opara L, Rowshan R, Abu Al-Rub RK, Vesenjak M, et al. Quasi-static and dynamic compressive behaviour of sheet TPMS cellular structures. Compos Struct 2021;266:113801. https://doi.org/10.1016/j.compstruct.2021.113801.

[173] Ramadani R, Pal S, Kegl M, Predan J, Drstvenšek I, Pehan S, et al. Topology optimization and additive manufacturing in producing lightweight and low vibration gear body. Int J Adv Manuf Technol 2021;113(11-12):3389–99.

[174] Ramadani R, Belsak A, Kegl M, Predan J, Pehan S. Topology optimization based design of lightweight and low vibration gear bodies. Artic Int J Simul Model 2018;17(1):92–104. https://doi.org/10.2507/IJSIMM17(1)419.

[175] Zochowski P, Bajkowski M, Grygoruk R, Magier M, Burian W, Pyka D, et al. Ballistic impact resistance of bulletproof vest inserts containing printed titanium structures. Metals (Basel) 2021;11(2):225. https://doi.org/10.3390/met11020225.

[176] Tomblin J, Lacy T, Smith B, Hooper S, Vizzini A, Lee S. Review of damage tolerance for composite sandwich airframe structures, 1999. https://www.researchgate.net/publication/235158415 (accessed July 1, 2021).

[177] Baroutaji A, Arjunan A, Robinson J, Ramadan M, Abdelkareem MA, Olabi A-G. Metamaterial for crashworthiness applications. In: Ref. Modul. Mater. Sci. Mater. Eng., Elsevier; 2021. Doi: 10.1016/b978-0-12-815732-9.00092-9.

[178] Zhou S, Usman I, Wang Y, Pan A. 3D printing for rechargeable lithium metal batteries. Energy Storage Mater 2021;38:141–56. https://doi.org/10.1016/j.ensm.2021.02.041.

[179] Dada M, Popoola P. Additive manufacturing of 3D microlattice lithium-ion battery electrodes: a review. In: Miner. Met. Mater. Ser., Springer Science and Business Media Deutschland GmbH; 2021: pp. 111–120. Doi: 10.1007/978-3-030-65647-8_8.

[180] Yadollahi A, Shamsaei N. Additive manufacturing of fatigue resistant materials: Challenges and opportunities. Int J Fatigue 2017;98:14–31. https://doi.org/10.1016/j.ijfatigue.2017.01.001.

[181] Zerbst U, Madia M, Klinger C, Bettge D, Murakami Y. Defects as a root cause of fatigue failure of metallic components. I: Basic aspects. Eng Fail Anal 2019;97: 777–92. https://doi.org/10.1016/j.engfailanal.2019.01.055.

[182] du Plessis A, Beretta S. Killer notches: The effect of as-built surface roughness on fatigue failure in AlSi10Mg produced by laser powder bed fusion. Addit Manuf 2020;35:101424. https://doi.org/10.1016/j.addma.2020.101424.

[183] Pyka G, Kerckhofs G, Papantoniou I, Speirs M, Schrooten J, Wevers M. Surface roughness and morphology customization of additive manufactured open porous Ti6Al4V structures. Materials (Basel) 2013;6:4737–57. https://doi.org/10.3390/ma6104737.

[184] Castro APG, Pires T, Santos JE, Gouveia BP, Fernandes PR. Permeability versus design in TPMS scaffolds. Materials (Basel) 2019;12. https://doi.org/10.3390/ma12081313.

[185] Timercan A, Sheremetyev V, Brailovski V. Mechanical properties and fluid permeability of gyroid and diamond lattice structures for intervertebral devices: Functional requirements and comparative analysis. Sci Technol Adv Mater 2021;22(1):285–300. https://doi.org/10.1080/14686996.2021.1907222.

[186] Ma S, Tang Q, Han X, Feng Q, Song J, Setchi R, et al. Manufacturability, mechanical properties, mass-transport properties and biocompatibility of triply periodic minimal surface (TPMS) porous scaffolds fabricated by selective laser melting. Mater Des 2020;195:109034. https://doi.org/10.1016/j.matdes.2020.109034.

[187] Barba D, Alabort E, Reed RC. Synthetic bone: Design by additive manufacturing. Acta Biomater 2019;97:637–56. https://doi.org/10.1016/j.actbio.2019.07.049.

[188] Xu P, Yu B. Developing a new form of permeability and Kozeny-Carman constant for homogeneous porous media by means of fractal geometry. Adv Water Resour 2008;31(1):74–81. https://doi.org/10.1016/j.advwatres.2007.06.003.

[189] Lv Y, Wang B, Liu G, Tang Y, Lu E, Xie K, et al. Metal material, properties and design methods of porous biomedical scaffolds for additive manufacturing: a review. Front Bioeng Biotechnol 2021;9. https://doi.org/10.3389/fbioe.2021.641130.

[190] Caiazzo F, Alfieri V, Bujazha BD. Additive manufacturing of biomorphic scaffolds for bone tissue engineering. Int J Adv Manuf Technol 2021;113(9-10): 2909–23. https://doi.org/10.1007/s00170-021-06773-5.

[191] Kemppainen JM, Hollister SJ. Differential effects of designed scaffold permeability on chondrogenesis by chondrocytes and bone marrow stromal cells. Biomaterials 2010;31(2):279–87. https://doi.org/10.1016/j.biomaterials.2009.09.041.

[192] Ali D, Ozalp M, Blanquer SBG, Onel S. Permeability and fluid flow-induced wall shear stress in bone scaffolds with TPMS and lattice architectures: A CFD analysis. Eur J Mech B/Fluids 2020;79:376–85. https://doi.org/10.1016/j.euromechflu.2019.09.015.

[193] Montazerian H, Mohamed MGA, Montazeri MM, Kheiri S, Milani AS, Kim K, et al. Permeability and mechanical properties of gradient porous PDMS scaffolds fabricated by 3D-printed sacrificial templates designed with minimal surfaces. Acta Biomater 2019;96:149–60. https://doi.org/10.1016/j.actbio.2019.06.040.

[194] Zhianmanesh M, Varmazyar M, Montazerian H. Fluid permeability of graded porosity scaffolds architectured with minimal surfaces. ACS Biomater Sci Eng 2019;5(3):1228–37. https://doi.org/10.1021/acsbiomaterials.8b01400.

[195] Loh GH, Pei E, Harrison D, Monzón MD. An overview of functionally graded additive manufacturing. Addit Manuf 2018;23:34–44. https://doi.org/10.1016/j.addma.2018.06.023.

[196] Zhang XY, Fang G, Leeflang S, Zadpoor AA, Zhou J. Topological design, permeability and mechanical behavior of additively manufactured functionally graded porous metallic biomaterials. Acta Biomater 2019;84:437–52. https://doi.org/10.1016/j.actbio.2018.12.013.

[197] Jafari D, Wits WW. The utilization of selective laser melting technology on heat transfer devices for thermal energy conversion applications: A review. Renew Sustain Energy Rev 2018;91:420–42. https://doi.org/10.1016/J.RSER.2018.03.109.

[198] Jafari D, Wits WW, Geurts BJ. Metal 3D-printed wick structures for heat pipe application: Capillary performance analysis. Appl Therm Eng 2018;143:403–14. https://doi.org/10.1016/j.applthermaleng.2018.07.111.

[199] Kirsch KL, Snyder JC, Stimpson CK, Thole KA, Mongillo D. Repeatability in performance of micro cooling geometries manufactured with laser powder bed fusion. In: 53rd AIAA/SAE/ASEE Jt. Propuls. Conf. 2017, American Institute of Aeronautics and Astronautics Inc, AIAA, 2017. Doi: 10.2514/6.2017-4706.

[200] Snyder JC, Stimpson CK, Thole KA, Mongillo DJ. Build direction effects on microchannel tolerance and surface roughness. J Mech Des 2015;137:111411. https://doi.org/10.1115/1.4031071.

[201] Nafis BM, Whitt R, Iradukunda A-C, Huitink D. Additive manufacturing for enhancing thermal dissipation in heat sink implementation: a review. Heat Transf Eng 2021;42(12):967–84. https://doi.org/10.1080/01457632.2020.1766246.

[202] Son YW, Kim T, Lu TJ, Chang S-M. On thermally managing lithium-ion battery cells by air-convection aspirated in tetrahedral lattice porous cold plates. Appl Therm Eng 2021;189:116711. https://doi.org/10.1016/j.applthermaleng.2021.116711.

[203] Ambrosetti M, Groppi G, Schwieger W, Tronconi E, Freund H. Packed periodic open cellular structures – an option for the intensification of non-adiabatic catalytic processes. Chem Eng Process - Process Intensif 2020;155:108057. https://doi.org/10.1016/j.cep.2020.108057.

[204] 3D printing a rocket engine, (n.d.). https://www.etmm-online.com/3d-printing-a-rocket-engine-a-886960/ (accessed June 28, 2021).

[205] Purdue students design award-winning 3D printed heat sink - 3D Printing Industry, (n.d.). https://3dprintingindustry.com/news/purdue-students-design-award-winning-3d-printed-heat-sink-174409/ (accessed June 28, 2021).

[206] Top 5 Advanced Heat Exchanger Design Videos | nTopology, (n.d.). https://ntopology.com/blog/2020/10/14/top-5-heat-exchanger-videos/ (accessed June 28, 2021).

[207] Designing the Optimal Heat Exchanger | nTopology, (n.d.). https://ntopology.com/blog/2019/12/16/heat-exchanger-design-high-performance/ (accessed June 28, 2021).

[208] Betatype and Progressive Technology heat up F1 additive manufacturing - 3D Printing Industry, (n.d.). https://3dprintingindustry.com/news/betatype-progressive-technology-heat-f1-additive-manufacturing-131102/ (accessed June 28, 2021).

[209] Zhao L, Ryan SM, Ortega JK, Ha S, Sharp KW, Guest JK, et al. Experimental investigation of 3D woven Cu lattices for heat exchanger applications. Int J Heat Mass Transf 2016;96:296–311. https://doi.org/10.1016/j.ijheatmasstransfer.2015.12.059.

[210] Liang D, Chen W, Ju Y, Chyu MK. Comparing endwall heat transfer among staggered pin fin, Kagome and body centered cubic arrays. Appl Therm Eng 2021;185:116306. https://doi.org/10.1016/j.applthermaleng.2020.116306.

[211] Chaudhari A, Ekade P, Krishnan S. Experimental investigation of heat transfer and fluid flow in octet-truss lattice geometry. Int J Therm Sci 2019;143:64–75. https://doi.org/10.1016/j.ijthermalsci.2019.05.003.

[212] Catchpole-Smith S, Sélo RRJ, Davis AW, Ashcroft IA, Tuck CJ, Clare A. Thermal conductivity of TPMS lattice structures manufactured via laser powder bed fusion. Addit Manuf 2019;30:100846. https://doi.org/10.1016/j.addma.2019.100846.

[213] Kaur I, Singh P. Critical evaluation of additively manufactured metal lattices for viability in advanced heat exchangers. Int J Heat Mass Transf 2021;168:120858. https://doi.org/10.1016/j.ijheatmasstransfer.2020.120858.

[214] Ekade P, Krishnan S. Fluid flow and heat transfer characteristics of octet truss lattice geometry. Int J Therm Sci 2019;137:253–61. https://doi.org/10.1016/j.ijthermalsci.2018.11.031.

[215] Broughton J, Joshi YK. Comparison of single-phase convection in additive manufactured versus traditional metal foams. J Heat Transfer 2020;142:1–12. https://doi.org/10.1115/1.4046972.

[216] Son KN, Weibel JA, Kumaresan V, Garimella SV. Design of multifunctional lattice-frame materials for compact heat exchangers. Int J Heat Mass Transf 2017;115:619–29. https://doi.org/10.1016/j.ijheatmasstransfer.2017.07.073.

[217] Attarzadeh R, Rovira M, Duwig C. Design analysis of the "Schwartz D" based heat exchanger: A numerical study. Int J Heat Mass Transf 2021;177:121415. https://doi.org/10.1016/j.ijheatmasstransfer.2021.121415.

[218] Bracconi M, Ambrosetti M, Maestri M, Groppi G, Tronconi E. A fundamental analysis of the influence of the geometrical properties on the effective thermal conductivity of open-cell foams. Chem Eng Process - Process Intensif 2018;129:181–9. https://doi.org/10.1016/j.cep.2018.04.018.

[219] Bianchi E, Schwieger W, Freund H. Assessment of periodic open cellular structures for enhanced heat conduction in catalytic fixed-bed reactors. Adv Eng Mater 2016;18(4):608–14. https://doi.org/10.1002/adem.201500356.

[220] Ferroni C, Bracconi M, Ambrosetti M, Maestri M, Groppi G, Tronconi E. A fundamental investigation of gas/solid heat and mass transfer in structured catalysts based on periodic open cellular structures (POCS). Ind Eng Chem Res 2021;60(29):10522–38. https://doi.org/10.1021/acs.iecr.1c0021510.1021/acs.iecr.1c00215.s001.

[221] Baillis D, Coquard RM. Radiative and conductive thermal properties of foams. In: Öchsner A, Murch GE, de Lemos MJS, editors. Cell. Porous Mater. Therm. Prop. Simul. Predict., WILEY-VCH Verlag, 2008: pp. 343–384.

[222] Vignoles GL, Ortona A. Numerical study of effective heat conductivities of foams by coupled conduction and radiation. Int J Therm Sci 2016;109:270–8. https://doi.org/10.1016/j.ijthermalsci.2016.06.013.

[223] Mellouli S, Dhaou H, Askri F, Jemni A, Ben Nasrallah S. Hydrogen storage in metal hydride tanks equipped with metal foam heat exchanger. Int J Hydrogen Energy 2009;34:9393–401. https://doi.org/10.1016/j.ijhydene.2009.09.043.

[224] Zhao CY, Lu W, Tian Y. Heat transfer enhancement for thermal energy storage using metal foams embedded within phase change materials (PCMs). Sol Energy 2010;84(8):1402–12. https://doi.org/10.1016/j.solener.2010.04.022.

[225] Kaplan Y. Effect of design parameters on enhancement of hydrogen charging in metal hydride reactors. Int J Hydrogen Energy 2009;34(5):2288–94. https://doi.org/10.1016/j.ijhydene.2008.12.096.

[226] Laurencelle F, Goyette J. Simulation of heat transfer in a metal hydride reactor with aluminium foam. Int J Hydrogen Energy 2007;32(14):2957–64. https://doi.org/10.1016/j.ijhydene.2006.12.007.

[227] Li Z, Wu Z-G. Numerical study on the thermal behavior of phase change materials (PCMs) embedded in porous metal matrix. Sol Energy 2014;99:172–84. https://doi.org/10.1016/j.solener.2013.11.017.

[228] Agyenim F, Hewitt N, Eames P, Smyth M. A review of materials, heat transfer and phase change problem formulation for latent heat thermal energy storage systems (LHTESS). Renew Sustain Energy Rev 2010;14(2):615–28. https://doi.org/10.1016/j.rser.2009.10.015.

[229] Gasia J, Miró L, Cabeza LF. Materials and system requirements of high temperature thermal energy storage systems: A review. Part 2: Thermal conductivity enhancement techniques. Renew Sustain Energy Rev 2016;60:1584–601. https://doi.org/10.1016/j.rser.2016.03.019.

[230] Chen J, Yang D, Jiang J, Ma A, Song D. Research progress of phase change materials (PCMs) embedded with metal foam (a review). Procedia Mater Sci 2014;4:389–94. https://doi.org/10.1016/j.mspro.2014.07.579.

[231] Fiedler T, Öchsner A, Belova IV, Murch GE. Thermal conductivity enhancement of compact heat sinks using cellular metals. Defect Diffus. Forum 2008;273–276:222–6. https://doi.org/10.4028/www.scientific.net/DDF.273-276.222.

[232] Kumar P, Topin F, Vicente J. Determination of effective thermal conductivity from geometrical properties: Application to open cell foams. Int J Therm Sci 2014;81:13–28. https://doi.org/10.1016/j.ijthermalsci.2014.02.005.

[233] Wong M, Owen I, Sutcliffe CJ, Puri A. Convective heat transfer and pressure losses across novel heat sinks fabricated by selective laser melting. Int J Heat Mass Transf 2009;52(1-2):281–8. https://doi.org/10.1016/j.ijheatmasstransfer.2008.06.002.

[234] Singh R. Thermal conduction through porous systems. In: Öchsner A, Murch GE, de Lemos MJS, editors. Cell. Porous Mater. Therm. Prop. Simul. Predict., WILEY-VCH Verlag, 2008: pp. 199–238.

[235] Fiedler T, Löffler R, Bernthaler T, Winkler R, Belova IV, Murch GE, et al. Numerical analyses of the thermal conductivity of random hollow sphere structures. Mater Lett 2009;63(13-14):1125–7. https://doi.org/10.1016/j.matlet.2008.10.030.

[236] Bakhvalov N, Panasenko G. Homogenisation: Averaging processes in periodic media. Kluwer Academic Publisher; 1989.

[237] Akbarzadeh AH, Fu JW, Liu L, Chen ZT, Pasini D. Electrically conducting sandwich cylinder with a planar lattice core under prescribed eigenstrain and magnetic field. Compos Struct 2016;153:632–44. https://doi.org/10.1016/j.compstruct.2016.06.058.

[238] Bai X, Zheng Z, Liu C, Nakayama A. Metal frame structures with controlled anisotropic thermal conductivity. Int J Heat Mass Transf 2020;148:119064. https://doi.org/10.1016/j.ijheatmasstransfer.2019.119064.

[239] Belova IV, Veyhl C, Fiedler T, Murch GE. Analysis of anisotropic behaviour of thermal conductivity in cellular metals. Scr Mater 2011;65(5):436–9. https://doi.org/10.1016/j.scriptamat.2011.05.029.

[240] Boldrin L, Scarpa F, Rajasekaran R. Thermal conductivities of iso-volume centre-symmetric honeycombs. Compos Struct 2014;113:498–506. https://doi.org/10.1016/j.compstruct.2014.03.013.

[241] Matsuura M. Gielis' superformula and regular polygons. J Geom 2015;106(2):383–403. https://doi.org/10.1007/s00022-015-0269-z.

[242] Abueidda DW, Abu Al-Rub RK, Dalaq AS, Lee D-W, Khan KA, Jasiuk I. Effective conductivities and elastic moduli of novel foams with triply periodic minimal surfaces. Mech Mater 2016;95:102–15. https://doi.org/10.1016/j.mechmat.2016.01.004.

[243] Park G, Kang S, Lee H, Choi W. Tunable multifunctional thermal metamaterials: manipulation of local heat flux via assembly of unit-cell thermal shifters. Sci Rep 2017;7:41000. https://doi.org/10.1038/srep41000.

[244] Vemuri KP, Bandaru PR. Geometrical considerations in the control and manipulation of conductive heat flux in multilayered thermal metamaterials. Appl Phys Lett 2013;103(13):133111. https://doi.org/10.1063/1.4823455.

[245] Vemuri KP, Canbazoglu FM, Bandaru PR. Guiding conductive heat flux through thermal metamaterials. Appl Phys Lett 2014;105(19):193904. https://doi.org/10.1063/1.4901885.

[246] Toropova MM, Steeves CA. Adaptive bimaterial lattices to mitigate thermal expansion mismatch stresses in satellite structures. Acta Astronaut 2015;113:132–41. https://doi.org/10.1016/j.actaastro.2015.03.022.

[247] Werner MR, Fahrner WR. Review on materials, microsensors, systems and devices for high-temperature and harsh-environment applications. IEEE Trans Ind Electron 2001;48:249–57. https://doi.org/10.1109/41.915402.

[248] Raimondi L, Tomesani L, Donati L, Zucchelli A. Lattice material infiltration for hybrid metal-composite joints: Manufacturing and static strenght. Compos Struct 2021;269:114069. https://doi.org/10.1016/j.compstruct.2021.114069.

[249] Gibiansky LV, Torquato S. Thermal expansion of isotropic multiphase composites and polycrystals. J Mech Phys Solids 1997;45(7):1223–52. https://doi.org/10.1016/S0022-5096(96)00129-9.

[250] Xu H, Pasini D. Structurally efficient three-dimensional metamaterials with controllable thermal expansion. Sci Rep 2016;6:34924. https://doi.org/10.1038/srep34924.

[251] Wei K, Peng Y, Wang K, Duan S, Yang X, Wen W. Three dimensional lightweight lattice structures with large positive, zero and negative thermal expansion. Compos Struct 2018;188:287–96. https://doi.org/10.1016/j.compstruct.2018.01.030.

[252] Ai L, Gao X-L. Three-dimensional metamaterials with a negative Poisson's ratio and a non-positive coefficient of thermal expansion. Int J Mech Sci 2018;135:101–13. https://doi.org/10.1016/j.ijmecsci.2017.10.042.

[253] Ai L, Gao X-L. Metamaterials with negative Poisson's ratio and non-positive thermal expansion. Compos Struct 2017;162:70–84. https://doi.org/10.1016/j.compstruct.2016.11.056.

[254] Parsons EM. Lightweight cellular metal composites with zero and tunable thermal expansion enabled by ultrasonic additive manufacturing: Modeling, manufacturing, and testing. Compos Struct 2019;223:110656. https://doi.org/10.1016/j.compstruct.2019.02.031.

[255] Steeves CA, dos Santos e Lucato SL, He M, Antinucci E, Hutchinson JW, Evans AG. Concepts for structurally robust materials that combine low thermal expansion with high stiffness. J Mech Phys Solids 2007;55(9):1803–22. https://doi.org/10.1016/j.jmps.2007.02.009.

[256] Wei K, Peng Y, Wen W, Pei Y, Fang D. Tailorable thermal expansion of lightweight and robust dual-constituent triangular lattice material. J Appl Mech 2017;84. https://doi.org/10.1115/1.4037589.

[257] Palumbo NMA, Smith CW, Miller W, Evans KE. Near-zero thermal expansivity 2-D lattice structures: Performance in terms of mass and mechanical properties. Acta Mater 2011;59(6):2392–403. https://doi.org/10.1016/j.actamat.2010.12.037.

[258] Ding Y, Akbari M, Gao X-L, Li A, Kovacevic R. Use of a robotized laser powder-feed metal additive manufacturing system for fabricating metallic metamaterials. In: Manuf. Tech. Mater. Eng., CRC Press, 2019: pp. 51–66.

[259] Askari M, Hutchins DA, Thomas PJ, Astolfi L, Watson RL, Abdi M, et al. Additive manufacturing of metamaterials: A review. Addit Manuf 2020;36:101562. https://doi.org/10.1016/j.addma.2020.101562.

[260] Vilardell AM, Takezawa A, du Plessis A, Takata N, Krakhmalev P, Kobashi M, et al. Mechanical behavior of in-situ alloyed Ti6Al4V(ELI)-3 at.% Cu lattice structures manufactured by laser powder bed fusion and designed for implant applications. J Mech Behav Biomed Mater 2021;113:104130. https://doi.org/10.1016/j.jmbbm.2020.104130.

[261] Burns N, Burns M, Travis D, Geekie L, Rennie AEW. Designing advanced filtration media through metal additive manufacturing. Chem Eng Technol 2016;39:535–42. https://doi.org/10.1002/ceat.201500353.

[262] Leary M. Design for additive manufacturing; 2019.

[263] Cooper N, Coles LA, Everton S, Maskery I, Campion RP, Madkhaly S, et al. Additively manufactured ultra-high vacuum chamber for portable quantum technologies. Addit Manuf 2021;40:101898. https://doi.org/10.1016/j.addma.2021.101898.

[264] Plocher J, Panesar A. Review on design and structural optimisation in additive manufacturing: Towards next-generation lightweight structures. Mater Des 2019;183:108164. https://doi.org/10.1016/j.matdes.2019.108164.

[265] Li T, Jiang Y, Yu K, Wang Q. Stretchable 3D lattice conductors. Soft Matter 2017;13(42):7731–9.

[266] Mitchell A, Lafont U, Hołyńska M, Semprimoschnig C. Additive manufacturing — A review of 4D printing and future applications. Addit Manuf 2018;24:606–26. https://doi.org/10.1016/J.ADDMA.2018.10.038.

[267] Niknam H, Yazdani Sarvestani H, Jakubinek MB, Ashrafi B, Akbarzadeh AH. 3D printed accordion-like materials: A design route to achieve ultrastretchability. Addit Manuf 2020;34:101215. https://doi.org/10.1016/j.addma.2020.101215.

[268] Saudan H, Kiener L, Perruchoud G, Kruis J, Liberatoscioli S, Dadras MM, et al. Compliant mechanisms and space grade product redesign based on additive manufacturing. SPIE-Intl Soc Optical Eng 2018:101. https://doi.org/10.1117/12.2312087.

[269] Kiener L, Saudan H, Cosandier F, Perruchoud G, Spanoudakis P, Rouvinet J. Additive manufacturing: Innovative concept of compliant mechanisms. In: Proc. 20th Int. Conf. Eur. Soc. Precis. Eng. Nanotechnology, EUSPEN 2020, euspen, 2020: pp. 137–140. Doi: 10.1117/12.2560906.

[270] Foley J, Dam A, Feiner S, Hughes J. Computer graphics: principles and practice, 1996. http://www.sidalc.net/cgi-bin/wxis.exe/?IsisScript=LIBRO.xis&method=post&formato=2&cantidad=1&expresion=mfn=028638 (accessed June 14, 2021).

[271] Leary M, Downing D, Lozanovski B, Harris J. Design principles. In: Fundam. Laser Powder Bed Fusion Met., Elsevier, 2021: pp. 119–154. Doi: 10.1016/B978-0-12-824090-8.00013-5.

[272] Osher S, Fedkiw R. Level Set Methods and Dynamic Implicit Surfaces, Springer New York, New York, NY, 2003. Doi: 10.1007/b98879.

[273] McMillan M, Jurg M, Leary M, Brandt M. Programmatic lattice generation for additive manufacture. Procedia Technol 2015;20:178–84. https://doi.org/10.1016/j.protcy.2015.07.029.

[274] Lee BN, Pei E, Um J. An overview of information technology standardization activities related to additive manufacturing. Prog Addit Manuf 2019;4(3):345–54. https://doi.org/10.1007/s40964-019-00087-5.

[275] Alghamdi A, Lozanovski B, McMillan M, Tino R, Downing D, Zhang X, et al. Effect of polygon order on additively manufactured lattice structures: a method for defining the threshold resolution for lattice geometry. Int J Adv Manuf Technol 2019;105(5-6):2501–11. https://doi.org/10.1007/s00170-019-04168-1.

[276] Gibson LJ, Ashby MF. The mechanics of three-dimensional cellular materials. Proc R Soc London, Ser A Math Phys Sci 382 (1982) 43–59. Doi: 10.1098/rspa.1982.0088.

[277] Lozanovski B, Downing D, Tino R, Tran P, Shidid D, Emmelmann C, et al. Image-based geometrical characterization of nodes in additively manufactured lattice structures. 3D Print Addit Manuf 2021;8(1):51–68. https://doi.org/10.1089/3dp.2020.0091.

[278] Lozanovski B, Downing D, Tino R, du Plessis A, Tran P, Jakeman J, et al. Non-destructive simulation of node defects in additively manufactured lattice structures. Addit Manuf 2020;36:101593. https://doi.org/10.1016/j.addma.2020.101593.

[279] Gunasegaram DR, Murphy AB, Matthews MJ, DebRoy T. The case for digital twins in metal additive manufacturing. J Phys Mater 2021;4(4):040401. https://doi.org/10.1088/2515-7639/ac09fb.

[280] Sumner DR, Galante JO. Determinants of Stress Shielding: Design versus materials versus interface, Clin Orthop Relat Res 274 (1992) 203–212. https://www.researchgate.net/profile/Dale-Sumner/publication/21426792_Determinants_of_Stress_Shielding_Design_Versus_Materials_Versus_Interface/links/58337b8508ae004f74c5adf8/Determinants-of-Stress-Shielding-Design-Versus-Materials-Versus-Interface.pdf (accessed June 14, 2021).

[281] Schaedler TA, Jacobsen AJ, Torrents A, Sorensen AE, Lian J, Greer JR, et al. Ultralight metallic microlattices. Science 2011;334(6058):962–5.

[282] Zheng X, Lee H, Weisgraber TH, Shusteff M, DeOtte J, Duoss EB, et al. Ultralight, ultrastiff mechanical metamaterials. Science 2014;344(6190):1373–7.

[283] Tancogne-Dejean T, Mohr D. Stiffness and specific energy absorption of additively-manufactured metallic BCC metamaterials composed of tapered beams. Int J Mech Sci 2018;141:101–16. https://doi.org/10.1016/j.ijmecsci.2018.03.027.

[284] Stiny G, JG-I. congress (2), undefined 1971, Shape grammars and the generative specification of painting and sculpture., n.d. http://home.fa.utl.pt/~lromao/2008_09/sg/aula_3/stiny_gips_aula_3.pdf (accessed July 2, 2021).

[285] Bendsoe MP, Sigmund O. Topology optimization: theory, methods and applications. Springer; 2003.

[286] Ruder S. An overview of gradient descent optimization algorithms; 2016. http://arxiv.org/abs/1609.04747 (accessed July 2, 2021).

[287] Jarraya B, Bouri A. Metaheuristic optimization backgrounds: a literature review, 2012. http://ssrn.com/abstract=2114335http://www.akpinsight.webs.com (accessed July 2, 2021).